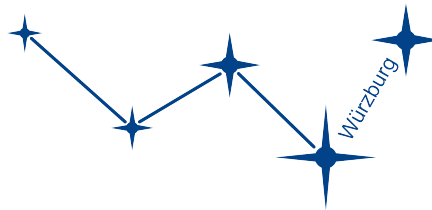# Indirect Search for Dark Matter in the Universe - the Multiwavelength and Multiobject Approach

Dissertation zur Erlangung des
naturwissenschaftlichen Doktorgrades
der Julius-Maximilians-Universität Würzburg

vorgelegt von
Dominik Martin Elsässer
geboren in: Alzenau

Abgabe: Würzburg, 2011

Eingereicht am

bei der Fakultät für Physik und Astronomie.

1. Gutachter: Prof. Dr. K. Mannheim

2. Gutachter: Prof. Dr. M. Kadler

3. Gutachter:

der Dissertation.

1. Prüfer: Prof. Dr. K. Mannheim

2. Prüfer: Prof. Dr. M. Kadler

3. Prüfer:

im Promotionskolloquium.

Tag des Promotionskolloquiums:

Doktorurkunde ausgehändigt am:

Contents

4

1 Zusammenfassung

Dunkle Materie ist ein zentraler Bestandteil der modernen Kosmologie, und damit von entscheidender Bedeutung für unser Verständnis der Strukturbildung im Universum. Seit ihrer Entdeckung durch spektroskopische Untersuchungen der Bewegung der Galaxien im Coma-Galaxienhaufen vor etwa 80 Jahren haben sich mehr und mehr starke Hinweise auf die gravitative Wirkung der Dunklen Materie auf allen Skalen, von Einzelgalaxien bis zum kosmologischen Hubble-Fluss ergeben. Das offensichtliche Fehlen von elektromagnetischer Wechselwirkung in Kombination mit unabhängigen Messungen der Energiedichte der baryonischen Materie über die Häufigkeit der primordialen leichten Elemente weisen auf eine nicht-baryonische Natur der Dunklen Materie hin. Die Wirkung der Dunklen Materie bei der Strukturbildung zeigt weiterhin dass ihre Konstituenten kalt sind, also zum Zeitpunkt des Gleichgewichts zwischen Strahlung und Materie eine Temperatur kleine als ihre Ruhemasse aufwiesen. Generische Kandidaten für das Dunkelmaterie-Teilchen sind stabile, schwach wechselwirkende Teilchen mit Ruhemassen von der Größenordnung der Skala der elektroschwachen Symmetriebrechung, wie sie zum Beispiel in der Supersymmetrie bei erhaltener R-Parität vorkommen. Derartige Teilchen frieren auf natürliche Weise im frühen Universum mit kosmologisch relevanten Reliktdichten aus. Die fortschreitende Strukturbildung im Universum führt dann zur Bildung von überdichten Regionen, in denen die Dunkelmaterie-Teilchen wiederum in signifikantem Ausmaß annihilieren können. Dadurch würde ein potentiell detektierbarer Fluß von Hochenergie-Teilchen einschließlich Photonen aus den instabilen Zwischenprodukten der Annihilationsereignisse erzeugt. Die Spektren dieser Teilchen würden Rückschlüsse auf die Masse und den Annihilations-Querschnitt als wichtige Größen zur mikrophysikalischen Identifikation der Dunkelmaterie-Teilchen erlauben. Darin liegt die zentrale Motivation für indirekte Suchen nach der Dunklen Materie.

Zum gegenwärtigen Zeitpunkt jedoch haben weder diese indirekten Suchen, noch direkte Methoden zur Suche nach elastischen Streuereignissen zwischen Dunkelmaterie-Teilchen und Atomkernen sowie Beschleunigerexperimente einen eindeutigen Nachweis von Dunkelmaterie-Teilchen erbracht. Das an sich stellt keine Überraschung dar, denn die zu erwartenden Signale sind aufgrund der schwachen Wechselwirkung der Teilchen nur von geringer Intensität. Im Falle der indirekten Suchen steht zu erwarten, dass selbst für die größten Massekonzentrationen im Universum die Stärke des Annihilationssignals der Dunklen Materie den durch astrophysikalische Quellen verursachten Untergrund nicht überschreitet. Die Möglichkeit der sicheren Unterscheidung zwischen einem möglichen Signal aus der Annihilation der Dunklen Materie und eben diesem Untergrund ist daher entscheidend für die Erfolgsaussichten der indirekten Suchen.

In der vorliegenden Arbeit wird eine neuartige Suchstrategie ausgearbeitet und vorgestellt, deren zentrale Komponente die Auswahl von Beobachtungszielen aus einem breiten Massebereich, die Kontrolle der astrophysikalischen Untergründe, und die Einbeziehung von Daten aus mehreren Wellenlängenbereichen ist. Die durchgeführten Beobachtungen werden vorgestellt und interpretiert. Ein Ergebnis ist, dass die Un-

sicherheiten in Bezug auf die Verteilung der Dunklen Materie in Halos und deren individuelle Dichtestruktur, sowie in Bezug auf die mögliche Verstärkung des Annihilationssignales durch Substruktur, im Falle der massearmen Halos (wie zum Beispiel bei den Zwerggalaxien) größer ist als bei massereichen Halos, wie denen der Galaxienhaufen. Andererseits weisen die massereichen Halos größere Unsicherheiten in Hinblick auf die zu erwartenden rein astrophysikalischen Untergründe auf. Die Unsicherheiten in Bezug auf die bisher unbekannte Teilchenphysik jenseits des Standardmodells schließlich sind unabhängig von der Masse der beobachteten Halos. Im Zusammenspiel ermöglichen es diese unterschiedlichen Skalierungsverhalten, die globale Unsicherheit durch eine kombinierte Analyse der Beobachtungen von Halos mit verschiedenen Massen, die einen bedeutenden Teil der Masseskala abdecken, nennenswert zu reduzieren.

Diese Strategie wurde im Rahmen des wissenschaftlichen Beobachtungsprogrammes des MAGIC Teleskopsystems implementiert. Es wurden Beobachtungen von Zwerggalaxien sowie des Virgo- und des Perseus-Galaxienhaufens durchgeführt. Die resultierenden Grenzen auf Gammastrahlung aus der Annihilation von schwach wechselwirkenden, massereichen Teilchen gehören zum Zeitpunkt dieser Niederschrift zu den stärksten Grenzen aus indirekten Suchen nach der Dunklen Materie. Die überragende Empfindlichkeit des MAGIC Teleskopsystems für niedrige Energien spielt hierbei eine Schlüsselrolle, da der überwiegende Anteil der Gammastrahlungs-Photonen aus dem Annihilationsprozess, bedingt durch die Produktion einer großen Anzahl von Standardmodell-Teilchen pro Annihilation, Energien deutlich unterhalb der Ruhemasse der Dunkelmaterie-Teilchen aufweist. Die so gewonnenen Grenzen auf die Annihilations-Flüsse schränken einige in der Literatur diskutierte und durch aussergewöhnlich große Annihilations-Flüsse gekennzeichnete Szenarien stark ein.

2 Abstract

Cold dark matter constitutes a basic tenet of modern cosmology, essential for our understanding of structure formation in the Universe. Since its first discovery by means of spectroscopic observations of the dynamics of the Coma cluster some 80 years ago, mounting evidence of its gravitational pull and its impact on the geometry of space-time has build up across a wide range of scales, from galaxies to the entire Hubble flow. The apparent lack of electromagnetic coupling and independent measurements of the energy density of baryonic matter from the primordial abundances of light elements show the non-baryonic nature of dark matter, and its clustering properties prove that it is cold, i.e. that it has a temperature lower than its mass during the time of radiation-matter equality. A generic particle candidate for cold dark matter are weakly interacting massive particles at the electroweak symmetry-breaking scale, such as the neutralinos in R-parity conserving supersymmetry. Such particles would naturally freeze-out with a cosmologically relevant relic density at early times in the expanding Universe. Subsequent clustering of matter would recover annihilation interactions between the dark matter particles to some extent and thus lead to potentially observable high-energy emission from the decaying unstable secondaries produced in annihilation events. The spectra of the secondaries would permit a determination of the mass and annihilation cross section, which are crucial for the microphysical identification of the dark matter. This the central motivation for indirect dark matter searches.

However, presently neither the indirect searches, nor the complementary direct searches based on the detection of elastic scattering events, nor the production of candidate particles in collider experiments, has yet provided unequivocal evidence for dark matter. This does not come as a surprise, since the dark matter particles interact only through weak interactions and therefore the corresponding secondary emission must be extremely faint. It turns out that even for the strongest mass concentrations in the Universe, the dark matter annihilation signal is expected to not exceed the level of competing astrophysical sources. Thus, the discrimination of the putative dark matter annihilation signal from the signals of the astrophysical inventory has become crucial for indirect search strategies.

In this thesis, a novel search strategy will be developed and exemplified in which target selection across a wide range of masses, astrophysical background estimation, and multi-wavelength signatures play the key role. It turns out that the uncertainties regarding the halo profile and the boost due to surviving substructure are bigger for halos at the lower end of the observed mass scales, i.e. in the regime of dwarf galaxies and below, while astrophysical backgrounds tend to become more severe for massive dark matter halos such as clusters of galaxies. By contrast, the uncertainties due to unknown details of particle physics are invariant under changes of the halo mass. Therefore, the different scaling behaviors can be employed to significantly cut down on the uncertainties in observations of different targets covering a major part of the involved mass scales. This strategical approach was implemented in the scientific program carried out with the MAGIC telescope system. Observations of dwarf galaxies and the Virgo- and Perseus

clusters of galaxies have been carried out and, at the time of writing, result in some of the most stringent constraints on weakly interacting massive particles from indirect searches. Here, the low-threshold design of the MAGIC telescope system plays a crucial role, since the bulk of the high-energy photons, produced with a high multiplicity during the fragmentation of unstable dark matter annihilation products, are emitted at energies well below the dark matter mass scale. The upper limits severely constrain less generic, but more prolific scenarios characterized by extraordinarily high annihilation efficiencies.

3 Dark Matter in the Universe

3.1 Historical Overview

The insight that the visible matter in the Universe, stars, cool and hot gas, molecular clouds and dust, is but a fraction of the total mass (and energy) content of the Cosmos is profound, and yet has non trivial ramifications. Many of the tools employed later in the discovery process of the Dark Matter were developed already in the 19 th century. As historical examples, the post-renaissance discovery of the planet Neptune by Johann Galle and Heinrich d'Arrest of the Berliner Sternwarte in 1864 was a consequence of the rigorous application of Keplerian dynamics by John Adams and Urbain Le Verrier to calculate the orbit of the planet Uranus, and to deduce the properties and position of a yet-invisible mass component in the solar system (the planet Neptune) [1]. Together with the prediction and subsequent observational discovery of companion stars to the bright fix stars Sirius and Procyon (both companions later turned out to be white dwarf stars) by means of astrometry (i.e. by observing tiny aberrations of the proper motion of the star, and ascribing these to the gravitational tug of a yet-unseen massive object in the system), this established as a scientific method what became a staple of the quest for the invisible Universe in the 20th century: the use of gravitational effects as a dynamical tracer of mass.

That the Universe might not only harbor scores of unseen stars, planets and gas or plasma too cold or too hot or simply too faint to be visible in the then-accessible parts of the electromagnetic spectrum first became evident in the third decade of the 20th century. Dutch astronomers and pioneers of Milky Way studies Jacobus Kapteyn and Jan Hendrik Oort surveyed both the motion of Milky Way stars in the plane of the Galactic disc, but also the vertical component perpendicular to the disc. In the 1920s it became clear that for the solar neighborhood, the allowable amount of gravitating matter is at least of the same order of magnitude as the visible mass. By 1932 it was then clear that the vertical velocity component of many stars was in fact larger by a factor of two than could be accounted for by the gravitational acceleration due to all known stars and visible gaseous components in the disc. Kapteyn was also the first scientist to use the term *Dark Matter* in reference to an invisible, but dynamically active mass component [2].

The point where the Dark Matter problem really went beyond being a possible nuisance hidden within the complex movement of stars in the relative solar neighborhood was ushered forward by Fritz Zwicky in the 1930s. Zwicky, a prolific thinker and certainly one of the most versatile astronomers, made spectroscopic studies of the movement of individual galaxies within the Coma Cluster. Being one of the prominent nearby mass concentrations on the northern sky, the Coma Cluster of galaxies was even then known to harbor hundreds to thousands of massive galaxies, and a yet unquantified amount of matter in between them. By spectroscopically measuring the velocities of galaxies gravitationally bound to the cluster and located at different distances from the cluster center, Zwicky was for the first time able to trace the velocity dispersion of the population of galaxies in the Coma Cluster [3].
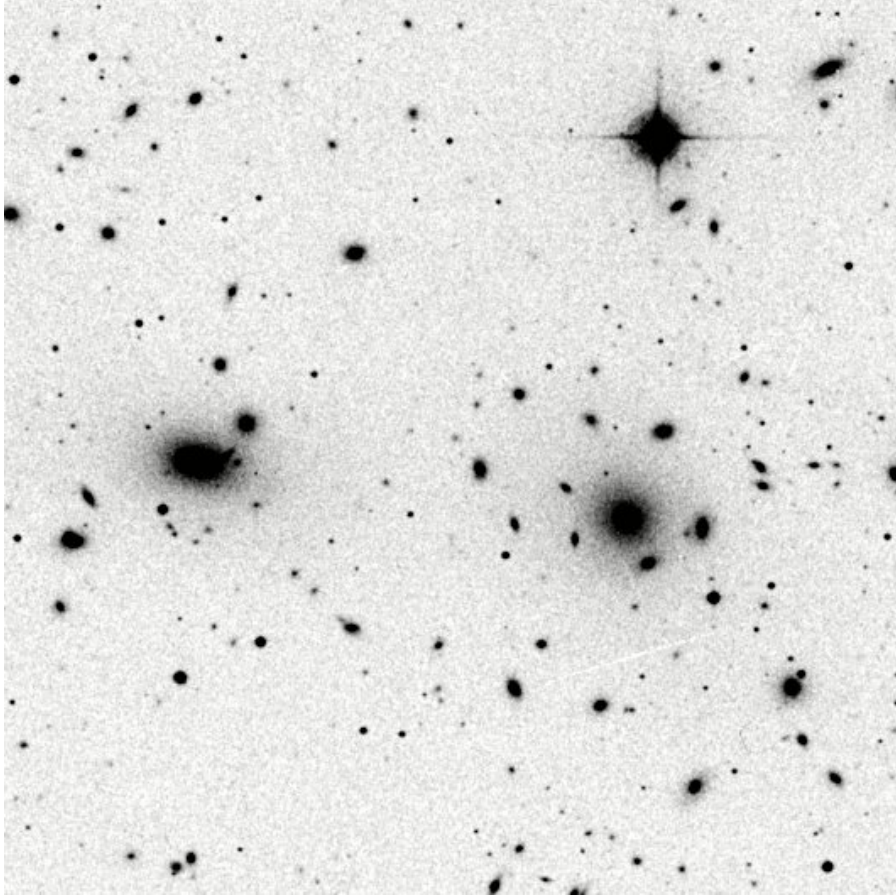
Figure 1: Visible light image of the Coma Cluster, taken with the Mt. Palomar Schmidt Telescope. Image Credit: NASA NED, $http://ned.ipac.caltech.edu/$.

He then used the virial theorem

$$T_{average} = -\frac{1}{2} \times U_{average} \tag{1}$$

to deduce from the observed velocity dispersion the amount of gravitating mass in the cluster and in each galaxy. The resulting value per galaxy, of which Zwicky counted close to 1000, was 4.5×10^{10} solar masses, and seems feeble, given modern knowledge of the total mass of the Milky Way approaching $1.5 \times 10^{12} M_\odot$ [4]. However, Zwicky had to compare this value to his estimate of the luminosity of each galaxy, which was 8.5×10^7 times the luminosity of our Sun. Although, again, his value falls short of modern estimates of bolometric luminosities of typical L^* galaxies by more than an order of magnitude, he immediately recognized the fundamental problem: With the ratio between gravitating mass and light

$$Y \equiv \frac{M}{L} \tag{2}$$

approaching a value of 500 in his study, the majority of the mass of the Coma Cluster could not possibly be concentrated in stars, or any other class of astronomical object emitting visible light.

It is instructive to remember here that Zwicky could not possibly know that much of the (baryonic) mass content of galaxies and clusters of galaxies is actually comprised of cold molecular clouds, hot gas and plasma, neither of which is prominent in the parts of the electromagnetic spectrum accessible to him. Also, he attributed all the gravitating mass to individual galaxies, not accounting for baryonic and other components in the medium in between the galaxies, but still bound to the cluster (confer Figures 1 and 2).
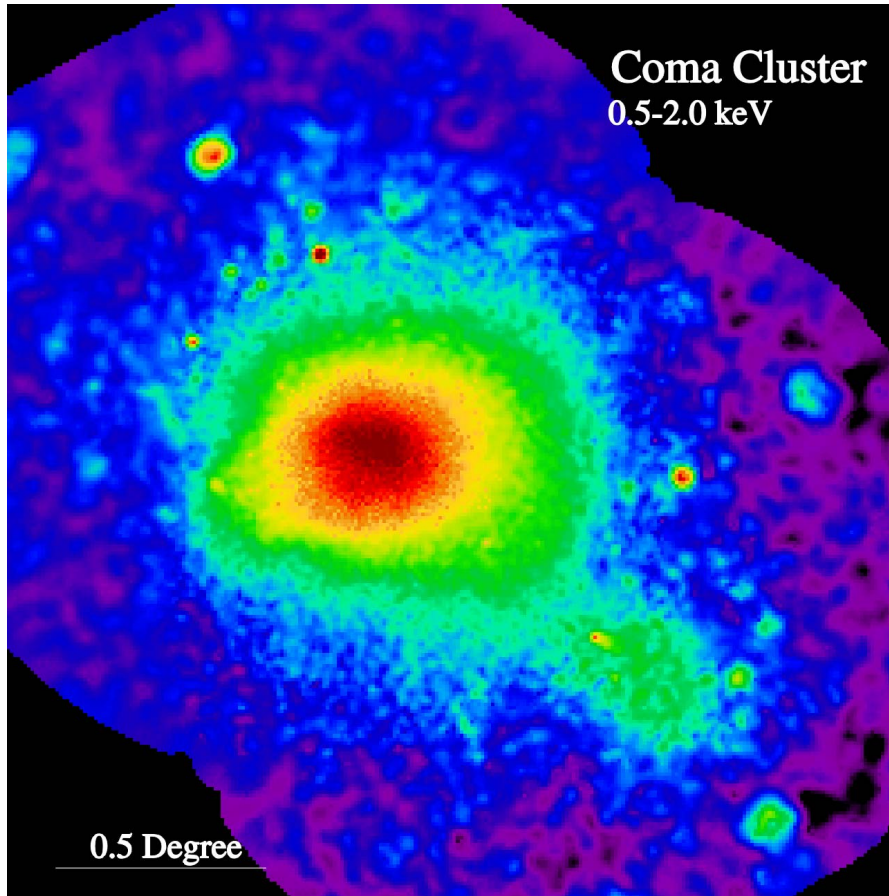

Figure 2: ROSAT X-ray image of the Coma Cluster. Intensity color coded. The dominating photon source here is neither individual L^* galaxies nor Active Galactic Nuclei, but the thermal emission of the hot intracluster medium, actually containing the majority of the baryonic mass in most clusters of galaxies. Image Credit: ROSAT Guest Observer Facility / HEASARC and S. L. Snowden USRA, NASA/GSFC.

Still, his inferred value for Y – largely of course by coincidence – was astonishingly

close to modern-day values ($Y_{Coma} = 300 - 400 \times h_0$ [5]).

Strong additional evidence for a large amount of Dark Matter in the Universe was then collected from measurements of the rotation curves of spiral galaxies. For such a system, Newtonian dynamics dictates that the orbital velocity of any tracer population (e.g. stars) outside of the radius containing the majority of the gravitating mass should fall of proportional to the inverse of the square root of the galactocentric distance, since

$$\frac{GMm}{r^2} = \frac{mv^2}{r} \Rightarrow v = \sqrt{\frac{GM}{r}} \tag{3}$$

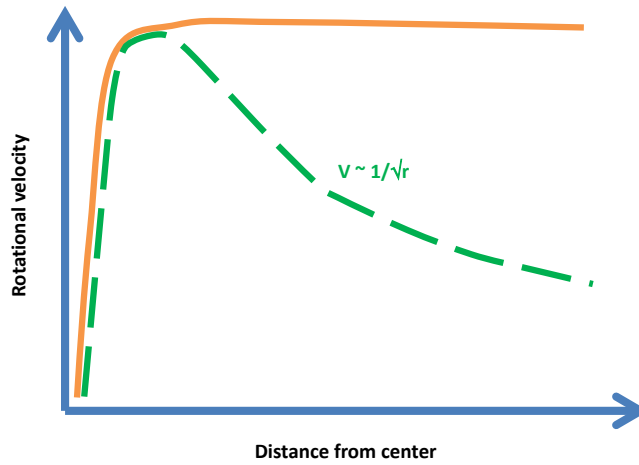See also Figure 3 for an instructive sketch.

Figure 3: Sketch of orbital velocities of stars in a spiral galaxy. Dashed line shows expected Keplerian decline with $1/\sqrt{r}$ outside of volume containing the majority of the visible mass. Solid line shows often observed "flat" rotational curve, extending far into the halo of the galaxy.

First, still inconclusive, observations in this regard were made for the Andromeda Galaxy, Messier 31, using stars [2] and the 21 cm emission of neutral hydrogen [6] as tracers. Both indicated a deviation from the expected decline at large radii. Much more sensitive observations were then undertaken by Vera Rubin, Norbert Thonnard and Kent Ford in the 1970s [7]. They took optical spectra of a large number of galaxies, and deduced rotation curves for the stellar populations therein. For a large fraction of such galaxies, they found flat rotational curves far outside the luminous mass concentrations, in some cases extending well into what was previously assumed to be intergalactic space (Fig. 4).
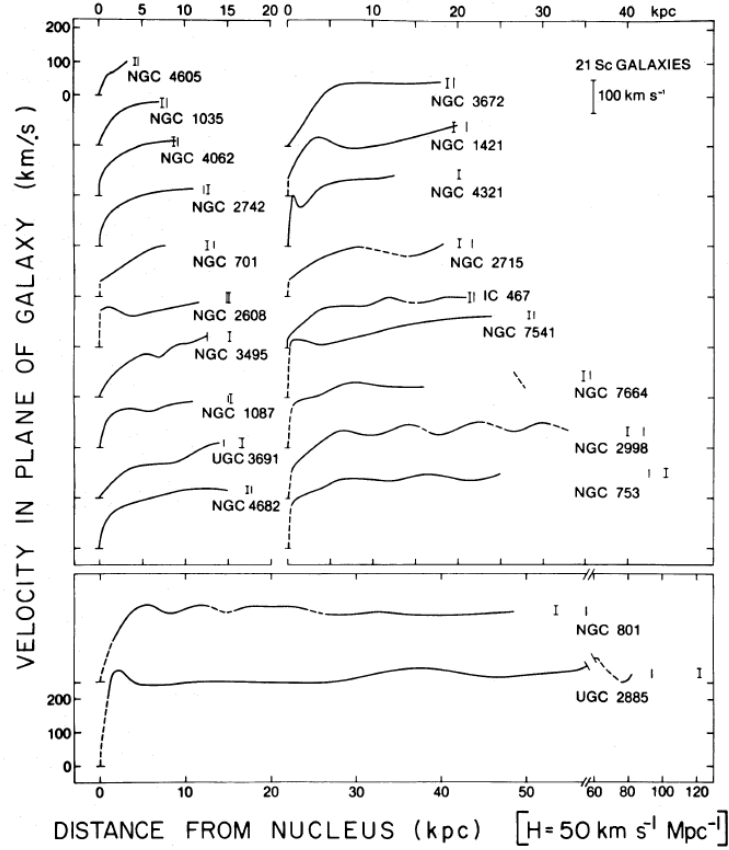
Figure 4: Measured rotational curves of various spiral galaxies. The trend towards flat rotation curves, with velocities in the galactic outskirts being far higher than predicted by Newtonian dynamics, is clearly evident. Image Credit: V. Rubin et al., 1978 [7]

Fundamentally, there are two possibilities to explain these results: First, Newtonian dynamics might not hold on very large scales. This possibility was first proposed in [8] as Modified Newtonian Dynamics, or *MOND*. The basic postulate of MOND is that the acceleration due to the gravitational interaction on large scales should be modified to

$$F_{MOND} = m\mu\frac{a}{a_0}a, \tag{4}$$

with a_0 being a constant of Nature with a value $a_0 \approx 10^{-10}m/s^2$, and μ an arbitrary function which goes to one for large and to $\frac{a}{a_0}$ for small arguments. Now, with orbits of stars approximated as circular, their acceleration goes as $a = v^2/r$, and, as introduced above,

$$a_{MOND} = \frac{\sqrt{GMa_0}}{r}, \tag{5}$$

13

it immediately follows that

$$v_{rotation,MOND} = \sqrt[4]{GMa_0}. \tag{6}$$

The rotation curves would therefore be "flat", matching the observations. It should be noted that this scenario does not make any prior assumptions about the underlying theoretical interpretation of both μ and a_0. These would rather have to be provided by a yet to be developed fundamental theory of gravity beyond general relativity.
As strikingly simply and elegant such an approach seems at first glance, there turned out to be severe observational constraints onto the idea of MOND: The gravitational redshifting of the emission of the hot intracluster medium in clusters of galaxies allows for an extremely precise mapping of the gravitational acceleration at large scales, and is in agreement with general relativity, but incompatible with MOND [9].

Thus, one has to turn to the second possibility, the existence of extended and massive, yet non-luminous halos around most galaxies, comprised of Dark Matter. A scenario that was also independently qualified in a pioneering numerical study of the stability of galactic discs [10], revealing the need for an extended and massive halo to stabilize the discs over relevant timescales.

3.2 Astrophysical Evidence

Presently, there is ample evidence for the geometrical and dynamical influence of the Dark Matter in the Universe. Rotational velocities of baryonic objects in galaxies can be employed to reveal the Dark Matter halos of these galaxies with great precision [11]. The advent of rocket, balloon-borne and orbital X-ray telescopes facilitated the discovery of a superheated plasma component in clusters of galaxies. This medium has temperatures in the range from 10 to 100 Megakelvins, thus thermally emitting X-rays [12] (Fig. 2). In fact, this Intracluster Medium (ICM) contains the majority of all baryonic mass of a galaxy cluster, exceeding the baryonic mass inside the galaxies themselves by factors of 3-5 [13]. Still, in comparison to the aforementioned mass-to-light ratios typical for clusters of galaxies ($\mathcal{O}(10-100)$), this component is sub dominant to the Dark Matter content of the halo, and in fact can be used as a tracer of the density profile and total mass of the Dark Matter halo. The basic assumption is that the gas is in hydrostatic equilibrium, i.e. the thermal pressure is balanced by the gravitational interaction. The velocity distribution in this simple but useful approximation then is held to be isotropic, and the relation between enclosed mass and the observable quantities in a X-ray exposure of the ICM – the electron density $n_e(r)$ and the temperature $T(r)$ follows [14] as

$$M(r) = -\frac{kT(r)r}{Gm_p\mu} \times (\frac{dln\,n_e}{dln\,r} + \frac{dln\,T}{dln\,r}), \tag{7}$$

with k being Boltzmann's constant, G the gravitational constant, m_p the mass of the proton, and μ the mean molecular weight. Results employing this method onto a sam-

ple of clusters, using the Chandra X-ray observatory, revealed mass-to-light ratios again compatible with the earlier results from the velocity dispersion of the cluster galaxies [15].

Another sensitive probe into the Dark Matter content content of galaxies and clusters is the gravitational lensing effect onto more distant background sources. The lensing effect is in a way unique as a tool, since it is not reliant on the dynamics of the system, but purely on the geometric effect of mass onto spacetime. In general relativity, the angle of deflection θ [11] for a light ray passing at a radius r from a mass M is

$$\theta = \frac{4GM}{rc^2}. \tag{8}$$

While challenging from an observational point of view, requiring either high resolution and yet deep imaging of an extended field using a space telescope like HST, or a huge sample of lower resolution images, this effect allows for a rather stringent calculation of the mass of the lens from readily observable quantities. Observations have been made of the strong gravitational lensing effect – the distortion of the image of background sources into giant "arcs" around large mass concentrations like clusters of galaxies (Fig. 5) in the foreground [16] – as well as of the statistical distortion of images of galaxies in large scale surveys by foreground masses, the so called weak lensing effect [17]. Both methods yield mass-to-light ratios again in good agreement with the findings from cluster dynamics, and from a very independent method.

In rare cases, both dynamical and geometrical action of the Dark Matter component in a cluster can be observed also in a single object. Most striking are those systems where two or more clusters undergo major merger events, and in this process different mass components are separated. Such systems allow do not only allow for a determination of the ratios between different constituents, but also for a rough indirect test of their interaction strength. The first such example was the so-called "Bullet Cluster" $1E0657 - 558$ [18] in the constellation Carina. In this system, the ICM has been frictionally slowed down and heated during the collision of two clusters, and subsequently settled in the center. The individual galaxies are dispersed enough that few collisions happen, and therefore the galaxy populations of both clusters could penetrate each other relatively undisturbed. The ICM can be pinpointed via X-ray observations of its thermal emission, while the galaxies are detectable at optical wavelengths. Weak lensing studies in turn reveal that the major part of the lensing mass (much greater than the masses of the galaxies summed up) is actually not co-located with the stripped ICM, but rather also penetrated undisturbed. This provides strong evidence of a dominant, non-luminous matter component additionally to the galaxies themselves and the ICM. Furthermore, the fact that this component was able to avoid frictional slowdown allows to conclude that the self-interaction strength of the constituent particles of this component must at least be smaller than the electromagnetic interaction. Presently, the conclusion that these systems (another example, "Pandora's Cluster" Abell 2744 [19], is depicted in Fig. 6) harbor roughly ten times as much weakly interacting matter compared to their baryonic content seems unavoidable.
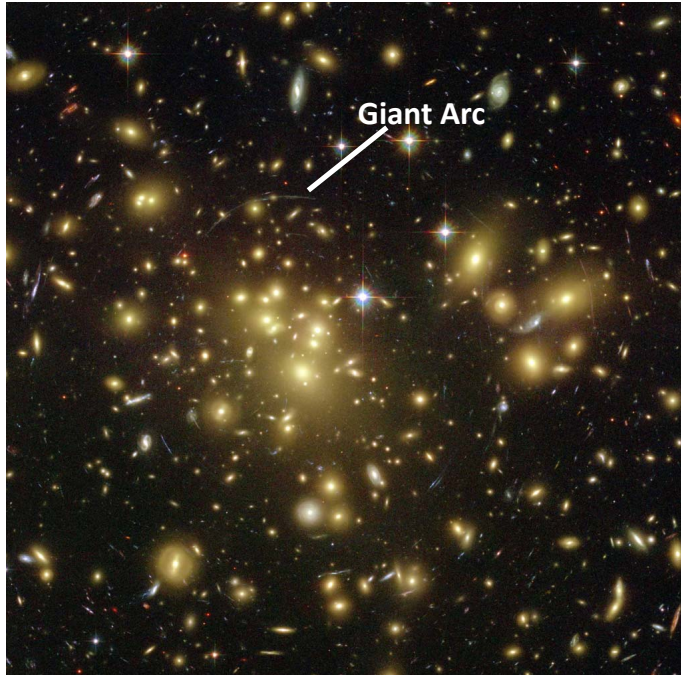
Figure 5: HST Advanced Camera for Surveys optical image of the galaxy cluster Abell 1689, depicting the foreground cluster galaxies as well as giant lensed arcs from distant background objects. Diameter of the imaged part of the cluster is close to 1 Mpc. Image Credit: NASA/ESA and own additions.

3.3 Cosmological Concordance Model

Apart from the description of the physical properties of individual objects, the Dark Matter is also evident within the framework of physical cosmology. The combination of observations of the power spectrum of the 3 K microwave background radiation [20,21], the X-ray surface brightness of distant clusters of galaxies [22,23], Type Ia supernovae [24–26] and the progress of structure formation, quantifiable e.g. via observations of the Lyman alpha forest [27], have led to the current cosmological standard model or "concordance cosmology", describing a Universe that began in a Big Bang 13.8 billion years ago, went through an inflationary era [28], is comprised of 4% baryonic matter, 23% cold Dark Matter, 73% Dark Energy (assumed here to be identified with the cosmological constant Λ), is of Euclidean flatness and shows accelerating expansion (see Fig. 7). The present-day value of the Hubble parameter is 0.7 [29]. This "$\Lambda - Cold - Dark - Matter$" or ΛCDM model will be used throughout this work.

In recent years, additional constraints pointing towards the ΛCDM model have been gained from measuring the imprint of the acoustic oscillations in the early universe on the visible baryonic matter component. These Baryon Acoustic Oscillations can be tracked via sky surveys, and strongly hint towards an amount of non-baryonic Dark Matter in

Figure 6: Composite image of the complex system of colliding clusters Abell 2744. X-ray surface brightness, indicating the ICM, depicted in red, superimposed on the optical image of the region. Weak lensing strength, tracing gravitating matter, indicated in blue. Image Credit: NASA/ESA. For detailed description of methods, see [19].

accordance with the ΛCDM model [30].

Independent support for the existence of cold Dark Matter also comes from precision studies of Big Bang nucleosynthesis.

Primordial abundances of hydrogen, helium, lithium, beryllium, and (in principle) boron can be spectroscopically measured from regions in the Galaxy relatively undisturbed by star formation activity, and also from low-metallicity population II stars. These abundances are a direct probe into the nuclear processes of the Big Bang. When the temperature dropped below 1 MeV, freeze-out of the weak interactions occurred, stopping the neutron-proton interconversion. Because the mass of the neutron is a bit larger than that of the proton, already at this time their relative abundance was 1/6 compared to the protons. At this time, the Universe was just close to one second old, but this is sufficiently close to the half-life of the free neutrons (890 seconds) for neutron decay to begin. Because of the large amount of thermal photons with energies of the order of typical nuclear binding energies (again, $\approx 1 MeV$), nucleosynthesis could only
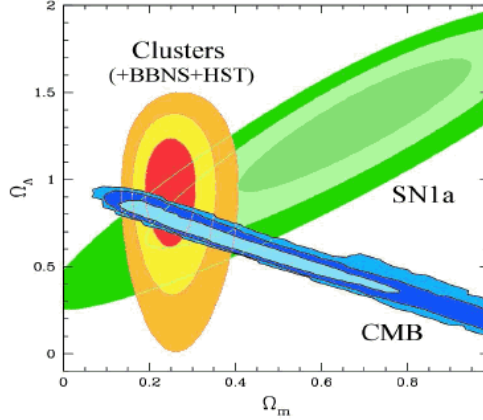
Figure 7: Different cosmological probes, and best fit region of overlap. Contours depict respective statistical confidence in terms of standard deviations. Image Credit: S. Allen et al., 2004 [23].

start at somewhat lower temperatures (approaching 100 keV), when the neutron/proton ratio was already down to 1/7. The relative minimal energy configuration of all light nuclei is the helium-4 nucleus. Therefore, from 2 neutrons and 14 protons (ratio 1/7!), 2 helium-4 nuclei and 12 remaining protons (hydrogen nuclei) result, immediately explaining the observed baryonic mass fraction of helium (25%). Other light isotopes are only produced in very small fractions, abundances being 10^{-5} for helium-3 and deuterium, and $\approx 10^{-10}$ for lithium. [31]

While actual measurement of these relative abundances is observationally challenging, their theoretical prediction hinges – due to the Universe being radiation dominated at the time of Big Bang nucleosynthesis – only on the parameter, the ratio between baryons and entropy

$$\eta = \frac{n_B}{S}. \tag{9}$$

Present observational constraints onto η and the relative abundances for the light elements are summed up in Fig. 8. Clearly, the Big Bang nucleosynthesis mandates that of the 27% cold matter content of the Universe, only 4% can actually be baryonic, in turn meaning that the Dark Matter cannot be of baryonic nature.

The non-baryonic nature of the Dark Matter is also corroborated by observations of the process of structure formation in the Universe. The rapid progress of hierarchical structure formation, and the already large amplitudes of the power spectrum of the 3 K background radiation (see Fig. 9 and also [33]), necessitate an onset of the formation of gravitational wells, into which the baryonic matter could then fall, already well before
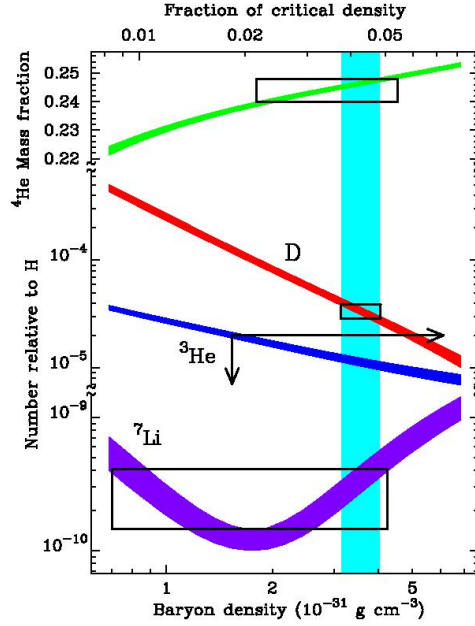
Figure 8: Allowable baryon density versus abundance for the light elements (theoretical predictions drawn as solid lines), and observational constraints (black boxes). Region of overlap around a baryon fraction of 4% shown as turquise area. Image Credit: D. Tytler et al., 2000 [32].

the surface of last scattering.

Observationally, and also from numerical experiments, it is evident that structure formation proceeded hierarchically, that the less massive halos collapsed at higher redshift, and the more massive halos later on formed through consecutive merger events [27, 34, 35]. The halo mass function is Press-Schechter [36] like.

In addition to the aforementioned observational indications of weakly interacting Dark Matter, there are also more theoretical arguments for its existence. Certainly, the most natural (though by no means the only viable) assumption is that the particles making up the Dark Matter would be thermally produced in the Big Bang, and then froze out. Since very light, weakly interacting particles (e.g. neutrinos with masses «eV) would be relativistic at the time of their freeze out, they would easily erase via free streaming all power on mass scales below superclusters, in obvious contradiction with the aforementioned observationally supported scenario of hierarchical structure formation. It is thereby possible to place a lower bound of the order 1 eV ("Cowsik-McClelland Bound", [37]) onto the mass of weakly interacting particles that are thermally produced in the Big Bang in quantities of the order of the Dark Matter relic density.

Generally, the number density evolution of any species is governed by the Boltzmann equation [38]

19
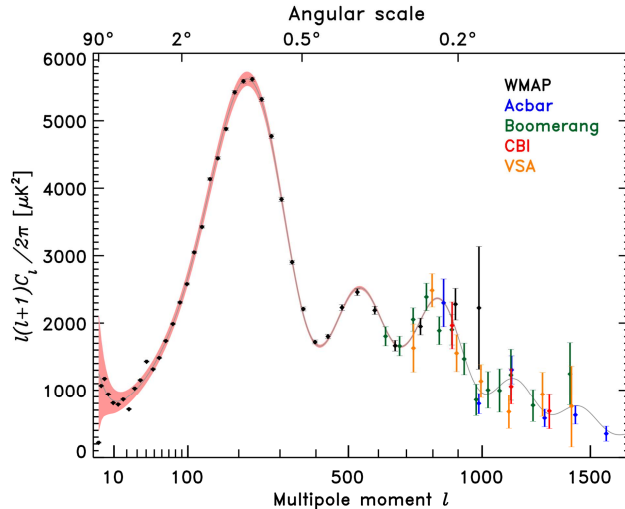
Figure 9: Power spectrum of the 3K cosmic background radiation. Depicted are measurements from different experiments with respective error bars, and shaded region of uncertainty for fit. Angular scale of the main (acoustic) peak is mostly sensitive to the curvature of the Universe (zero in case of $l \approx 200$, as observed), while ratio between the odd and even peaks, and the third peak probe reduced baryon and Dark Matter density, respectively. Image Credit: NASA.

$$\frac{dn_\chi}{dt} + 3Hn_\chi = - <\sigma v> (n_\chi^2 - n_{\chi,eq.}^2). \tag{10}$$

Freeze out will happen when the interaction rate of the particles becomes smaller than the Hubble rate of expansion:

$$\Gamma < H. \tag{11}$$

In this framework, it is already possible to track the number density evolution of a given species, and also resulting number densities in the present Universe, which have to be compared to ΛCDM. Before freeze out, the number density scales as

$$n_\chi \propto e^{-m_\chi/T}, \tag{12}$$

for a particle with mass m_χ, and H goes with

$$H \propto \frac{T^2}{m_{Planck}}. \tag{13}$$

Freeze out thus occurs roughly at a temperature

$$T_{fo} \approx \frac{m_\chi}{20}. \tag{14}$$
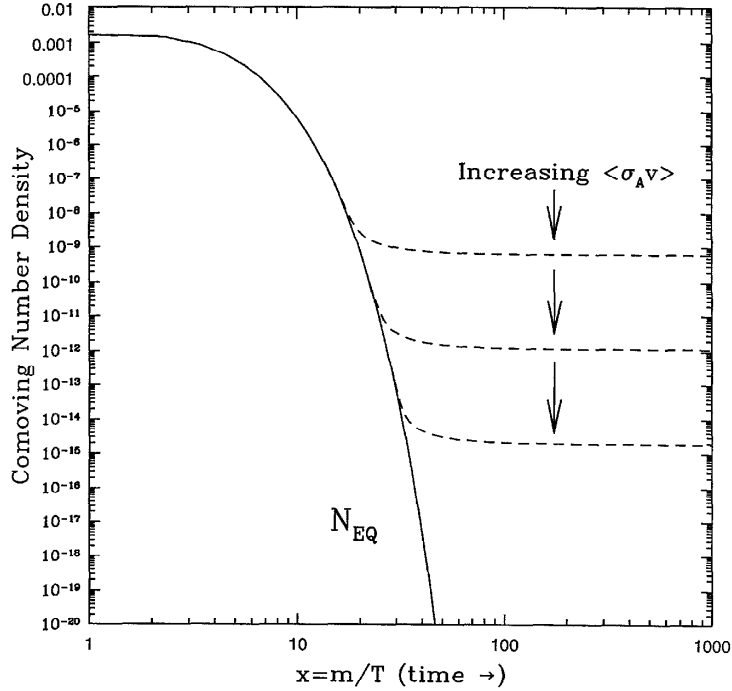
Figure 10: Number density of particle species before and after freeze out, and resulting relic density for different thermally averaged cross sections. Image Credit: Jungman et al., 1996 [38].

An immediate result is that the resulting "relic" number density Ω_χ scales inversely with the cross section (see also Fig. 10) as

$$\Omega_\chi h^2 = \frac{0.1pb \times c}{<\sigma v>}. \tag{15}$$

For weakly interacting particles, it has long been known [39] that the mass of such a relic particle would have to be larger than $\approx 2GeV$, to avoid exceeding the observed matter density in the Universe. The observed Dark Matter relic density times the square of the dimensionless Hubble parameter $\Omega_{DM}h^2 \approx 0.1$ thus is naturally reached via thermal freeze out of a massive relic particle with interaction strength of the order of the weak interaction:

$$<\sigma v>_\chi \approx 3 \times 10^{-26} \frac{cm^3}{s}. \tag{16}$$

The remarkable observation, that a relic that lacks electromagnetic interaction (i.e. is "dark"), but exhibits weak interaction and a mass roughly of the order of the scale of the electroweak symmetry breaking scale

$$(G_F\sqrt{2})^{-1/2} \approx 246GeV, \tag{17}$$

21

with G_F being the Fermi coupling constant, and thermally freezes out in the Big Bang, will reproduce the independently observed Dark Matter relic density, is sometimes even termed the "WIMP miracle". It should be stressed that, such prosaic terminology aside, the naturalness argument put forward above in fact lends substantial support to the paradigm of Weakly Interacting Massive Particles (or "WIMPs") as constituents of the Dark Matter in the Universe.

3.4 Collider Experiments, Direct and Indirect Searches for Dark Matter

The evident presence of large quantities of (at most) weakly interacting Dark Matter in the Cosmos leads to the question of the physical identification of its constituents. Since there are no stable and neutral standard model particles in the relevant mass range for WIMPs, some sort or another of beyond standard model physics would have to provide for the existence of the WIMPs.

An obvious possibility to search for this physics would be collider experiments like LEP [40], Tevatron [41] and LHC [42]. In the collision of standard model particles at center of mass energies »GeV, WIMPs (along with other potentially charged or unstable beyond standard model particles) could be produced. For the neutral and stable WIMPs, it should be noted that their actual detection would be non-trivial, since after their production in the collisions, the vast majority of them could cross the detector without interaction. However, with the detector being calorimetric, and the energies of the colliding particles known, it is still possible to search for the missing transversal energy carried away by the WIMPs.

A potentially more promising strategy for collider experiments is however the search for either direct signatures of charged particles, or for the decay products of short lived particles, within a certain framework of beyond standard model physics that also includes WIMP candidates (e.g. Supersymmetry). At the time of this writing, searches are ongoing, with most efforts centered on the LHC experiments at CERN. As an example for the status of constraining supersymmetric models via collider experiments, confer Fig. 11 and [43].

In case of a positive detection of either a Dark Matter candidate particle at these collider experiments, or of the confirmation of a beyond standard model physics scenario containing a yet-undetected WIMP candidate, the question would still remain whether the Dark Matter in the Universe really is made of this specific particle. To answer this question, various methods to search for Dark Matter in astrophysical objects can be employed.

At the location of the solar system in the Galaxy, the average Dark Matter density is $0.3 \pm 0.1 GeV/cm^3$ [44]. The solar system movement along the Sun's orbit around the center of the Milky Way leads to a flux of Dark Matter particles through the Earth, and any laboratory apparatus. In principle, it is possible to directly search for scattering
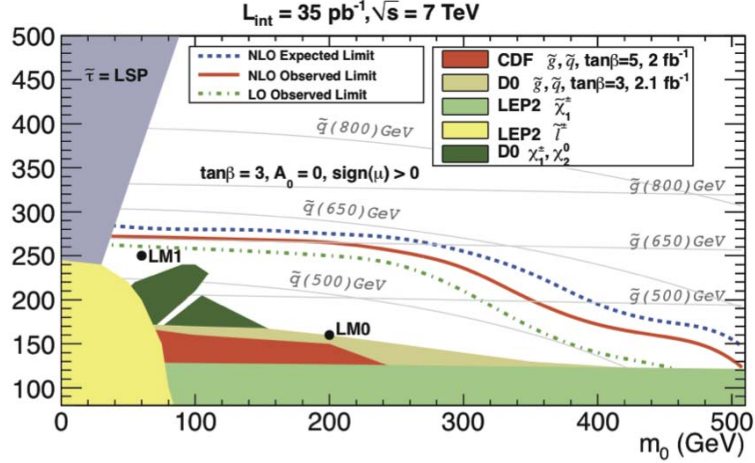
Figure 11: Exclusion limits plotted in the plane of the unified gaugino mass vs. unified scalar mass parameters in the framework of supersymmetry. Included data are from searches for missing transversal energy and also other channels from LHC and various other collider experiments. Image Credit: CMS Collaboration, 2011 [43].

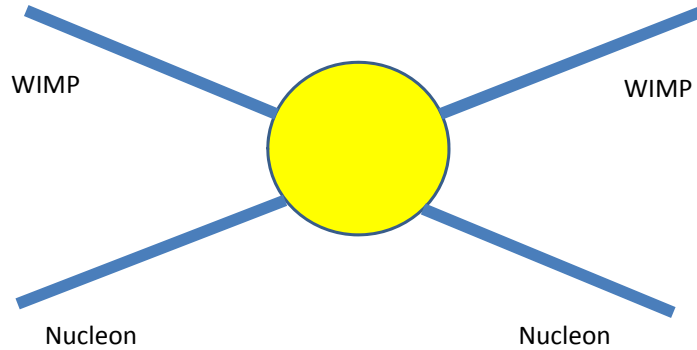events between nuclei and those Dark Matter particles (see Fig. 12).

Figure 12: Process of elastic scattering between WIMP and nucleon.

Typical velocities of thermal WIMPs in the halo of the Galaxy depend on the halo model adopted for the Milky Way, but generally peak around 300km/s [45] (confer also the orbital velocity of the Sun in the Galaxy of $\approx 225km/s$). Superimposed onto this is the orbit of the Earth around the Sun, annually modulating the resulting velocity of this "WIMP wind" by 29.8km/s.
Elastic scattering searches make use of the deposited energy via the resulting heating of

the absorber material, ionization or emission of photons. Often, a combination of more than one channel is used to improve background rejection (see Fig. 13).
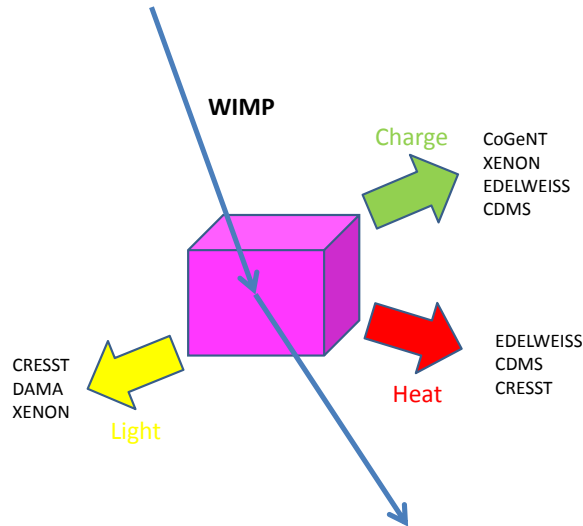
Figure 13: Different detection channels for experiments to search for elastic WIMP-nucleon scattering events. Provided is also a list of contemporary experiments and the respective channels employed.

It has to be stressed that there are considerable experimental obstacles to be overcome in with respect to background suppression in these experiments (see [46] for an overview of current experimental efforts). The detectors have to be placed in deep underground laboratories to shield them against energy deposition by the Cosmic Ray flux. Extensive shielding against ambient radioactivity, and meticulous isotope cleaning for all parts of the detector has to be performed. There have been various hints in data from several experiments of events that could possibly be attributed to WIMPs [47–50]. In the cases of DAMA and CoGeNT, observation of an annual modulation due to the different effective velocities of the WIMPs because of the orbital motion of the Earth has been claimed. However, it has to be noted that at the moment, the various hints do not seem to be obviously compatible with each other (see Fig. 14), and also upper limits from other experiments [46]. There have been proposals that some of the results could be reconciled by considering spin dependent interactions with the different absorber materials [51]. Up to now, consensus has however not been reached. There have been proposals to construct directionally sensitive detectors, which would drastically reduce experimental uncertainties [52].
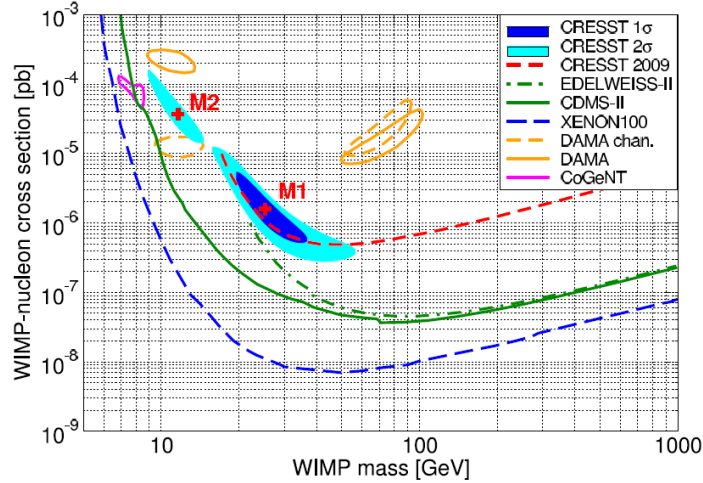
Figure 14: Exclusion limits / confidence contours for upper limits and claimed signals from various elastic scattering experiments. Plotted is spin-independent cross section vs. WIMP mass. Image Credit: G. Angloher et al., 2011 [50].

A very relevant cross-correspondence between these direct detection efforts described above, and indirect searches for standard model decay or annihilation products of WIMPs should be noted: In the (likely) case of a not completely homogeneous distribution of the Dark Matter particles within the halo of the Milky Way, because of the expected Press-Schechter like mass function (cut off at some yet to be determined small mass scale) of substructure in the Dark Matter, the volume filling factor for these substructure clumps would inevitably be quite low. It is then likely, that at any given point in time, a direct Dark Matter detection experiment would find itself within an underdense region, compared to the generally assumed $0.3 GeV/cm^3$. Event rates scaling linearily with the Dark Matter particle density, this means that the more substructure forms and survives within the Dark Matter halo, the lower the detection prospects with direct searches become, from a purely statistical viewpoint (small chances of the solar system actually crossing such a subclump with drastically enhanced density at this moment in time notwithstanding, of course). For indirect detection efforts, in many cases the inverse is true: Since the efficiency of annihilation will scale quadratically, not linearily, with the Dark Matter density, rates and therefore detection prospects can be boosted considerably by the existence of substructure, making direct and indirect efforts complemental.

Indirect search efforts rely on the detectability of standard model products - photons, neutrinos/antineutrinos, electrons/positrons and protons/antiprotons of the annihilation or decay of Dark Matter particles.

Since Dark Matter has to be presumed to be stable over cosmological timescales (otherwise the Dark Matter energy density would have decreased already drastically), the

most relevant channel is WIMP annihilation (Fig. 15). Astrophysical detection e.g. of a gamma ray line from

$$\chi\chi \to \gamma\gamma \tag{18}$$

or

$$\chi\chi \to Z^0\gamma \tag{19}$$
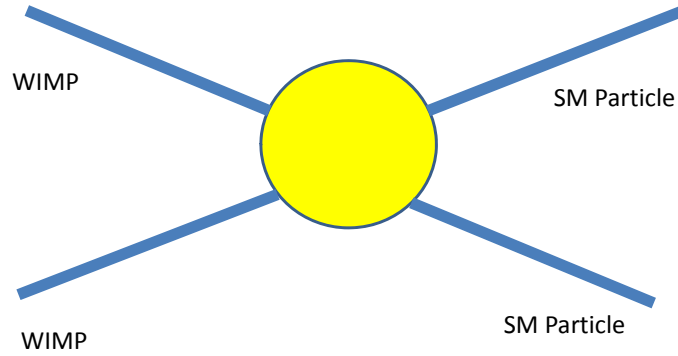
Figure 15: WIMP annihilation.

with resulting gamma ray energies far beyond the proton mass would obviously be a clear indication of detection of a new particle. However, since the Dark Matter particle cannot have electromagnetic interaction and thereby couple to the photon on tree level, fluxes from these processes will only result from loop level interactions, and therefor be strongly suppressed.

The most promising channels rather seem to arise from jet fragmentation and hadronization, with subsequent production and decay of pions:

$$\chi\chi \to (...) \to \pi^+,\, \pi^-,\, \pi^0 \to leptons, neutrinos, gammas. \tag{20}$$

This processes will result in spectra not as conspicuous as a sharp line, but rather following the decay spectra of the pions, exhibiting a maximum at roughly $m_\chi/20$, as simple analysis of the multiplicities in above processes reveals.

Still, these spectra are distinct from the power-law like spectra owing to acceleration processes often encountered in astrophysical high-energy sources, lending themselves in principle to efforts of indirect Dark Matter detection.

The annihilation isotropic and bolometric flux from a unit volume within a sufficiently large volume containing a number density of WIMPs n_χ will scale as

$$F_{ann.} \propto n_\chi^2 \times <\sigma v> \times N_{SM}, \tag{21}$$

with N_{SM} being the number of standard model particles in the respective channel produced per annihilation event.

Note that here the assumption is made that the WIMPs are Majorana particles, i.e. their own antiparticles, as is the case in many concrete models discussed later on.

For a gamma-ray detector, the flux from an annihilation source at distance r will then be

$$F_\gamma = \frac{1}{4\pi \, r^2} \times <\sigma v> \times N_\gamma \times \int_{l.o.s.} n_\chi^2 \, ds, \tag{22}$$

with $\int_{l.o.s.} n_\chi^2 \, ds$ being the integral along the line of sight over the field of view of the respective detector. It is often instructive to factor out the particle mass m_χ:

$$F_y = \frac{1}{4\pi \, r^2} \times \frac{<\sigma v>}{m_\chi^2} \times N_\gamma \times \int_{l.o.s.} \rho_\chi^2 \, ds, \tag{23}$$

with ρ being the Dark Matter density. This way, the equation consists of one part in which the particle physics setup is encoded:

$$\frac{<\sigma v>}{m_\chi^2} \times N_\gamma, \tag{24}$$

and a second part which contains the astrophysical properties of the studied Dark Matter halo:

$$\int_{l.o.s.} \rho_\chi^2 \, ds. \tag{25}$$

The presence of substructure might enhance the flux, which then could be accounted for by including factors.

For the case of the detection of charged annihilation products like electrons/positrons or protons/antiprotons, the transport and energy losses of these particles have to be considered. The magnetic fields in the galaxy will isotropize the particles on comparatively small scales, while the transport can in general be described by a transport equation [53] of the form:

$$\frac{\partial \phi}{\partial t} - K(x, E)\nabla^2 \phi - \frac{\partial}{\partial E}[b(E)\phi] = q(x, E), \tag{26}$$

where q(x,E) is the charged particle source term, and ϕ their number density per energy.

Energy loss mechanisms can be grouped into two classes:

The turbulent diffusive energy loss is parameterized by

$$K(x, E) = K_0 \epsilon^\delta, \tag{27}$$

with

$$\epsilon = \frac{E}{E_0}. \tag{28}$$

The energy losses due to radiative processes b(E) mainly consist of inverse Compton losses due to up scattering of CMB and starlight photons, and synchrotron radiation in the microgauss magnetic field of the Galaxy:

$$b(E) = b_{IC}(E) + b_{syn.}(E, B). \tag{29}$$

For a given radiation field (predominantly starlight or the CMB)the inverse Compton losses can be parameterized with

$$b_{IC}(E) \propto \frac{E_0 \epsilon^2}{\tau_E}, \tag{30}$$

with typical lifetimes approaching 10^{16}s.

The synchrotron losses are described by

$$b_{syn.}(E, B) = \frac{2e^4 B^2}{3m^4 c^8} E^2. \tag{31}$$

While in principle, this type of equation is analytically solvable, it can be more straightforward to implement the transport and energy losses along with the assumed configuration of the magnetic- and radiation fields into a numerical code, e.g. [54].

Incidentally, in the Galaxy, there is nearly equipartition between the energy densities of the CMB, starlight, and the interstellar magnetic field, since

$$\frac{P_{IC}}{P_{syn.}} = \frac{U_{rad.}}{U_B}. \tag{32}$$

The radiative losses of the leptons from Dark Matter annihilation will lead to in principle detectable photon fluxes, in addition to the gamma rays from the π^0-decay. While the energy of the bump from the π^0-decay will scale linearily with the WIMP mass, the location of the maxima from IC and synchrotron losses during the propagation of the charged particles scales with γ^2. Detection of such a "multi-bump" annihilation spectrum, with the IC bump in the X-rays, and the synchrotron bump in the radio/microwave regime would go a long way in identifying Dark Matter [55].

Searches for neutrinos from Dark Matter annihilation represent a distinct case. In general, the energy and intensity of the neutrinos will be comparable to those of the photons from the π^0-decay. From a source at astronomical distances, the resulting mixture between neutrino flavors at Earth will be 1:1:1. At typical (GeV-)energies, fluxes at a neutrino detector will be overwhelmed by atmospheric neutrinos. This could be remedied if a feasible concept for a flavor sensitive neutrino detector was put forward, to discriminate the tau neutrinos against the atmospheric background.

There is, however, another possibility, in which neutrino fluxes could be much higher

than those of distant sources: Via scattering from nucleons, WIMPs can occasionally be captured in the gravitational potential of the Sun, Earth or Moon. Once in a bound orbit, multiple subsequent scatterings can occur while the WIMP repeatedly crosses the body of the Sun or planet, with the result of the WIMP settling down at the center of the mass on relatively short timescales, leading to a drastical enrichment of the core with WIMPs (see Fig. 16).

Annihilation of WIMPs can then occur efficiently, with only neutrinos of all annihilation
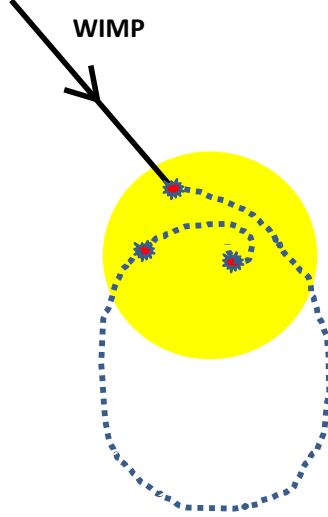
Figure 16: WIMP capture into the Sun.

products being able to leave the core, and result in a detectable signal in neutrino telescopes.

The change of the total number N of WIMPs in the core of the Sun will then be given by [56]

$$\frac{d}{dt}N = C^\odot - A^\odot N^2, \tag{33}$$

where $C^\odot$ is the rate of WIMP capture, depending on the elastic scattering cross section of the WIMPs, the local WIMP density and velocity distribution, and the properties of the Sun, and $A^\odot$ is given by

$$A^\odot = \frac{<\sigma v>}{V_{core}}. \tag{34}$$

V_{core} is the effective volume of the core of the Sun, characterized by the boundary where the core temperature equals the gravitational binding energy of a WIMP at the radius of the core.

The present-day WIMP annihilation rate is then

$$\Gamma = \frac{1}{2}A^\odot N^2 = \frac{1}{2}C^\odot tanh^2(\sqrt{A^\odot C^\odot}t_\odot), \tag{35}$$

with the age of the Sun $t_{\odot}$ being ≈ 4.6 gigayears.

The maximum rate of annihilations, and thereby the largest prospects for detection of those neutrino fluxes at a neutrino telescope, will result for

$$\sqrt{A^{\odot}C^{\odot}}t_{\odot} >> 1, \tag{36}$$

a condition that is reached within the age of the solar system for the Sun, but not for the Earth, due to the much smaller amount of scattering targets in the Earth, and the less deep potential well this much smaller mass provides [56]. Therefore, the Sun is the most promising target for Dark Matter searches with neutrino telescopes. Valuable limits have already been derived (see Fig. 17 and [57]).
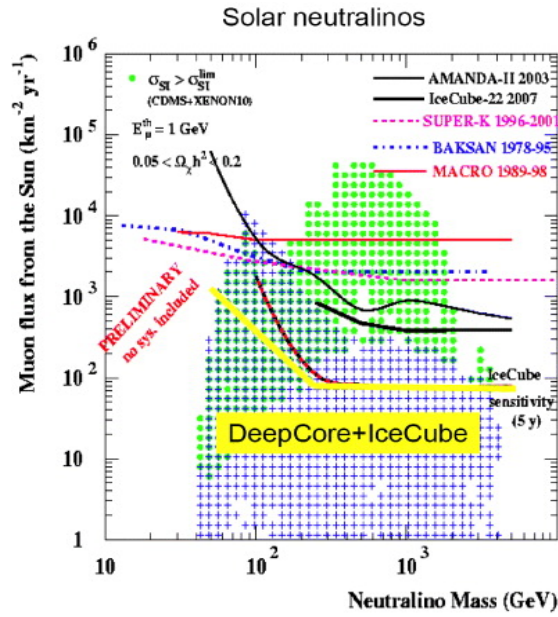
Figure 17: Limits on the muon flux in different neutrino detectors from neutrinos produced by WIMP annihilations in the Sun. Shaded regions denote supersymmetric models where the lightest neutralino is a WIMP candidate particle and is produced thermally in the Big Bang in cosmologically relevant quantities. Image Credit: Halzen and Hooper, 2009 [57].

It should be noted that, due to the capture rate being dependent from the elastic scattering cross section and local Dark Matter density, akin to laboratory elastic scattering searches, but the production rate of neutrinos also being governed by the annihilation cross section, this provides for a unique tool to explore the WIMP parameter space due to this cross-combination of dependencies.

It is furthermore possible to constrain the presence of Dark Matter in the core of the Sun via searching for its effect on the heat transport in the Sun by means of helioseismology [58].

4 Dark Matter Candidates

4.1 MACHOs and Constraints from Microlensing

Accepting the observational and phenomenological evidence for the existence of Dark Matter, the task of identifying it with a concrete class of objects or particles arises. It had long been thought that the Dark Matter could consist of large numbers of cold astrophysical objects like isolated planetary bodies, brown dwarfs, very low mass M dwarfs, cooled down white dwarfs or neutron stars, or even black holes. Such objects have often been termed "Massive Astrophysical Compact Halo Objects" or MACHOs. Those MACHOs could populate the halos of the galaxies. However, even at very low temperatures, the would of course not be completely dark, but exhibit thermal emission, the sum signal of which would show up at some point in sensitive measurements of cosmic radiation backgrounds. Also, if they Dark Matter would consist of such objects, this would mean that within the present age of the Universe, more than 80% of all matter would already have undergone gravitational collapse of one type or another (formation of stars or planets, or direct formation of black holes), in obvious conflict with the well-established paradigm of structure formation.

The most stringent constraints on MACHOs come from searches for microlensing events: Statistically, such objects would sometimes pass in front of background stars, and the gravitational lensing effect would then imprint an achromatic variation onto the brightness of the background star, easily discernible from intrinsic stellar brightness variations (which typically show considerable frequency dependence).

Searches for these kinds of lensing events have been undertaken, e.g. in the field of the Large Magellanic Cloud, which acted as a large ensemble of background stars prone to lensing by potential MACHOs in the halo of the Milky Way.

While lensing events have in fact been found these surveys, their frequency and geometric characteristics actually refute the hypothesis that most or all of the Dark Matter in the halo consists of such objects [59]. Rather, the lens population seems to consist mostly of low mass stars.

There exists also the possibility that the Magellanic Stream does not only contain gas as tidal debris, but also a low mass stellar population, which would bias the count of lensing events in the chosen search fields towards higher numbers, therefore overestimating the lens population in the halo of the Galaxy.

In turn, this results strongly encourage an identification of the missing mass with a yet unidentified particle, or several particles.

4.2 WIMPs

As outlined in the previous section, there is strong phenomenological motivation for the Dark Matter consisting of particles that have electroweak-scale masses and weak interactions. For these WIMPs, there are a number of promising candidates from particle physics scenarios beyond the standard model.

4.2.1 Supersymmetry

One of the most prolific of these scenarios is supersymmetry ("SUSY"). Supersymmetry is a symmetry between fermions and bosons, relating particles with integer and half integer spin:

$$Q|Fermion >= |Boson > \tag{37}$$

and

$$Q|Boson >= |Fermion > . \tag{38}$$

In 1974, Wess and Zumino [60] showed that such a supersymmetric quantum field theory, containing fermionic generators obeying anti-commutation relations besides the usual bosonic Lie algebra generators can provide a way to circumvent the Coleman-Mandula theorem [61]. this result sparked a great deal of research interest, continuing to the present day.

Apart from being a fundamentally allowed symmetry of Nature, therefore raising the question whether the supersymmetry is actually realized in our Universe, supersymmetric extensions of the standard model of particle physics potentially offer substantial phenomenological benefits: in the standard model, the renormalizations of the Higgs mass squared are quadratically divergent, baring cancellations making the Higgs mass the highest natural scale possible. This has often been termed the "hierarchy problem". The addition of the superpartners however leads to additional contributions, canceling this corrections (for an illustrative example, see Fig. 18).

Another asset of supersymmetry is that the running gauge coupling constants do not quite meet at a common energy scale in the standard model, while minimal supersymmetric extensions of the standard model can provide for unification [62] at an energy scale of

$$\Lambda_{GUT} \approx 10^{16} GeV. \tag{39}$$

While of course unification of the forces is not mandatorily inherent in Nature, the features mentioned above lead to supersymmetry being an integral part of many extensions of the standard model.

Since there are no suitable superpartners for the standard model particles among the particle inventory of the standard model itself, this leads to the prediction of additional particles. Up to now, none of this "superpartners" have been found experimentally.

The natural solution to the hierarchy problem inherent to SUSY can however be salvaged even if supersymmetry is a broken symmetry at scales below $\mathcal{O}(TeV)$.

"Soft" SUSY breaking scenarios have been put forward [63], which allow for SUSY being a broken symmetry, to reconcile with observational facts, while at the same time avoiding the appearance of ultraviolet divergences in scalar masses. Supersymmetry breaking can therefore allow for masses of the superpartners far above standard model particle masses.

There is an additional problem that needs to be tackled: In supersymmetric extensions
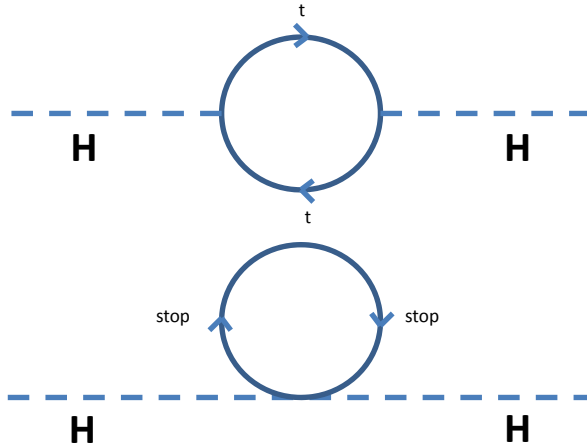
Figure 18: Canceling of fermionic top loop and scalar stop tadpole in supersymmetric extensions of the particle physics standard model.

of the standard model, baryon- and lepton numbers are not conserved for all renormalizable couplings. This is obviously in conflict e.g. with the apparent stability of the proton over at least many times the age of the Universe. Therefore, a "R-parity" forbidding these couplings is introduced:

$$P_R = (-1)^{2s+3B+L}, \tag{40}$$

with s being spin, B the baryon-, and L the lepton-number.

A viable supersymmetric extension of the standard model, which includes soft SUSY breaking and R-parity is the Minimal Supersymmetric Standard Model ("MSSM"), also first proposed in [63].

Natural generation of the soft SUSY breaking terms by a "super Higgs mechanism" (with gravity mediating the breaking through existence of a hidden sector) has been shown to lead to interesting low energy phenomenology while needing only four input parameters and a sign:

- the gaugino mass parameter $m_{1/2}$

- the scalar mass parameter m_0

- the soft breaking trilinear coupling constant A_0

- the ratio of the vacuum expectation values of the Higgs bosons $tan\beta$

- and the sign of the Higgsino mass parameter

at the GUT scale. This class of models is known as minimal supergravity or "mSugra", and has been thoroughly investigated [64].

For the context of this work, the prediction of new particles with masses of order of the electroweak scale, of which the lightest one would have to be stable over cosmological timescales due to R-parity, makes supersymmetry a highly relevant framework, providing candidate WIMPs.

The superpartners of the neutral Higgs, of the photon, and of the W have identical quantum numbers, and can therefore mix to form four mass eigenstates [65]. Interestingly, in many supersymmetric models, one these electrically neutral "neutralinos"

$$\chi_i^0 = N_{i1}\tilde{B} + N_{i2}\tilde{W} + N_{i3}\tilde{H}_1^0 + N_{i4}\tilde{H}_2^0 \tag{41}$$

is the lightest superpartner ("LSP").

This way, supersymmetry provides for a quite natural WIMP candidate.
The properties of the neutralino WIMPs in specific supersymmetric models, and their ensuing relic density from freeze-out, including loop corrections and the effects of co-annihilations, can readily be calculated by numerical codes like DarkSUSY ([66], and $http://www.physto.se/\tilde{e}dsjo/darksusy/$) and Micromegas ([67] and $http://lapth.in2p3.fr/micromegas/$), and the resulting models checked against a database of up to date constraints from elastic scattering and collider searches, as well as against constraints on the Dark Matter relic density from cosmology. Production of models is done by randomly generating input parameters, and then checking the output parameters for physicality and against violation of experimental constraints, rather than restricting the input parameter space. While this approach of course statistically produces a very large amount of models that are not viable and have to be discarded, it is still sound since output data volumes are very small in all cases, and on the other hand there are not compelling experimental constraints onto all input parameters.

It should be noted that some alternative scenarios for supersymmetry breaking, like the anomaly mediated supersymmetry breaking ("AMSB"), where supersymmetry breaking is communicated via a conformal anomaly, can also provide the cosmologically correct amount of Dark Matter, while allowing for very high annihilation cross sections [68].

4.2.2 Neutralino Model Database

In this work, a large database of 10^5 neutralino models, that are cosmologically valid, meaning they thermally reproduce within a factor of 2 the WMAP 7-year best fit Dark Matter relic density of $\Omega_{DM}h^2 = 0.1123 \pm 0.0035$ with the dimensionless Hubble parameter $h = 0.705 \pm 0.013$ [21], MSSM neutralino models has been calculated using the DarkSUSY 5 code. All these models were checked against up to date collider constraints on SUSY discovery [43]. Also, it is of course checked whether a neutralino is in fact the

LSP in the respective model.

For a scatter plot of neutralino mass versus $<\sigma v>$ of these models, see Fig. 19.
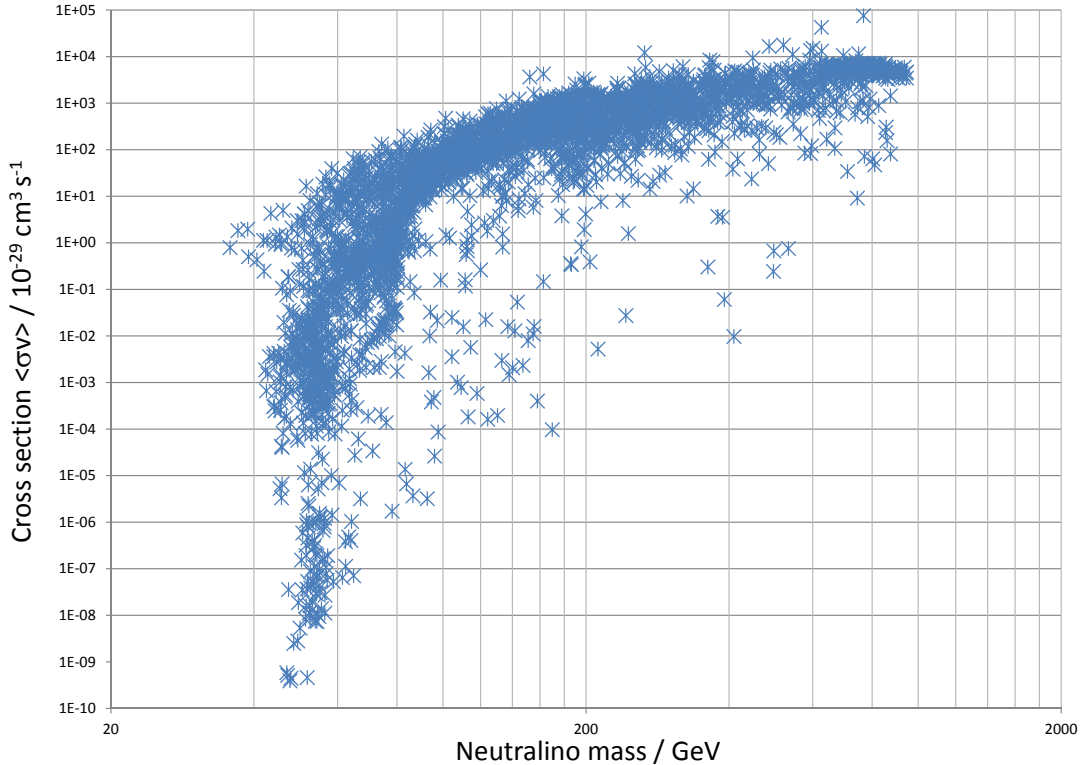
Figure 19: Scatter plot of neutralino mass in GeV versus $<\sigma v>$ in units of $10^{-29} cm^3 s^{-1}$ for the Wuerzburg model database. Obviously, there is considerable scatter even among experimentally and cosmologically valid models.

For each of these models, input parameters as well as resulting particle masses and cross sections have been saved as well to the database. Also, the total number of photons above 100GeV, and photon numbers for energy bins of width 100GeV per annihilation event have been computed using tables generated with the PYTHIA 8 code ([69] and $http : //home.thep.lu.se/torbjorn/Pythia.html$). Note that this spacing is rather coarse, but still sufficient to interpret observations in light of the limited energy resolution of VHE gamma ray telescopes.

4.3 Candidates from Extra Dimensions

While supersymmetric WIMPs certainly are among the most natural candidates, the astrophysical evidence for particle Dark Matter is in this regard not exclusive.

For example, already 90 years ago it was proposed [70,71] that particles could propagate

in "extra" spacetime dimensions, resulting in an infinite "tower" of states with identical quantum numbers.

In the case of Universal Extra Dimensions [72], where all standard model particles propagate, concrete candidates can be identified in the form of so-called Kaluza Klein particles, which in terms of thermal production at the required relic density have analogous properties compared to SUSY WIMPs [73]. Although the first Kaluza-Klein excitation of the hypercharge gauge boson (the B^1) is the best studied case, there also exist other candidates like the KK-excitation of the neutral SU(2) gauge boson [74, 75].
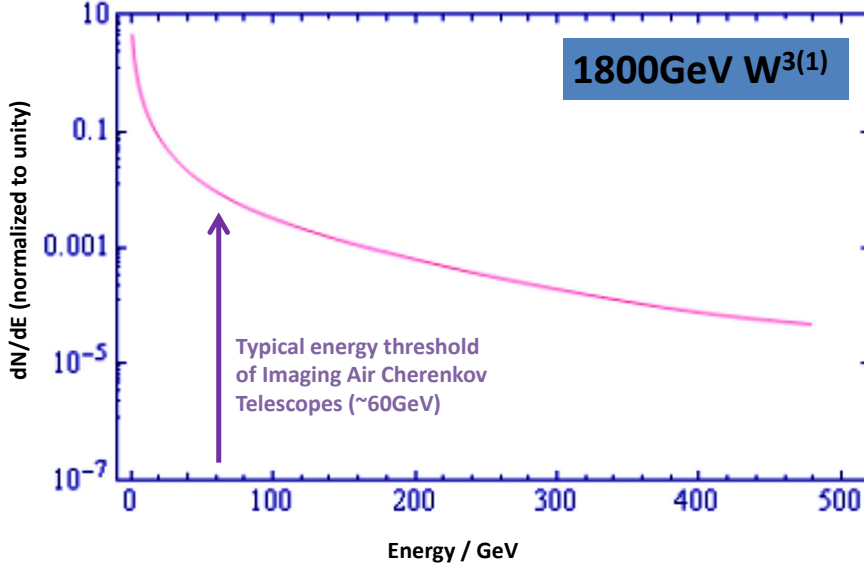
Figure 20: Differential spectrum of photons produced in the annihilation of $W^{3(1)}$ KK-WIMPs with a mass of 1800 GeV. Significant portion of flux above typical IACT energy thresholds of $\approx 60\ GeV$. Niederhausen, Elsässer and Flacke, in prep. ([76]).

Such KK-WIMPs can provide for annihilation spectra accessible to ground based gamma ray telescopes, warranting further studies. (Fig. 20).

4.4 Other Candidates – Axions, WIMPzillas and Sterile Neutrinos

Apart from this WIMP candidates, there are also other possible particle Dark Matter candidates.

Quantum Chromo Dynamics predicts an electrical dipole moment of the neutron of order $d_n \approx 10^{-16} e \times cm$. Experimental limits however are some 9 orders of magnitude more stringent: $d_{n,exp.} \leq 10^{-25} c \times cm$ [77].

To solve this "strong CP problem", it was proposed to introduce a new, spontaneously broken global symmetry into the standard model, the Peccei-Quinn Symmetry.

From the breaking of this symmetry, a new particle ensues - the axion [78, 79].

Axions could be produced in the early Universe at the QCD phase transition in the form of a Bose-Einstein-condensate, or through the decay of strings produced at the Peccei-Quinn phase transition. they therefore would behave as cold Dark Matter, in accordance with astrophysical observations [77].

To avoid violating bounds for the energy loss of stars and during Supernova 1987A from axion production, the axion mass has to be smaller than $10^{-2} eV$, while overproduction of the observed Dark Matter density would occur for axion masses smaller than $\approx \mu eV$ [80].

Experimental searches for axions are undertaken exploiting the interconversion of axions and photons in an exterior magnetic field (Primakoff-effect) [81, 82], either with the Sun or an intense laboratory light source providing the photons.

While considerable progress has been made in excluding parts of the parameter space, no decisive result on the existence of axion Dark Matter could yet be put forward (see Fig. 21).

It is also possible to search for axions using polarized light from distant astrophysical sources, and exploiting the effect that photon-axion interconversion in cosmic magnetic fields would have on the polarization of this sources [85].

There are also ways in which the seemingly rather stringent bounds from the observed relic density onto very massive and weakly interacting particles can be circumvented: if very massive WIMPs were created at very early times, at temperature T_* and with a relic density smaller than $\Omega_{WIMPZILLA} \approx 1$, it can be shown [86] that they never attain equilibrium if

$$\frac{200 TeV}{M_{WIMPZILLA}}^2 \times \frac{T_*}{M_{WIMPZILLA}} < 1. \tag{42}$$

Such "WIMPzillas", with masses of the order of the GUT scale or even higher, could thus populate the Universe in cosmologically relevant quantities. Any detection efforts, however, would be rendered exceedingly challenging by the comparatively extremely small number densities implied by the high masses.

Another class of particles motivated by theory are the sterile neutrinos, implied by the seesaw mechanism [87]. In principle, it would be possible to search for sterile neu-
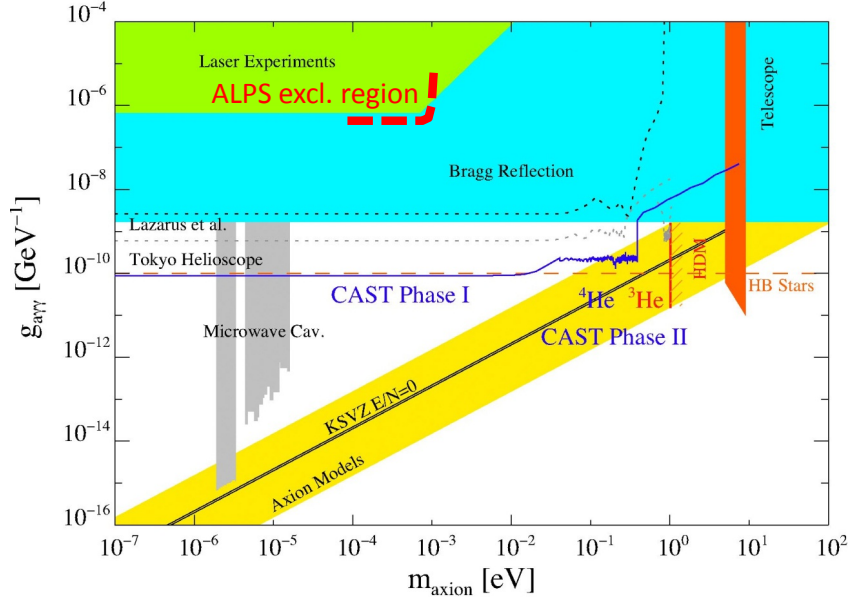
Figure 21: Experimental and observational exclusion regions for axions, using data from different experiments, in the plane of coupling to the photon versus axion mass. Underlying plot from [83], exclusion region for ALPS 2009 from [84] added by D. Elsässer.

trinos not only via collider experiments, but also via detection of X-ray photons from their decays in astrophysical objects, if they were the Dark Matter constituent particle. Some limits for individual objects have been placed [88], and there are ongoing efforts to exploit archival data from the ROSAT mission [89] for an allsky-search by A. Gewering-Peine and J. Schmitt (from Hamburger Sternwarte), and the author of this work.

5 Astrophysical Distribution of Dark Matter

5.1 Basics and Isothermal Approximation

After decoupling of the particle Dark Matter in the early Universe, structure formation via gravitational interaction can begin.

As has been outlined in Section 3, the mass function of collapsed Dark Matter halos will follow a Press-Schechter function [36]

$$N(M)dM = \frac{1}{2\sqrt{\pi}}(1 + \frac{n}{3})(\frac{\overline{\rho}}{M^2})(\frac{M}{M^*})^{\frac{3+n}{6}} \times e^{-(\frac{M}{M^*})^{3+n/3}}, \tag{43}$$

with M being the mass of the halo, M^* some to be determined critical mass scale, $\overline{\rho}$ the mean matter density of the Universe, and n the index of the fluctuation power spectrum $(P(k) \propto k^n)$.

Observationally, this means that there is some maximum mass scale, and a power-law like behavior for lower masses. The total number of overdensities is determined by a presumed low mass cut off of this function. This plays an important role for indirect Dark Matter searches.

For the internal density profile of Dark Matter halos, a natural first approximation would be the formation of a virialized, quasi-isothermal sphere, truncated to a core of quasi-constant density, as proposed already by [12]:

$$\rho(R) = \frac{\rho_0}{1 + (\frac{R}{R_c})^2}. \tag{44}$$

Here, only to parameters, the density ρ_0 and radius R_c of a constant density core have to be chosen, in order to make the enclosed mass and central density finite and thereby physical.

The orbital velocity at radius R can then simply be deduced by employing

$$V(R) = \sqrt{\frac{GM(R)}{R}} \tag{45}$$

which yields

$$V(R) = \sqrt{4\pi G \rho_0 R_c^2 (1 - \frac{R}{R_c} arctan) \frac{R}{R_c}}. \tag{46}$$

The velocity at infinity evaluates to

$$V_\infty = \sqrt{4\pi G \rho_0 R_c^2}. \tag{47}$$

While this description thus seems a viable approximation, the exact choice of the parameters R_c and ρ_0 for the constant density core can not easily be motivated.

5.2 Numerical Experiments

Substantial progress for modeling Dark Matter halos has been made with the introduction of numerical codes and high-performance computing. These facilitated the numerical solution of the N-body problem at scales and resolution / test particle numbers sufficient for modeling the process of structure formation.

In 1996, it was shown [90] that a mean overdensity of

$$< \overline{\rho} > \approx 200 \, \rho_{crit.}(z), \tag{48}$$

with the density of the critical Einstein-deSitter-Universe

$$\rho_{crit.}(z) = \frac{3H(z)^2}{8\pi G}, \tag{49}$$

is the discriminator between infall and virialized regions in a halo. This radius is commonly termed R_{200}.

The enclosed mass then is

$$M = \frac{4\pi}{3} R_{200}^3 \times 200 \rho_{crit.}(z), \tag{50}$$

or, using the definition of $\rho_{crit.}$ given above:

$$M = \frac{100 R_{200}^3 H(z)^2}{G}. \tag{51}$$

Again using the velocity for a circular orbit

$$V_{200} = \sqrt{\frac{GM}{R_{200}}}, \tag{52}$$

we obtain

$$M = \frac{V_{200}^3}{10GH(z)} \tag{53}$$

and

$$R_{200} = \frac{V_{200}}{10H(z)}. \tag{54}$$

In ΛCDM cosmology for large z holds:

$$H(z) > H_0. \tag{55}$$

Thus, at a given mass scale, halos that collapsed at higher redshift have a higher degree of compactness.

In case of hierarchical structure formation, in which halos of lower mass collapse at higher z, this generally means that lower mass halos have higher concentrations than those of higher masses. A result which will be relevant regarding the contribution to any annihilation signal from surviving lower mass halos within a larger one.

The simulations made it also possible to study the properties and density profiles of the halos they produced, in some respects performing a "numerical experiment".

Although results vary considerably, dependent from the exact numerical approach used, the simulated halos tend to form density profiles which can be described as [91]

$$\rho(r) = \frac{\rho_0}{\frac{R}{R_s}(1 + \frac{R}{R_s})^2}. \tag{56}$$

The parameters R_s (the "scale radius") and ρ_0 depend on halo size and formation epoch.
In literature, this class of profile is generally termed a "Navarro-Frenk-White" (NFW-) profile.
It is possible to link the scale radius to the virial radius through

$$R_s = \frac{R_{200}}{c}, \tag{57}$$

where c is a dimensionless parameter, encoding the redshift-dependent compactness as outlined above.

The total enclosed mass inside the virial radius then becomes finite:

$$M = \int_0^{R_{200}} = 4\pi R^2 \rho(R) dR. \tag{58}$$

Again using the concentration parameter c:

$$M = 4\pi \rho_0 R_s^3 (ln(1 + c) - \frac{c}{1 + c}). \tag{59}$$

While there was considerable debate about the validity of these type of profile in the past [92], it became more and more clear that it offers indeed a workable description of many types of Dark Matter halo [93].

It has however to be recognized that there are severe limitations, part of them imposed by computational resources (limiting e.g. the resolution), part of them however probably inherent:

- While it is possible to simulate spherically symmetric, as well as tri-axial halos, the global shape of real halos especially for spiral galaxies is not readily observable, due to lack of baryonic tracers far away from the disc

- While the Dark Matter potential wells facilitate the collapse of baryons early in the history of the Universe, later on, and especially for regions of high baryonic matter density, baryons may modify the Dark Matter halo, e.g. contract the inner slope of the profile [94]

- Even large computational resources limit the available numerical resolution to scales of order 10^5 solar masses, if consistent simulation of large (host-) halo is desired. This does not correspond to any possible physical lower mass cut off of the Press-Schechter function

- Even at the lowest mass scales not yet numerically compromised in the simulations, results seem to predict an excess in small scale power, compared with observations ("missing satellite problem"). For example, simulations predict up to 500 dwarf galaxy sized halos orbiting the Milky Way [95], while actual observations turn up ten times less objects. It is presently unclear whether more sensitive observations will remedy this discrepancy (by detecting more dwarfs)

There have also been long standing proposals for other types of profiles, like the Einasto class of profile [96]

$$\rho(r) \propto e^{-A\,R^{\alpha}}, \tag{60}$$

where A is a constant parameter, and α describes the curvature of the slope. Interestingly, this type of profile can be shown to be in satisfactory agreement with a substantial range of observations [97].

For the purpose of Dark Matter searches, because of the scaling of the annihilation intensities, the integral over the square of the density of a given profile is the quantity that directly enters the limits deduced here. For the NFW-profile, this evaluates to

$$\int_0^{R_{out}} 4\pi R^2 \rho(R)^2 dR = \frac{4}{3}\pi R_s^3 \rho_0^2 (1 - \frac{R_s^3}{(R_s + R_{out})^3}), \tag{61}$$

where the outer radius R_{out} is chosen by observed (or assumed) extend of the halo as relevant to the specific observation carried out.

For the purpose of deducing limits from the cluster observations reported in this work, numerical simulations of cluster-sized halos were carried out using the Adaptive Refinement Tree code. This code is a N-body algorithm employing particle-mesh techniques on a cubic grid, and recursive relaxations of the meshes [98].

Fig. 22 shows a snapshot out of one of this simulations, the central region of a cluster with a mass of $3 \times 10^{14} M_\odot$, and resolved substructure down to $3 \times 10^7 M_\odot$.
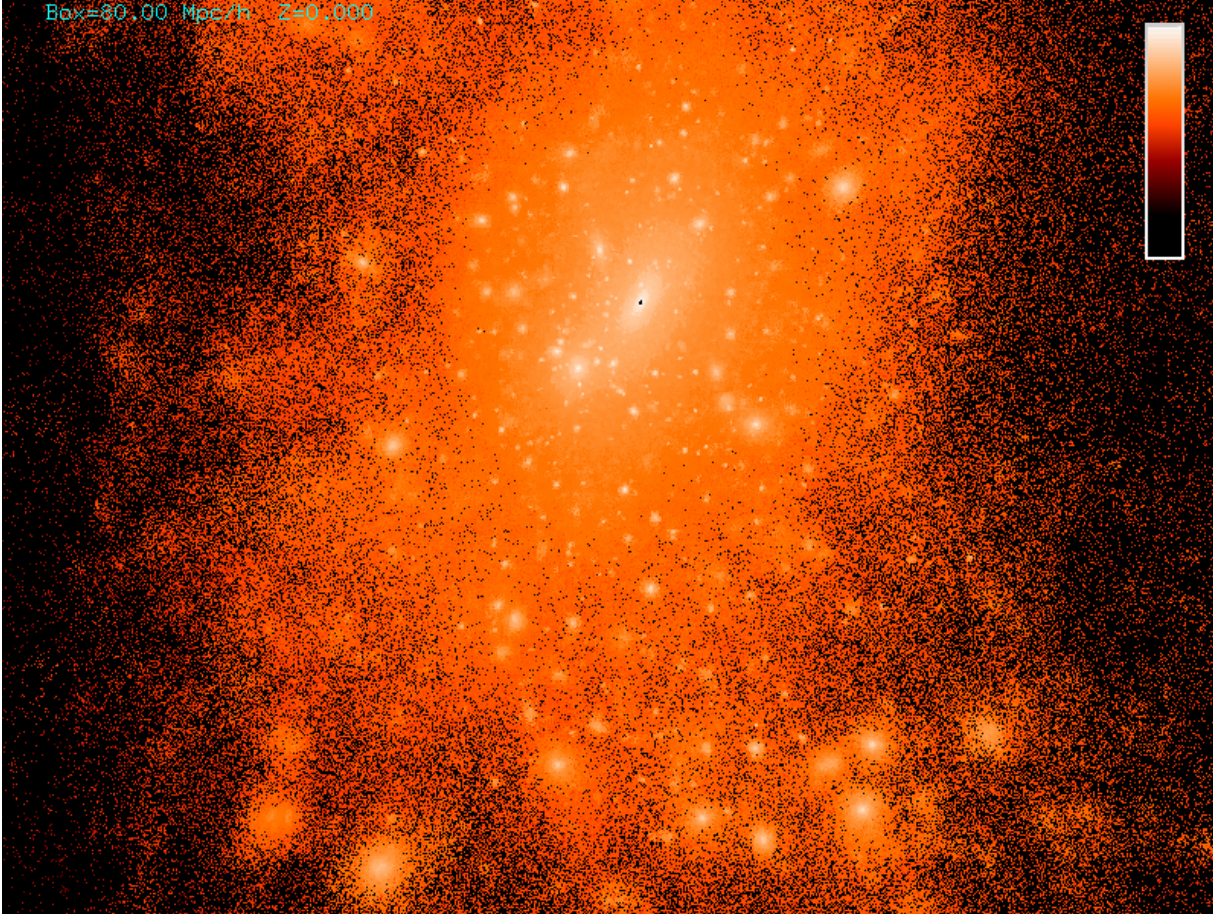
Figure 22: Center of large cluster simulated with ART. Total mass of cluster is $3 \times 10^{14} M_\odot$, and substructure resolved down to $3 \times 10^7 M_\odot$. Color coded is the normalized square of the Dark Matter density, the quantity determining WIMP annihilation luminosity per volume. Diagonal of image corresponds to 1.5Mpc.

Even for this relatively limited numerical resolution, substructure in this case contributes twice as much to the integral over density squared compared to the "host halo".

While there remains of course the substantial question of the physical lower mass cut off of the subhalos, and of the actual survival of these clumps in the presence of baryons, this corresponds quite well to results using other codes [99], where "boost factors" of order 10^2 where identified for large halos and a simulation lower mass cut off of $10^5 M_\odot$.

5.3 Substructure Formation

As outlined above, gravitational collapse and subsequent gravitational interaction will lead to a power-law like mass function of Dark Matter halos, with higher mass objects forming by subsequent merging and infall of lower mass halos. Obviously, not all infalling lower mass objects will be completely disrupted and included into a smooth new halo, but there will be surviving low mass halos inside a larger one. As is evident from simulations, owing to the ρ^2-scaling of the annihilation signal, this substructure will lead to significant boosting of the total signal from a given halo.
The exact factors by which the signal will be boosted depend mainly on two questions:

- Where is the physical lower end of the Dark Matter halo mass function?

- What fraction of small mass halos that once formed actually survives over cosmological timescales?

5.3.1 Minimal Mass of WIMP Halos

The first question posed above is actually to be answered from a particle physics point of view. There are two processes mainly limiting growth on small mass scales, collisional damping and free streaming due to non-zero temperature of the WIMPs.
Since after freeze-out, WIMPs could actually continue interacting kinetically (scatter elastically) with photons for considerable time (depending on exact cross sections), kinetic decoupling actually happens later than chemical decoupling. This means that prior to kinetic decoupling, energy transfer will erase very small structures. After kinetic decoupling, free streaming will become the most important effect damping structure on small scales.
While strongly dependent from the (unknown, lacking an identification with a concrete particle) microphysics of the WIMPs, it is possible to approximately track both of these effects [100]. The result is a fundamental mass cut off estimated for generic SUSY WIMPs at

$$M_{min,SUSY} \approx 10^{-6} M_\odot, \tag{62}$$

and

$$M_{min,Axion} \approx 10^{-12} M_\odot, \tag{63}$$

for the case of the other prolific CDM candidate, the axion. See also Fig. 23 for a fiducial example.
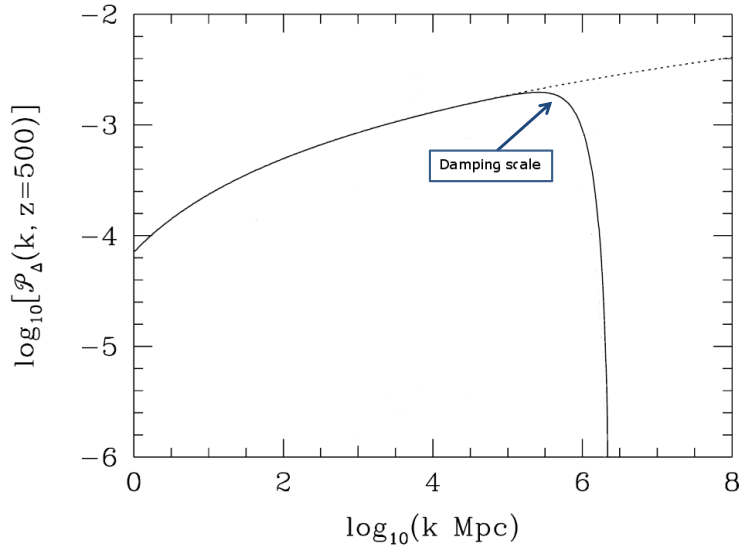
Figure 23: Dimensionless CDM power spectrum at z=500 for a fiducial SUSY WIMP of mass 100GeV, and for generic sfermion mass of 230GeV. Solid line including collisional damping and free streaming, dotted line neglecting these effects. Adapted from A. Green et al., 2004 [100].

Since there is no proposed way to damp structure formation on higher mass scales, in principle the existence of those very small mass (sub-)halos should lead to very high annihilation efficiencies, boosting expected signals by up to factors $\gg 10^3$.

5.3.2 Survival Probability of Subhalos and Implications for Search Strategy

The decisive question regarding the real boost factor is however rather which fraction of these once-formed subhalos will survive to the present time (or, e.g. for the case of the extragalactic background, to the earliest time a signal detectable by the respective instrument is emitted).

The main process responsible for the destruction of low mass halos is tidal disruption, either by interaction with the host halo, or other subhalos, or baryonic objects like stars. While each of these processes is difficult to track over cosmological timescales and all relevant mass scales, here a generic approach, building upon the proposal made in [101] is taken:

As outlined above, the (sub-)halo mass function is taken to follow the Press-Schechter law

$$N(M)dM = \frac{1}{2\sqrt{\pi}}(1+\frac{n}{3})(\frac{\overline{\rho}}{M^2})(\frac{M}{M^*})^{\frac{3+n}{6}} \times e^{-(\frac{M}{M^*})^{3+n/3}}. \tag{64}$$

All subhalos are assumed to have circular orbits inside the host halo, and their density distribution as well as their own internal density profile should again follow a NFW-profile:

$$\rho(r) \propto \frac{\rho_0}{\frac{R}{R_s}(1+\frac{R}{R_s})^2} \tag{65}$$

and accordingly a velocity distribution

$$\frac{V(R)}{V_{200}} = \sqrt{\frac{R_{200}}{R}\frac{ln(1+c \times R/R_{200}) - \frac{c \times R/R_{200}}{1+c \times R/R_{200}}}{ln(1+c) - \frac{c}{1+c}}}. \tag{66}$$

Collision probabilities can then be directly obtained. While absolute boost factors retain significant uncertainties, the net result is that the collision probability (with which the survival probability is taken to inversely scale) is lower for subhalos in extended (i.e. high mass) host halos, than for dwarf galaxy size hosts, largely owing to the scaling of the volume filling factor with $\frac{1}{R_s^3}$, steeper than the NFW slope. At the same time, statistical uncertainties will be smaller for larger halos, since for individual dwarf-sized halos there is the possibility of catastrophic disruption events e.g. from crossing the baryonic disc of the host halo, as observed for the Milky Way Sagittarius dwarf [102]. Fig. 24 sums up the results for prospective targets for indirect searches.
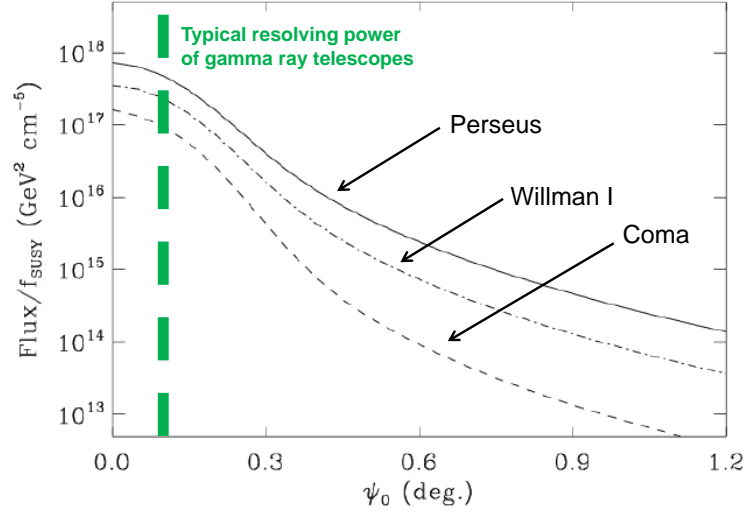
Figure 24: Expected flux including clumps versus angular scale for three prospective tar-
gets for indirect searches, one Milky Way dwarf galaxy (Willman I), and two
nearby clusters of galaxies (Coma and Perseus). Typical angular resolution
of gamma ray telescopes (≈ 0.1 degrees) indicated. Raw figure from our pro-
posal to observe the Perseus cluster with MAGIC (F. Zandanel, D. Elsässer,
C. Pfrommer, M. A. Sanchez-Conde et al., 2009), presented here in modified
form.

6 Observational Framework for Indirect Searches

6.1 Gamma Ray Astronomy

6.1.1 Ground-based Facilities, MAGIC

As outlined in Section 3, for annihilation of electroweak scale masses, the energy spectrum of the prompt pion decay gammas will peak in the tens of GeVs [103]. The opacity of the Earth's atmosphere to gamma rays in general inhibits observations from the ground at these energies from several eV to several GeVs. For gamma rays of GeVs and above however, it is possible to detect the Cerenkov light from charged particles produced in extensive air showers originating from the interaction of the gammas in the atmosphere, and traveling faster than the speed of light in the atmosphere.

Although backgrounds due to hadronic showers produced from Cosmic Ray protons and nuclei (which dominate by three orders of magnitude, even compared to strong gamma ray sources), as well as leptonic showers from electrons and positrons (which differ from showers due to gammas only by the first interaction point) are severe, it is possible to discriminate the gamma ray induced showers using a large reflecting surface, a fast camera and advanced shower image reconstruction methods [104, 105].

The positive aspect of this technique is that a telescope on the surface of the Earth will be sensitive to any particle hitting a surface of the atmosphere above the telescope with an area equal to the area of the the Cerenkov light pool at ground – typically $(10^4 - 10^5)m^2$, but depending on primary gamma ray energy, due to the Cerenkov angle

$$cos(\theta) = (n\beta)^{-1}. \tag{67}$$

This equally results in very large effective detector areas for such instruments, facilitating the detection of weak signals, and a sensitivity extending well into the TeV regime.

The breakthrough for this method certainly was the detection of the Crab nebula by the Whipple collaboration [106] in 1989. Since then, a number of facilities has been constructed around the world, among the presently operating telescope systems most notably H.E.S.S. in Namibia [107], VERITAS in Arizona [108], MAGIC and FACT in La Palma [109, 110].

Among those projects, the MAGIC telescope system (Fig. 25) is unique in that the large collecting areas of $236m^2$ (diameter of segmented primary mirrors: 17m), advanced photomultiplier cameras and 2 gigasample readout result in a sensitivity in the energy regime critical for indirect Dark Matter searches (10GeV-100GeV) that is unmatched by any other facility.

Fig. 26 displays the sensitivity curve of the MAGIC system.

Figure 25: MAGIC site at 2200m above sea level, Roque de los Muchachos Observatory, La Palma. In between the MAGIC telescopes, the control building can be seen. FACT telescope on the right side. Image Credit: S. Rügamer.

A lower energy threshold of 60GeV [111] has been consistently achieved and demonstrated by observations of the Crab Nebula – commonly used as the standard candle in Very High Energy (VHE) astronomy. Using a sum trigger logic, it was also possible to detect the pulsed emission from the Crab pulsar down to 25GeV [112].

These features make the MAGIC system one of the foremost tools for indirect Dark Matter searches presently available. As a member of the MAGIC collaboration and the fundamental physics and clusters working groups inside the collaboration, the author of this writing has therefore been part of several Dark Matter detection oriented proposals, which were carried out, with results being used and interpreted throughout this work.
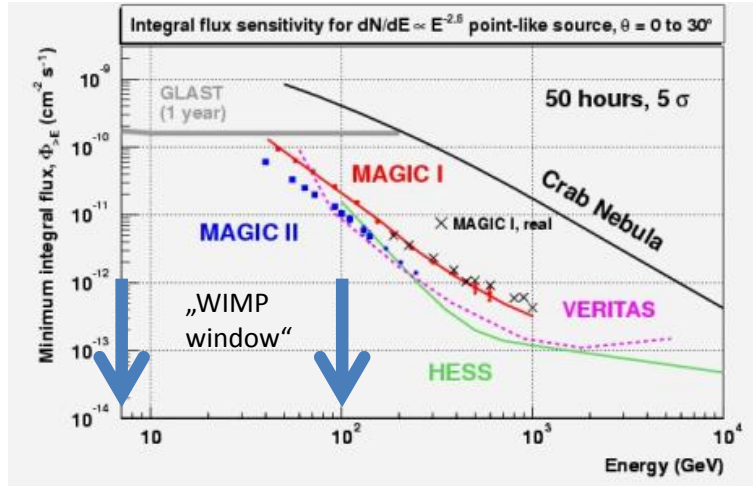
Figure 26: Sensitivity for the MAGIC I telescope and the MAGIC System, from Monte Carlos and Crab Nebula observations, as well as sensitivities for other space- and ground based gamma ray observatories. Relevant window for the prompt pion decay gamma rays from WIMP annihilation indicated. Energy resolution for the MAGIC system is $\approx 20\%$ above 150 GeV.

6.1.2 Satellite Observatories

EGRET and Fermi

At lower energies, inaccessible for the Imaging Air Cerenkov Telescopes, satellite detectors can directly detect gamma rays from cosmic sources. While effective areas are rather limited by launcher dimensions and weight constraints, the detector can operate at comparatively very low background levels, provided that charged particle and Earth albedo events can be controlled by vetoes and shielding.

In the MeV to GeV regime, measurements were made from 1991 to 2000 with the EGRET spark chamber detector on the NASA Compton Gamma Ray Observatory (CGRO) [113]. The EGRET energy range extended from 20MeV to 30GeV, and the all-sky survey resulted in the detection of 271 individual sources, including 66(+27 probable) identifications with known blazars, Centaurus A, the LMC, five pulsars and a solar flare. 170 of the sources in the catalog as of yet lack identification with any counterpart from other wavelengths [114].

Relevant for Dark Matter searches is also the detection of both diffuse galactic [115] and extragalactic [116, 117] gamma ray backgrounds.

By now, there have been new measurements in this energy regime by the pair telescopes on board AGILE [118] and the Fermi satellite (Fermi Large Area Telescope) [119]. For the Fermi-LAT, a significant advantage for cataloging the gamma ray sky is the very

large field of view, >1 steradian, allowing for operation of the telescope in a nearly continuous scanning mode.

The Fermi-LAT census of sources presently (2FGL catalog) contains 1874 individual sources, with not only individual numbers being higher than for EGRET, but also a more diverse source population (see Table 1) [120].

Source Class	Number of Objects in the 2FGL
Active Galactic Nuclei	1091
Unidentified	577
Pulsars (Pulses detected)	83
SNRs/PWNs	71
Pulsars (no Pulses yet detected)	25
Globular Star Clusters	11
Other Types of Galaxies	10
Stellar/Compact Object Binaries	5

Table 1: Second Fermi-LAT source catalog: Source census

While the sensitivity of the LAT-survey is higher than for EGRET, a sizable fraction of sources remains without identified counterpart.

The higher sensitivity of the Fermi-LAT survey, with a higher fraction of individual sources (see Fig. 27 for a view of the sky as seen by Fermi-LAT), has also resulted in new determinations of both galactic [121] and extragalactic diffuse gamma ray backgrounds. For the extragalactic background, results indicate that the intensity is in general lower than the EGRET value (presumably due to the higher fraction of resolved sources), but still can not completely be explained by extrapolating from detected extragalactic sources [122]. It should however be noted that these are ongoing efforts, with results still being preliminary.
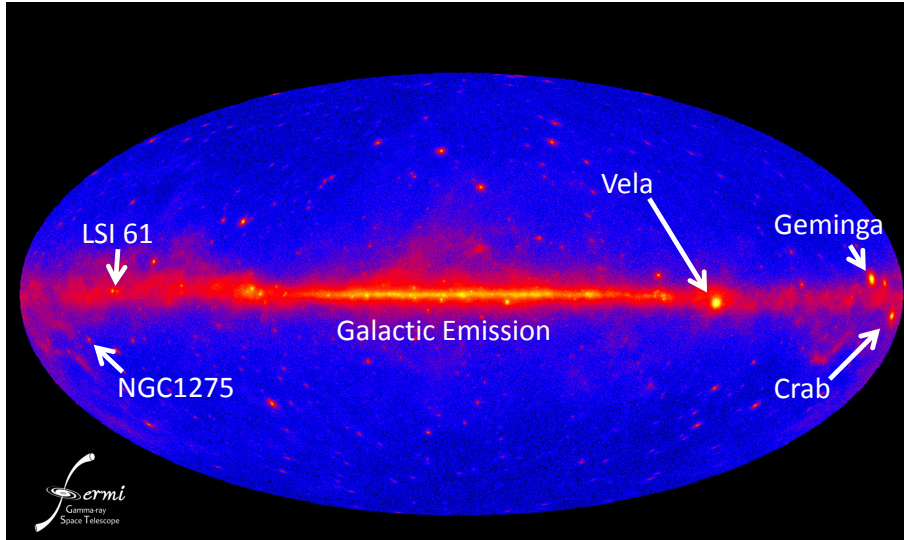
Figure 27: The sky as seen by the Fermi-LAT, using data from 12 months of operation. Intensity color coded. Image Credit: NASA/Fermi-LAT collaboration. Labels for galactic emission and prominent point sources added by D. Elsässer. NGC1275 in the Perseus cluster, treated in more detail in this work, to be seen in the left part of the image.

COMPTEL and GRIPS

At still lower energies than probed by EGRET and Fermi-LAT, Compton telescopes become the most powerful tools for photon detection.

While these energies lie outside the primary window for the prompt pion decay gammas from generic WIMP annihilation, the 100keV-MeV range is still relevant to indirect Dark Matter searches for three reasons:

- Scenarios in which the Dark Matter particle is unusually light can lead to annihilation into photons, or into electrons / positrons, in turn giving rise to annihilation signals (e.g. the positronium line, which for more massive WIMPs is not a very stringent tracer since cooling losses would overproduce diffuse intensities in other wavelength regimes) [123]. MeV-Observatories could in these cases place relevant limits on Dark Matter annihilation.

- For generic WIMPs, the radiation due to inverse-Compton scattering of the leptons from the annihilation with the CMB or starlight can produce potentially detectable signals in this band.

- A more thorough survey of MeV sources might allow to pinpoint the sources of the galactic Cosmic Ray components, and this in turn could lead to an improved understanding of charged particle propagation in the Galaxy, relevant for searches for the charged particle WIMP annihilation products.

COMPTEL, also on board the NASA CGRO, produced a catalog of 63 point sources in the energy regime from 750keV to 30MeV [124]. Apart from detection of several prominent AGN, like 3C273 and 3C279, line emission from radioactive decay of elements released into the ISM in recent supernova explosions, like the 1.8 MeV decay line of Al-26, were found [125, 126]. These act as tracers of recent ($\leq 10^6 yrs$) supernova activity.

Advanced Compton detectors with a sensitivity enhanced by a factor of 40, compared to COMPTEL, as proposed by the GRIPS consortium [127] might not only allow for placement of more stringent limits onto the positronium line emission from light Dark Matter annihilation, but also to search for nuclear de-excitation lines due to local interactions of Cosmic Rays accelerated in supernova remnants [128].
For the case of the young Wolf-Rayet supernova remnant Cassiopeia A, in collaboration with A. Summa and K. Mannheim (Universität Würzburg), the author of this work calculated – using a well-proven numerical code [129] by R. Ramaty – the expected intensities of de-excitation lines [128], which lie well into the region accessible by GRIPS-type future missions. Such a detection would constitute an unambiguous prove of Cosmic Ray acceleration by galactic supernova remnants. See Fig. 28 for resulting line fluxes and comparison with estimated GRIPS sensitivity.
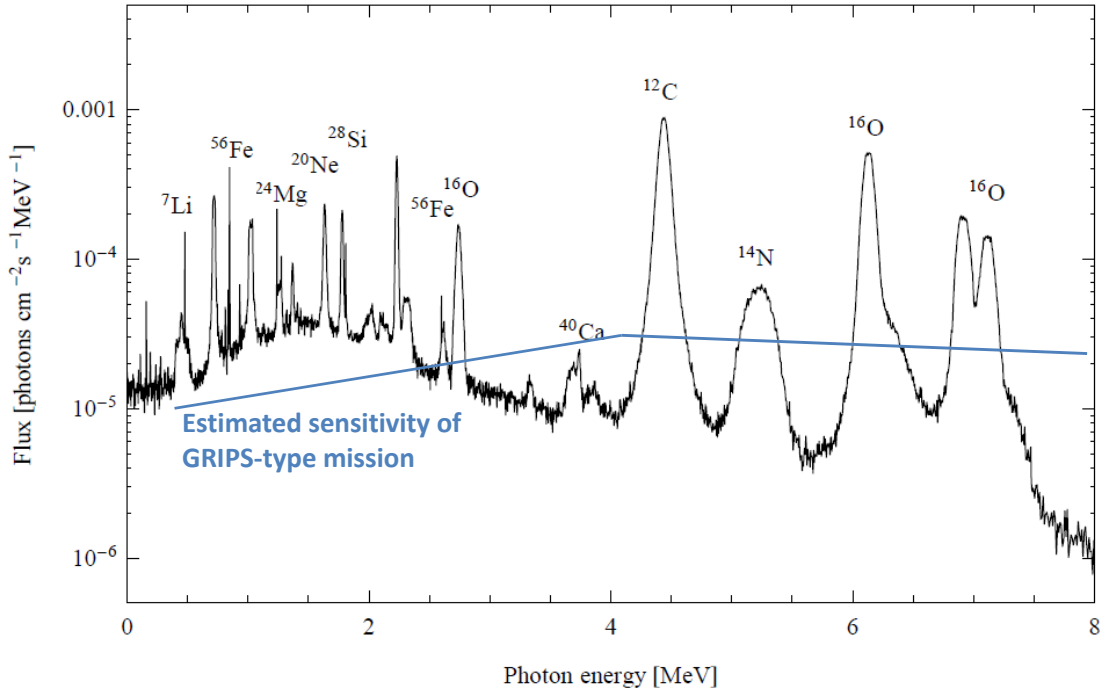
Figure 28: Predict nuclear de-excitation line fluxes from Cassiopeia A (without continuum), and comparison with estimated sensitivity of a GRIPS-type detector.

6.2 Charged Particle Detectors

While Photons certainly are the most direct tracers for pinpointing any location of Dark Matter annihilation, in the Galaxy also leptons, protons and antiprotons can be used as probes [130].

Searches have been undertaken especially for the lepton component by the PAMELA and ATIC collaborations.

Both collaborations reported excesses of the cosmic positron [131] respectively global lepton [132] flux in the GeV-TeV range. From the spectral slopes and normalizations of both results, a common origin might be expected. Proposals were made to interpret these anomalies in terms of annihilation of Dark Matter particles, in case of the ATIC excess requiring a WIMP with $\mathcal{O}(TeV)$ mass and annihilating predominantly into electron/positron pairs [133]. However, in these cases, one has to consider that a consistent explanation of the observed signals has to take radiative cooling losses of the produced leptons into account. In fact, those losses are even an integral part in producing the observed lepton energy distribution (Fig. 29).
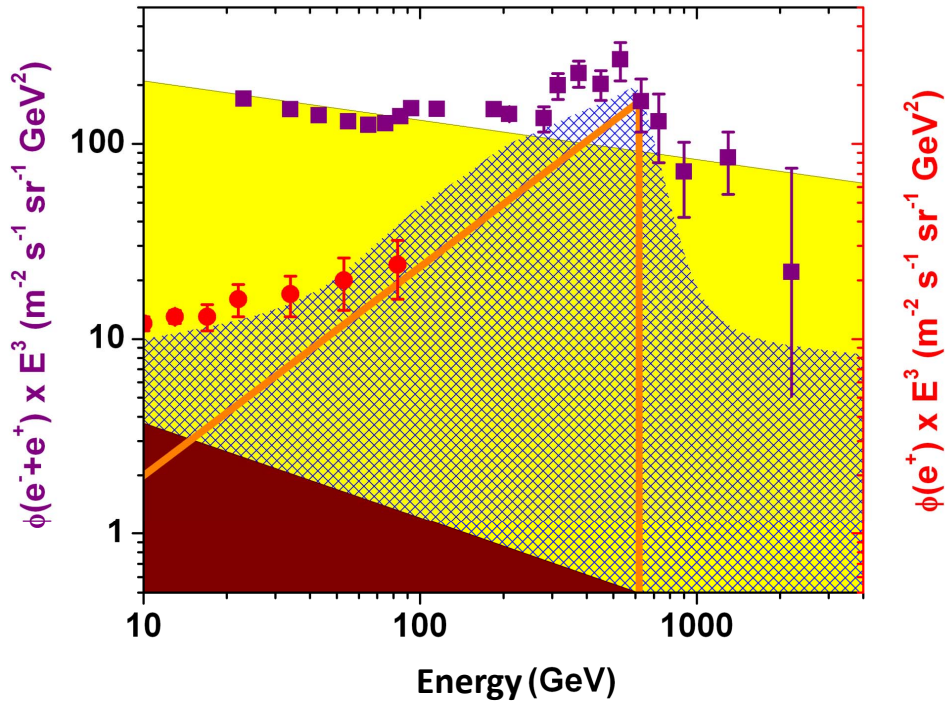
Figure 29: ATIC lepton (purple) and PAMELA positron (red) intensities, compared to standard propagation models (GALPROP) (shaded). Orange line denotes fiducial annihilation of generic 0.6 TeV WIMP and subsequent radiative cooling. For comparison, in blue shaded region shows fiducial intensity due to nearby pulsars, modeled following [134]. For an introductory review of this situation, see also [135].

Let us consider the case of a delta function injection of leptons from Dark Matter annihilation at the mass scale of the DM particles, which would be implied to be $\approx 0.6\ TeV$ by the ATIC results. The measured $\propto E^{-2}$ particle spectrum extending up to the WIMP mass (the energy scale where our fiducial pairs would be produced) can certainly be built up from the delta injection function by cooling losses. In this case however, energy conservation mandates that radiative losses of the order of the dissipated energy from synchrotron cooling would end up in the GHz–THz regime:

$$\mathcal{P}_{int,GHz-THz} \approx 0.1 \frac{GeV}{m^2\, sr\, s}, \tag{68}$$

which is incompatible with actually allowable excess radiation in these bands [136]. If the ATIC and PAMELA anomalies hold up to further scrutiny by existing [137] and future detectors like AMS-02 [138], nearby pulsars would offer an explanation alternative to Dark Matter, not suffering from this cooling disaster [134].

This underscores the power of a multiwavelength approach in ruling out certain scenarios, or in turn placing much stronger upper limits on WIMP annihilation.

6.3 Neutrino Telescopes

As outlined in section 3.4, annihilations in the core of the Sun are the most prospective detection channel for neutrino telescopes. It should however be noted that in theory, annihilation in cosmologically distributed Dark Matter halos could lead to a detectable cosmological neutrino background [139]. However, the overwhelmingly strong background from atmospheric neutrinos at GeV energies severely hampers actual searches. If flavor discriminating detectors for astronomical neutrino sources could be constructed, a search for the ν_τ component might become viable.

Another factor limiting the prospects would however be the limited angular resolution (of order degrees) of present telescope layouts.

6.4 Extragalactic Gamma Ray Background (EGB)

As an explanation for the EGRET measured excess over models including only AGN, a contribution from WIMPs with a mass of 500GeV annihilating in NFW-halos had been proposed by Elsässer and Mannheim [140].

Such a contribution can be calculated by integrating over the mean Dark Matter annihilation luminosity per comoving volume over the redshift:

$$\Phi_\gamma(E) = \frac{c}{4\pi \, H_0} \times \frac{1/2 <\sigma v> \Omega_{DM}^2 \rho_{crit.}^2}{m_\chi^2} \times \int_0^{z_{max.}} \frac{(1+z)^3 \kappa(E,z) \Gamma(z) f_{E(1+z)}}{\sqrt{\Omega_M(1+z)^3 + \Omega_K(1+z)^2 + \Omega_\Lambda}} \; dz.$$
(69)

Here, $\kappa(E,z)$ parameterizes the attenuation of gamma rays in metagalactic radiation fields, $f_{E(1+z)}$ is the spectrum of gamma rays from the annihilation process as calculated from the respective model, and $\Gamma(z)$ parameterizes the boost to the annihilation signal through the process of structure formation.

The new determination of the EGB by the Fermi-LAT team [122] does not readily confirm the EGRET excess, but rather supports an unbroken power-law like spectrum for the EGB above 200MeV (the lowermost LAT data point) with index 2.41 ± 0.05. See also Fig. 30.

However, the composition of sources of the EGB is still not determined. There will also be additional components to those discussed in the previous paragraph (blazars and Dark Matter annihilation), like starburst galaxies, which recently have been detected as extragalactic gamma ray sources [141–143].

In these works, a production of the detected gamma rays from interactions of the diffuse Cosmic Rays previously accelerated by shell supernova remnants has been assumed. However, this neglects a component that inevitably also accompanies star formation
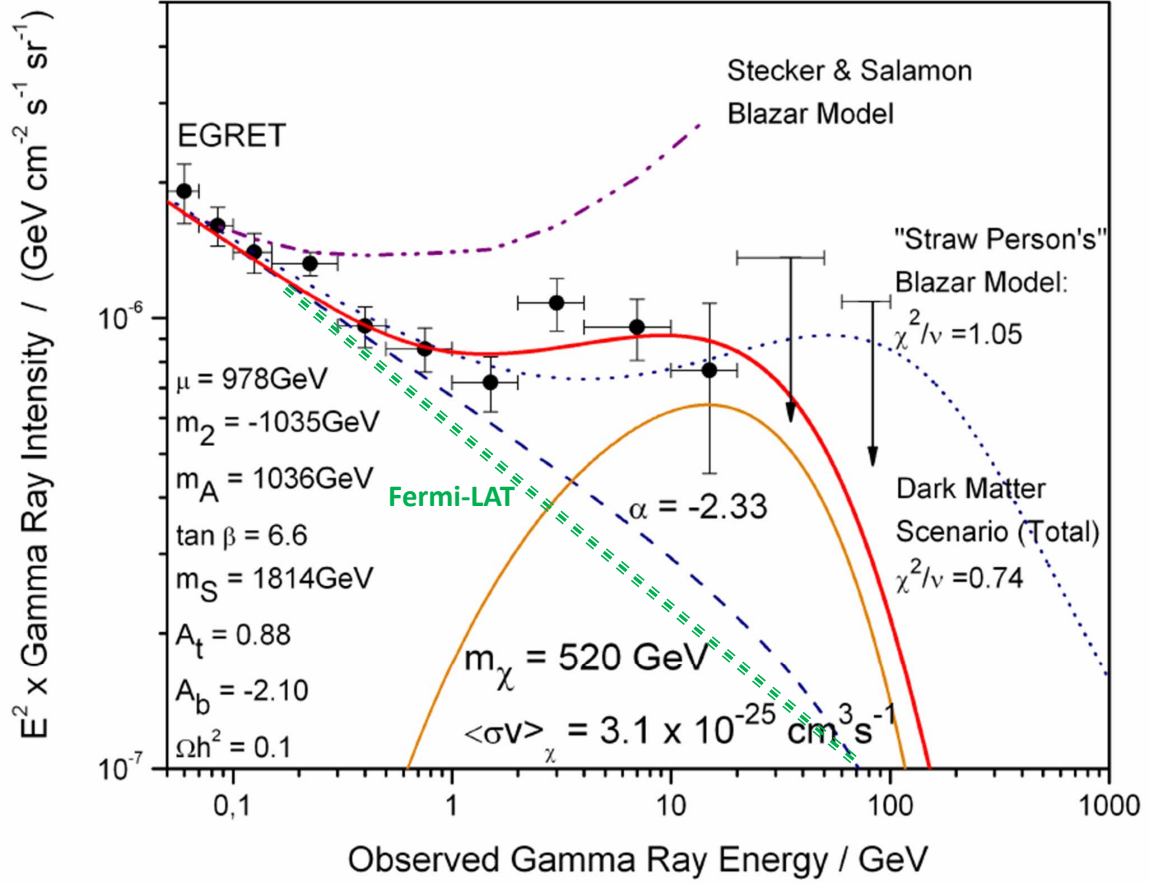
Figure 30: Extragalactic gamma ray background. Measurements by EGRET and Fermi-LAT, and comparison with a simplified model of two blazar populations (each contributing a simple power law, break chosen for best fit to data), an attenuated simple power law, and a scenario including annihilation of a WIMP with mass 520GeV.

(and thus supernova) activity: the emission from pulsar wind nebulae (PWN). As has been calculated in [144], their contribution, extrapolated from the known PWN in the Galaxy, at least for TeV energies will be sizable

$$L_{PWN}(E) = 7 \times 10^{38} (\frac{R}{0.2} yr)(\frac{E}{TeV})^{-0.3} \; erg/s, \tag{70}$$

where R is the mean supernova rate of the starburst galaxy. Such a model is strikingly able to fit the observed gamma ray luminosities of various star forming galaxies. See also Fig. 31.

Extrapolation to lower energies more relevant to WIMP searches is however not
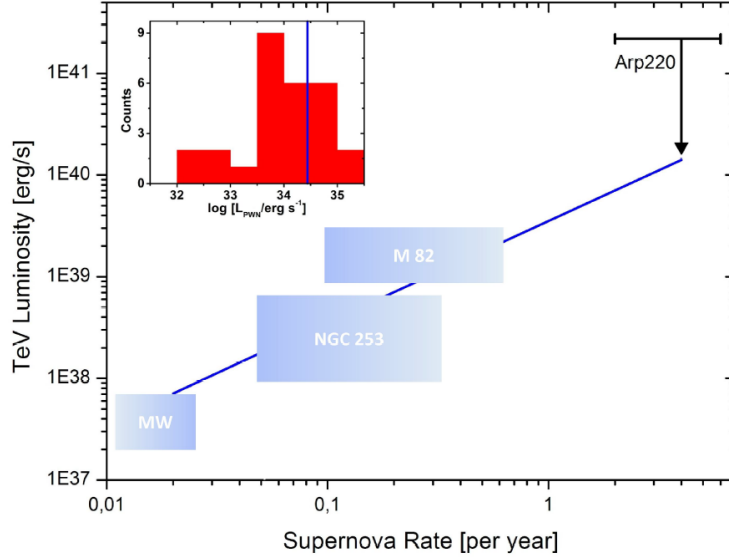
Figure 31: Luminosity due to PWN produced in starburst activity versus supernova rate. Inset shows sample of Milky Way PWN with extracted mean luminosity, used to construct scaling law (solid line). Detected fluxes / upper limits for different star forming galaxies and their supernova rates indicated by boxes. Figure also used in Mannheim, Elsässer and Tibolla, 2010 ([144]).

straightforward, due to the largely unknown effect of the cooling break in PWN spectra for a sizable statistical sample of these sources.

Still, the developing picture of the EGB is rather more complex than previously thought, thereby mandating confirmation or rejection any contribution of WIMP annihilation also by observation of other targets.

Since the Dark Matter properties are universal, and the most straightforward assumption would also be a universal type of halo profile, expected fluxes from individual halos can directly be computed from the assumed EGB contribution. For the central part of the Milky Way, for mentioned criterion of universality taken to be a NFW-halo with the center at a distance of 8.3 kpc from the Sun, scale radius of 20kpc, and the density fixed by the value of 0.3 $GeV\,cm^{-3}$ as measured for the local vicinity of the Sun [145], this yields a flux of $(1-9) \times 10^{-}10\frac{GeV}{cm^2 s}$ at 500GeV, depending on the assumed boost factor for the specific halo of the Milky Way. See Fig. 32.

Compared to the point source sensitivity of MAGIC ($5 \times 10^{-10}GeV\,cm^{-2}s^{-1}$ for 50hrs of observations, cf. Fig. 26), this should in principle make a detection feasibly by a deep observation.
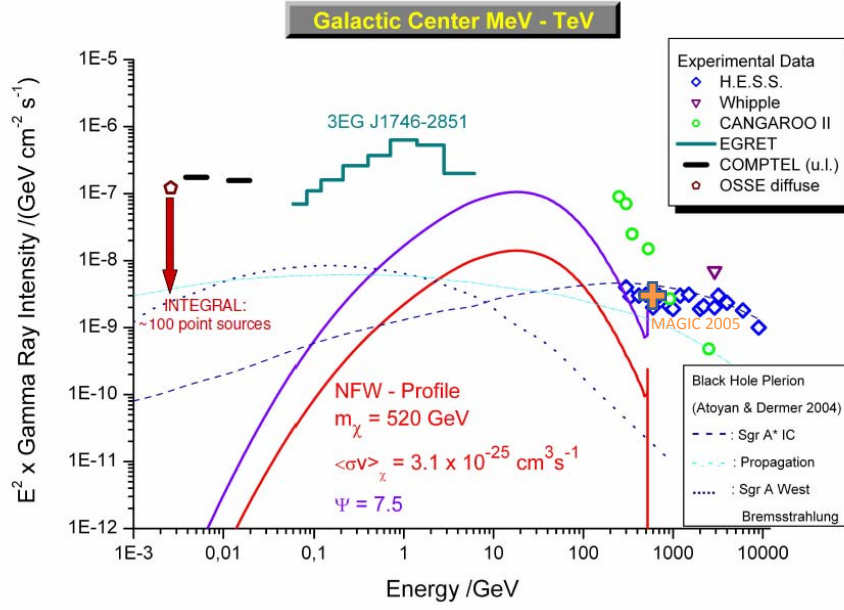
Figure 32: Dark Matter annihilation luminosity of the galactic center as inferred from the EGB. Plotted are the baseline model (solid red line), and a model including potential boost from the (unknown) amount of additional substructure in the line of sight (solid purple line). For comparison, data from H.E.S.S. [146], CANGAROO [147], Whipple [148], MAGIC [149], EGRET [150], upper limits from COMPTEL [151] and OSSE [152] are shown, along with a purely astrophysical fit to the TeV-data by the H.E.S.S. instrument by [153]. Also note that a large part of the OSSE measured flux is very probably identified with astrophysical point sources detected by INTEGRAL [154]. Line fluxes from loop-suppressed annihilation in photons with energies at or close to the Dark Matter mass can also be seen in the spectra.

In 2004/2005, efforts were undertaken to observe the galactic center with the MAGIC I telescope. This observations resulted in a detection [149], with the lowermost energy bin containing $9 \times 10^{-12} TeV cm^{-2} s^{-1}$, and extending down to 500GeV. Lower energies were unfortunately not accessible due to geometric constraints (northern latitude of La Palma).
The TeV detection by MAGIC however clearly confirms the presence of an astrophysical VHE gamma ray source in the galactic center.

6.5 Implications for Search Strategy

The implications of these border conditions for the strategy to implemented for further indirect searches is rather clear: the limited angular resolution of Cerenkov- and satellite observatories in the GeV-TeV regime of order $10^{-5} sr$ renders any astrophysical backgrounds, typically encountered in regions of high baryonic matter density, and present in the form of emission from accreting compact objects, shell supernova remnants, interacting Cosmic Rays, pulsars and pulsar wind nebulae considerable obstacles to discriminate putative weak signals due to Dark Matter annihilation. These backgrounds have to be characterized and subtracted.

On the other hand it is clear that also the uncertainty due to potential boost from surviving substructure has to be taken into account. This uncertainty is less severe for large halos, and for distant targets like clusters of galaxies, actually a sizable part of the relatively undisturbed outer reaches of the cluster lie within the field of view of Cerenkov instruments. See Fig. 33 for a simulated example.

Also, the total expected signal from suitable candidate clusters like the Perseus cluster is larger than for even the brightest Milky Way satellites (Fig. 24). Also, one should note that even dwarf galaxies with seemingly very small baryonic mass content obviously have undergone star formation at some point, leaving the possibility of compact remnants like pulsars being present in them. Therefore, a detection of a gamma ray signal from one of these objects would not be a "silver bullet" that constitutes automatic proof of Dark Matter discovery.

The implemented search strategy therefore is two-fold: clusters of galaxies as well as dwarf galaxies in the halo of the Milky Way were observed (see also [155, 156]). From the respective upper limits on a signal due to Dark Matter annihilation, and using the universality of Dark Matter annihilation spectra, a combined limit is deduced.
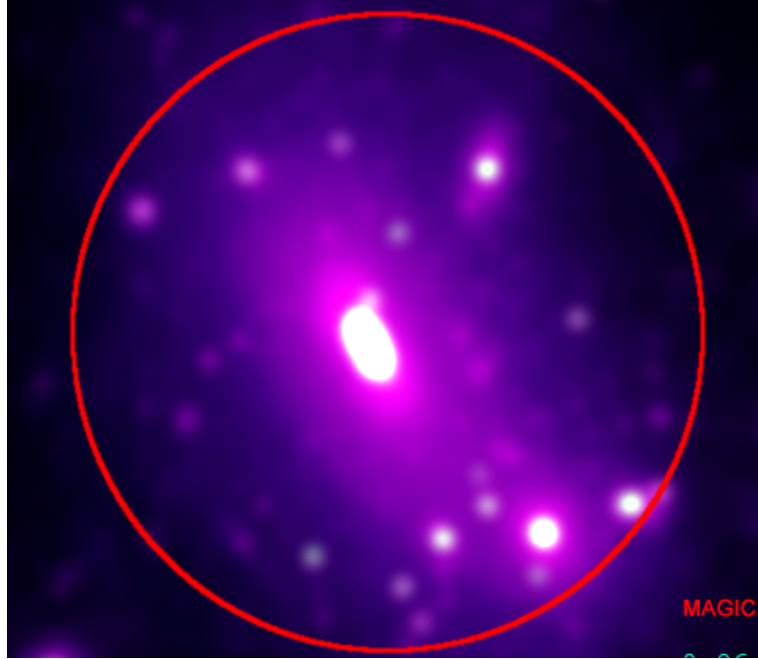
Figure 33: This image shows the central part of the simulated cluster shown in Fig. 22. This cluster was now artificially placed at a distance of 16Mpc (corresponding to the distance of the Virgo cluster), and then artificially smoothed with a Gaussian filter corresponding to a resolution of $10^{-5}sr$. Red circle denotes the central trigger area of the MAGIC telescopes for comparison. Color code this time displays the integral of the Dark Matter density squared along the line of sight through the cluster. So, what is depicted gives an idea of the result of such an idealized observation. It is readily seen that sizable contribution (again a factor of ≈ 2) of the total integrated signal is due to surviving substructure still inside the trigger area for such a distant source.

7 Dwarf Galaxy Observations

Within the MAGIC collaboration, observations of dwarf galaxies with high mass to luminosity ratios were proposed and carried out. Target selection was done according to visibility under small zenith angles from the Roque de los Muchachos observatory site, distance from the galactic plane, and especially availability of stellar velocity data to constrain the Dark Matter halo profiles.

7.1 Segue I

Segue I is a dwarf spheroidal galaxy identified in the Sloan Extension for Galactic Understanding and Exploration [157]. This object is located at RA 10.12h and DEC 16.08° in the constellation Leo. The galactocentric distance is $\approx 28\,kpc$, and the distance from the Sun $23 \pm 2\,kpc$.

While initially, there was considerable debate as to the validity of the classification as a dwarf galaxy [158], the detection of additional stars belonging to the object, bringing the total number of identified member stars to 66, placed the identification on much more solid ground [159].

On grounds of being suspected as a highly Dark Matter dominated system [160], Segue I seemed to warrant further studies as a target for indirect Dark Matter searches, and eventual observation.

Observations of Segue I with the MAGIC I telescope were carried out between November 2008 and March 2009 in wobble mode.

Total time of data taken was 43.2 hours, with zenith angles reaching from 12.7 to 33.9 degrees.

After cuts due to data quality and weather conditions, 29.4 hours of good quality data remained for analysis. Special care had to be taken to remove time slices compromised by the optical light from the V=3.5mag star η-Leonis, located just 0.68° from Segue I, and thus within the MAGIC trigger area.

The remaining good data were analyzed with the MAGIC I standard analysis package [161].

No significant signal was detected, and upper limits for the energy range 100GeV–10TeV were extracted [162]. Since the analysis of data taken by Cerenkov instruments is dependent from a coarse assumption of the slope of the spectrum to be reconstructed, here the upper limits for a rather soft spectral index of -2.4 are used, to comply with the decline of the annihilation spectra at energies above $\approx m_\chi/10$. A skymap of the region from the MAGIC data is shown in Fig. 34, and the resulting differential and integral upper limits on gamma ray emission above the MAGIC threshold energy of 100GeV are given in Tables 2 and 3.

The calculation of limits on annihilation of Dark Matter particles in the parameter space spanned up by WIMP mass and cross section now is done by again using equation 23:
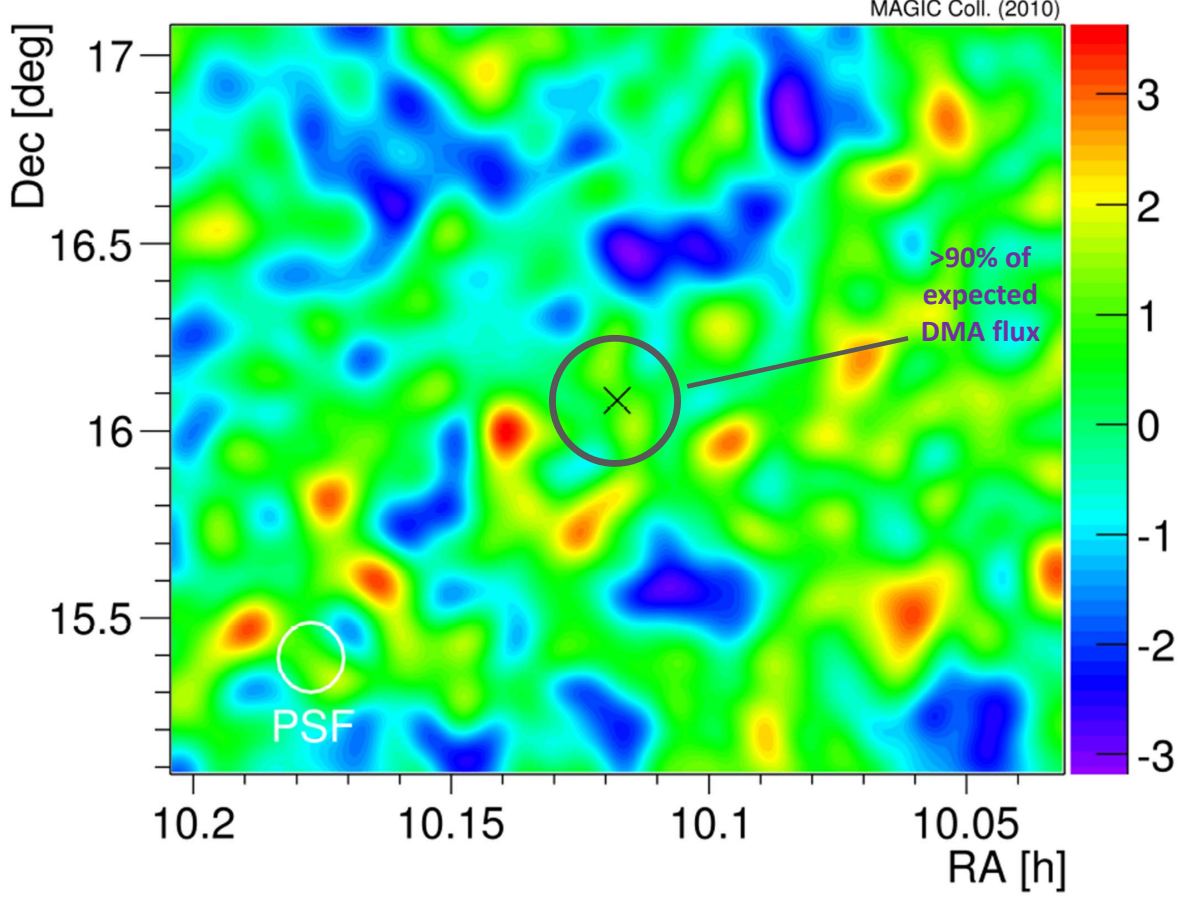
Figure 34: Sky map of the region around Segue I, as seen by the MAGIC telescope for gamma ray energies above 200 GeV. Black cross marks position of the barycenter of Segue I, white circle denotes MAGIC point spread function. Grey circle indicates region enclosing 90% of expected total flux from Dark Matter annihilation (DMA) in the Dark Matter halo hosting Segue I. Significance of excess gamma rays color coded, scale indicating standard deviations. The distribution is compatible with only background events. Plot from [162], but further additions included for this work by D. Elsässer.

$$F_y = \frac{1}{4\pi\,r^2} \times \frac{<\sigma v>}{m_\chi^2} \times N_\gamma \times \int_{l.o.s.} \rho_\chi^2 \, ds. \tag{71}$$

To physically evaluate

$$\int_{l.o.s.} \rho_\chi^2 \, ds, \tag{72}$$

the halo model for Segue I and the angular resolution of the telescope now have to be specified.

64

Energy [GeV]	No. ex. ev.	Stat. sign.	Diff. U. L. $[TeV^{-1}\,cm^{-2}\,s^{-1}]]$
100–320	399	-1.2	6.5×10^{-11}
320–1000	156	1.1	4.2×10^{-12}
1000–3200	72	1.7	4.5×10^{-13}
3200–10000	48	1.1	7.4×10^{-14}

Table 2: Differential flux upper limits for the Segue I observations carried out by the MAGIC I telescope, as also published in [162]. Limits given for a spectral index of -2.4.

Energy threshold [GeV]	No. excess ev.	Stat. sign.	Flux U. L. $[10^{-12}\,cm^{-2}\,s^{-1}]$
100	453	-0.99	13.7
126	174	-2.04	4.6
158	93	-2.25	2.1
200	110	-0.97	2.2
251	194	0.57	3.5
316	250	1.67	4.1
398	147	0.79	2.2
501	140	0.96	2.0
631	124	0.84	1.6
794	146	1.34	1.8
1000	135	1.36	1.6

Table 3: Integral flux upper limits for the Segue I observations carried out by the MAGIC I telescope, as also published in [162]. Limits given for a spectral index of -2.4.

For the observation carried out with MAGIC I, the resolution was 0.1 degrees. Since data were not taken in stereo mode, but only with a single dish system, extended source sensitivity is marginal, and the solid angle effectively covered by the observation will thus be taken to be equal to the point spread function.

The best-fit halo model from stellar dynamical observations for Segue I was found to be an Einasto-profile of type

$$\rho_{Seg}R = \rho_s e^{-2n((R/R_s)^{1/n}-1)}, \tag{73}$$

with parameters $\rho_s = 1.1 \times 10^8 M_\odot \, kpc^{-3}$, $R_s = 150 \, pc$ and $n = 3.3$ by [163], and is used here accordingly. This halo has a mass of 600 000 solar masses, providing for a mass-to-light ratio of ≈ 1000.

Therefore, the equation for the expected flux from Dark Matter annihilation in Segue I now reads

$$F_y = \frac{1}{4\pi \, r^2} \times \frac{<\sigma v>}{m_\chi^2} \times N_\gamma \times \int_{\Delta\Omega} \int_{l.o.s.} \rho_{Seg}^2(R(s, \, \Omega)) \, ds \, d\Omega, \tag{74}$$

with $d\Omega$ being the solid angle covered by the point-source analysis of the MAGIC observation. The radius emitting 90% of the predicted flux for this halo model is indicated in Fig. 34. The total value of the density integral for Segue I is $J(\Delta\Omega) = 1.78 \times 10^{19} \, GeV^2 \, cm^{-5}$. The MAGIC point spread function after analysis still contains $\approx 65\%$ (or, in terms of the density integral $J(\Delta\Omega)_{PSF} = 1.14 \times 10^{19} \, GeV^2 \, cm^{-5}$) of the total expected flux. It should be noted that – as is generally the case for these high-mass-to-light dwarfs identified from surveys – the measured stellar population is a small fraction of the total mass content, and contamination by interloper stars poses severe risks to the fit. Conservatively, the global uncertainty on the astrophysics setup is an estimated one order of magnitude at 2σ confidence level.

To attain the exclusion limit in the $m_\chi - <\sigma v>$–plane, the maximum allowable effective (i.e. including any additional boosting) cross-section times number of photons above the energy threshold of the observation so as to not overproduce with the result of Eq. 74 the integrated MAGIC flux limit has been calculated. This is compared to the actual models from the Würzburg database (Section 4.2.2).

The resulting exclusion line is shown in Fig. 35. As can readily be seen, the MAGIC excluded region actually does not yet permit to constrain the parameter space without additional boosting of the signal. Large boost factors $b > 10^3$ however can already be excluded for a significant part of the parameter space with these observations.
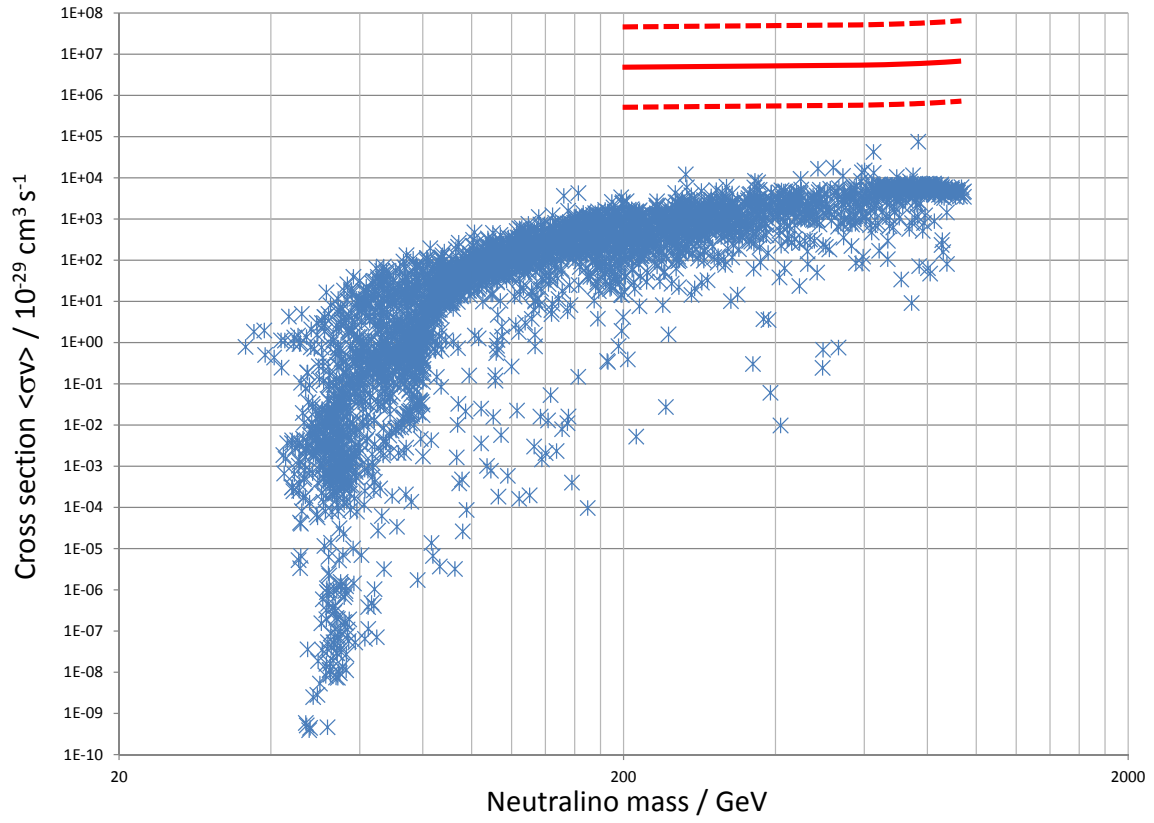
Figure 35: MAGIC exclusion limits from the Segue I observations (red solid line, astrophysical uncertainties indicated by dashed lines). Higher mass models with boost factors above order 10^3 can be constrained from this campaign.

7.2 Willman I

Another system well suited to indirect Dark Matter searches by VHE telescopes is the dwarf galaxy Willman I in the constellation Ursa Major (the Larger Bear). Exact location is RA 10h40m22s and DEC 51°03'04", at a distance of $38 \pm 7\,kpc$ from the solar system.

This Milky Way companion was discovered in 2005 in Sloan Digitized Sky Survey data [164]. This observations indicate a total mass of 400 000 solar masses, with an absolute magnitude of only -2.7 ± 0.7. This yields a mass-to-light ratio of 800, obviously a strongly Dark Matter dominated system.

Between March and May of 2008, Willman I was thus observed with the MAGIC I telescope for 16.8 hours in ON and 9.3 hours in OFF (for background determination) mode. Zenith angles during the observations ranged from 22 to 30 degrees. 7% of the data had to be rejected due to atmospheric conditions, leaving 15.5 hours which were analyzed.

Analysis was done with a branch of the MAGIC analysis software package optimized also for slightly extended sources [165].

No significant excess of gamma rays was found, and upper limits on the flux from Willman I above an energy threshold of 100GeV were deduced [166].

Figure 36 shows the resulting alpha-plot for this observation, and Table 4 the respective upper limits.

Energy [GeV]	Flux U. L. $[10^{-12}\,cm^{-2}\,s^{-1}]$
100–170	9.94
170–350	4.75
350–1000	0.68
1000–20000	0.35

Table 4: Integral flux upper limits for the Willman I observations carried out by MAGIC I, as also published in [166].
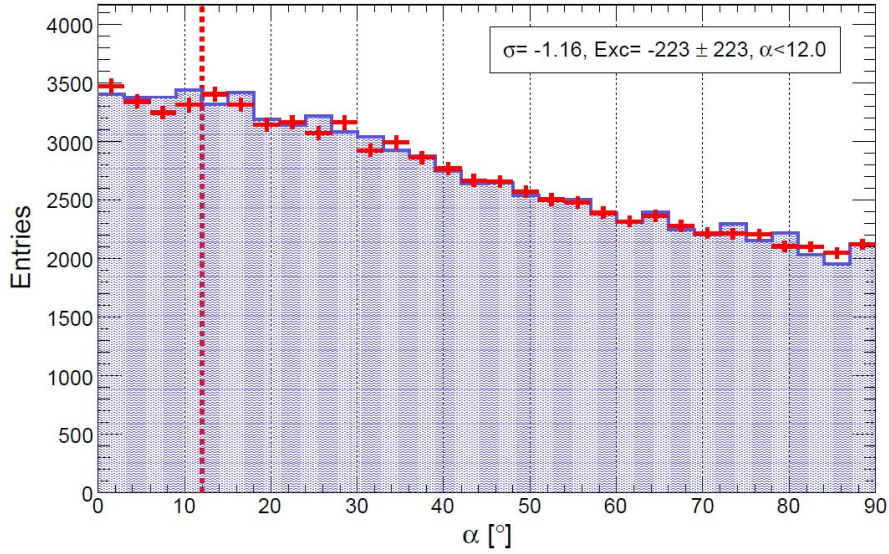
Figure 36: Distribution of angles between orientation of events and direction to the camera center for the events from the MAGIC campaign on Willman I ("alpha-plot"), for ON source pointing (red crosses) and background (OFF source, plotted as blue shade) data. Any significant detection would manifest itself by an excess of ON events at small angles (to the left of the red dotted line). Result is compatible with the null hypothesis. Plot from [166].

Best-fit Dark Matter halo models to the stellar velocity data for Willman I [167] are of the NFW-type:

$$\rho_{Will}(R) = \rho_s (\frac{R}{R_s})^{-1}(1 + \frac{R}{R_s})^{-2}, \tag{75}$$

with $\rho_s = 4 \times 10^8 M_\odot \, kpc^{-3}$ and $R_s = 0.18 \, kpc$. The resulting value for the density integral is $J(\Delta\Omega) = 3.5 \times 10^{17} \, GeV^2 \, cm^{-5}$. Again, global uncertainties on the astrophysical model are considerable, and are an estimated 1 order of magnitude at 2σ confidence level.

The procedure to deduce exclusion limits in the $m_\chi - <\sigma v>$–plane was done in the same fashion as described for Segue I, again using Eq. 74.

The resulting limit is presented in Figure 37.

As could already be judged from comparing the observational flux upper limits and differing values for the density integrals, resulting exclusion limits are roughly an order of magnitude less stringent than for Segue I. Again, large additional
boost factors >(1000–10000) can be constrained from these observations.
Partly counter-balancing the stronger limits in case of Segue I however is the fact that the Willman I observations are not influenced at low energies by the presence of a bright star in the field of view.
Again, it is noteworthy that these differences underline the considerable astrophysical uncertainties regarding dwarf galaxy observations, mandating a diversified approach.
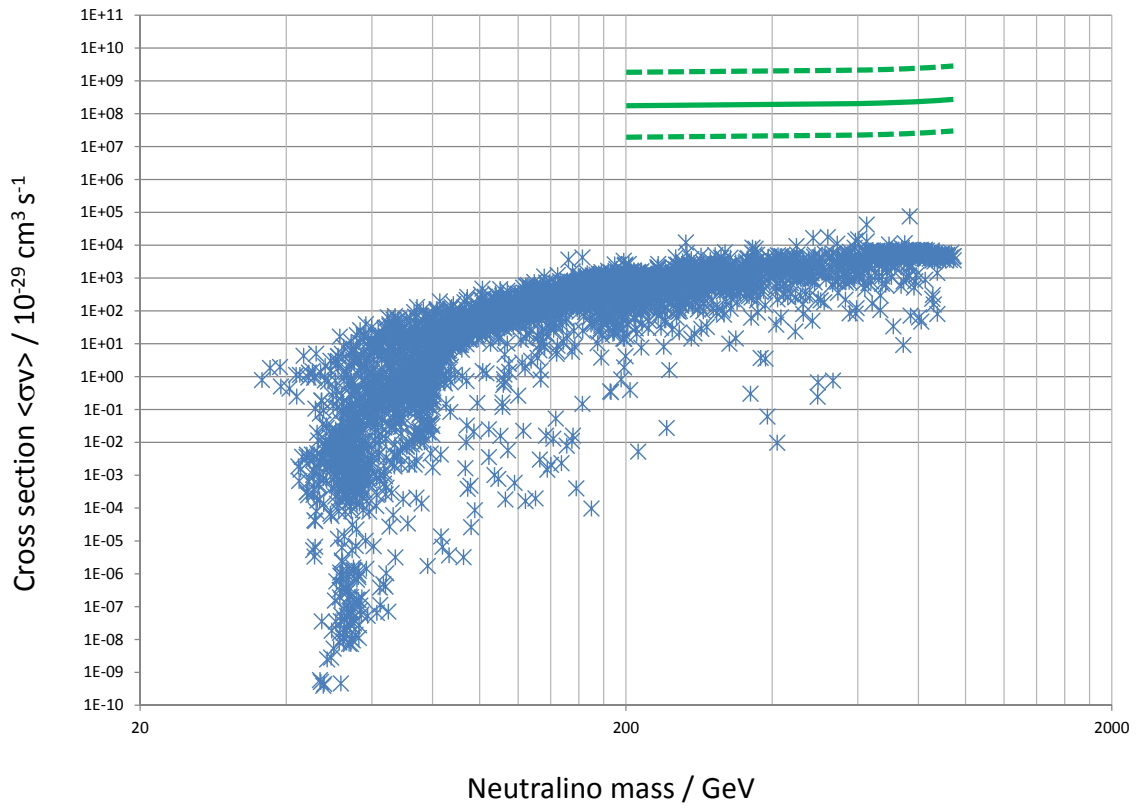
Figure 37: MAGIC exclusion limits from the Willman I observations (green solid line, astrophysical uncertainties indicated by dashed lines).

7.3 Unidentified Fermi Sources

Cerenkov observations as described in the previous two sections of course rely on a priori knowledge of the location of prospective objects, typically from large scale surveys producing stellar velocity data.

On the other hand, N-body simulations predict the presence of a larger number of Dark Matter subhalos in the Galaxy. Some of them might be among the best targets for indirect Dark Matter searches. However, prospective candidates may at the same time evade discovery by mentioned surveys, e.g. because their stellar content is simply too small to result in detection of a bound system, or they may have lost their baryonic content altogether due to tidal interactions with the Milky Way halo.

The Cerenkov method as employed in current instruments unfortunately does not lend itself well to surveying the entire sky for a population of faint sources, because of limited field of view and rather large amounts of overhead time for background determination. Estimates however show that a small number of order unity of these subhalos may also be detectable by Fermi-LAT as point sources [168, 169].

It has to be conceded that searching for such a population in the Fermi-LAT all sky survey is challenging, since without knowledge of either the density profile of the clumps or their masses and distances (lacking any baryonic tracers), or the WIMP properties, the problem is severely under-defined. A survey of Fermi-LAT data on 10 known Milky Way satellites recently turned up no evidence of Dark Matter annihilation [170, 171].

Therefore, it rather makes sense to turn to an approach even less dependent from prior assumptions, and survey all unidentified Fermi-LAT sources (numbering 577 at the moment, see Table 1) for those that have properties fitting for annihilating Dark Matter subhalos.

The imposed criteria were:

- No obvious association with baryonic sources, also in other wavelength regimes

- No confirmed variability (a strong confirmation or rejection is in any case however challenging due to the limited number of photons for many sources)

- Detection of at least one photon at energies >10 GeV; also facilitates follow-up observations with more sensitive Cerenkov telescopes [172]

- Galactic latitude >20 degrees

The last criterion is of course not mandated by subhalo or WIMP physics, but serves to cut down on the otherwise unavoidable confusion with galactic sources due to the limited angular resolution of the LAT.

Somewhat surprisingly, among the surviving sources there is only a single one from which at least one photon was detected above 80 GeV (the lower energy threshold of the MAGIC telescope system), and this is 1FGL J0030.7+0724 [169].

Of this source, in total 6 photons have been detected by the LAT (see Fig. 38). Probabilities of each of them being background photons are negligible.
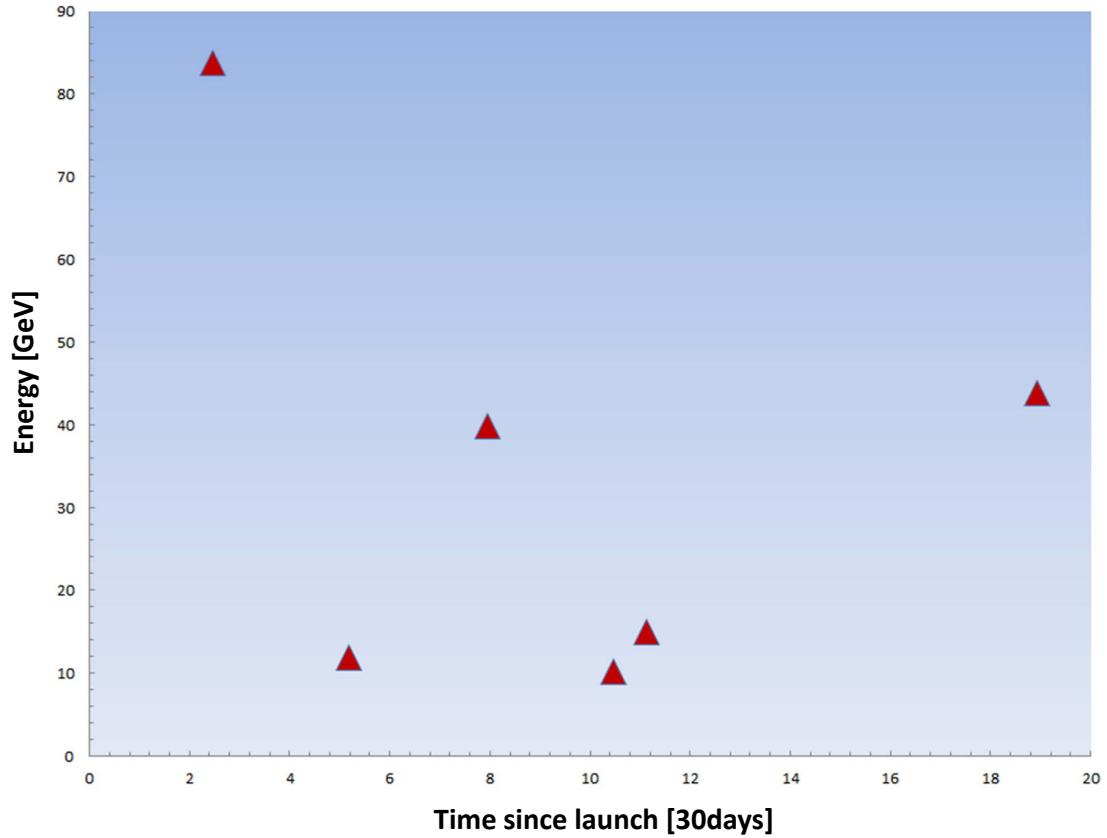
Figure 38: Fermi-LAT detected photons from 1FGL J0030.7+0724. Plotted is photon energy vs. elapsed time since mission start.

A subsequent survey of the region around this source using the NASA Extragalactic Database (ned.ipac.caltech.edu) turned up two weak (milliJansky) radio source (NVSS J003119 and J003030) as candidate counterparts.

SWIFT [173] observations of this region were proposed, and 10.1ksecs of data taken in November 2010 (Obs. ID 00041265001).

Standard calibration and analysis (xrtpipeline/HEAsoft and Xspec, using up to date calibration files and response matrices) revealed 7 X-ray sources in the field, down to a flux level of $4 \times 10^{-14} \, cm^{-2} \, s^{-1}$ [169].

Fig. 39 displays the region after the SWIFT observations.
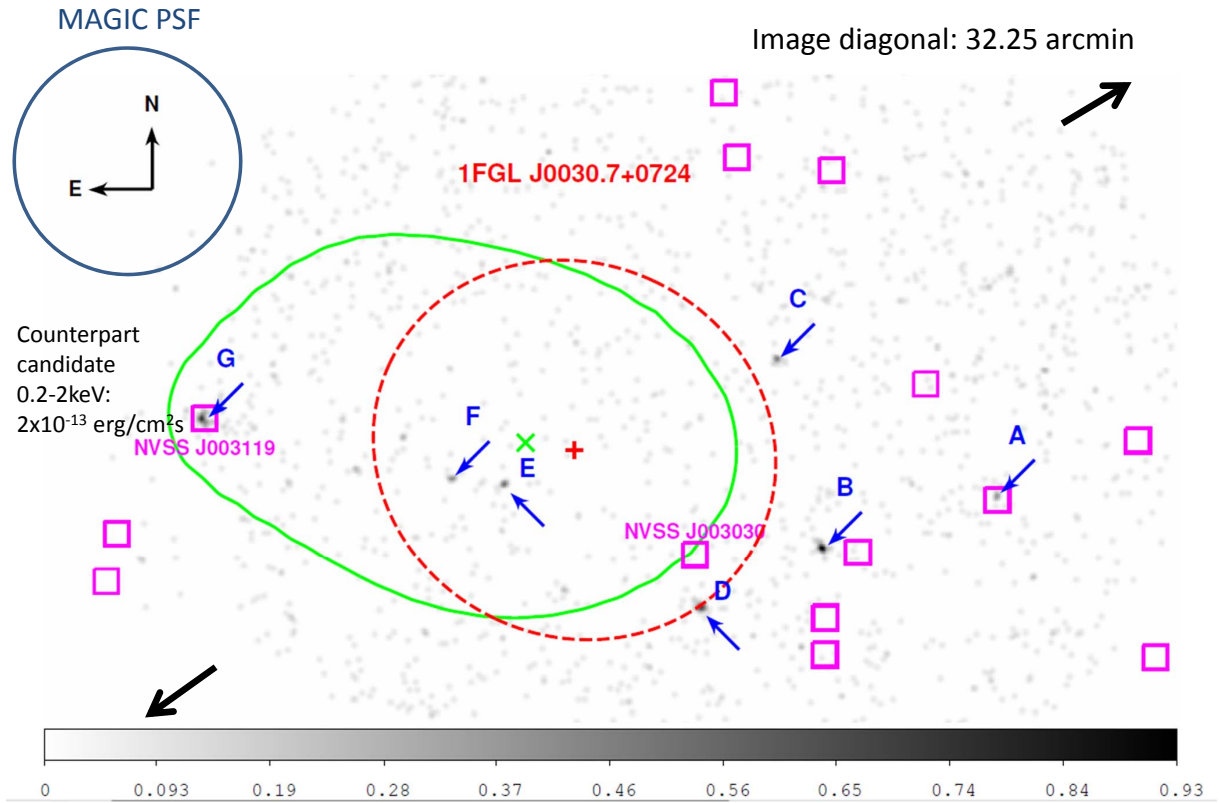
Figure 39: Region around $1FGLJ0030.7 + 0724$. Black and white color code displays SWIFT observations (Obs. ID 00041265001). Seven new X-ray sources labeled in blue with arrows and capital letters. Red cross/circle denotes 12 month Fermi-LAT best fit position and 95% positional confidence level. Green cross/circle denotes position and 95% C.L. for 24 months of LAT data. Superimposed in magenta are the known NVSS radio sources in the field. SWIFT source G as most likely candidate counterpart indicated, as well as MAGIC point spread function for purpose of comparison. Basic plot from our publication [169], but with additions for this work.

As can be seen, the only remaining counterpart candidate after including all data is NVSS J003119. The X-ray emission with a
H-corrected flux $\nu F_\nu = 20.7^{+8.8}_{-4.7} \times 10^{-14}\, erg\, cm^{-2}\, s^{-1}$ in the SWIFT band between 0.2 and 2 keV may suggest that it is a distant blazar or flat spectrum radio quasar.
H.E.S.S. and MAGIC observations are planned/proposed to gather further data for placing more stringent constraints on either scenario, and to decide whether the NVSS/SWIFT source is just positionally coincident, or identical with the Fermi-LAT source.

8 Observations of Clusters of Galaxies

8.1 Target Selection

At the upper end of the mass scale of gravitationally bound objects, clusters of galaxies represent strongly Dark Matter dominated objects accessible to indirect searches.
In addition to halo modeling, here astrophysical backgrounds have to be considered when extracting limits. Those consist mainly of

- Active Galactic Nuclei naturally present among the thousands of cluster galaxies

- VHE emission due to interactions of Cosmic Rays in the cluster

While AGN have long been known as prominent emitters of high energy gamma rays, as of yet no observational evidence of hadronic Cosmic Ray induced emission has been found from clusters of galaxies. From the presence of radio "mini"-halos associated with many clusters [174], the presence of relativistic electrons can be deduced. Corresponding to the situation in the Galaxy (where the ratio of relativistic protons to electrons at GeV energies is about 100) [175], the sites of origin of these synchrotron-emitting electrons should also be accelerators of high-energy protons and nuclei. Since the radiative cooling times scale with the square of the mass ratio

$$\frac{\tau_p}{\tau_e} \propto (\frac{m_p}{m_e})^2, \tag{76}$$

those protons could naturally be stored over the Hubble time in clusters, and losses due to inelastic interactions with nuclei become important. In hadronic mini-halo models, the relativistic electrons are produced by proton-proton interactions [176] of Cosmic Rays with the intracluster medium (ICM), with Cosmic Rays making up a few per cent of the thermal pressure in the cluster. Those clusters that exhibit cool cores [177], with lower central temperatures and correspondingly higher densities, provide especially high target densities for these interactions [178].
While this means that the gamma rays from the decays of neutral pions inevitably also produced in such interactions act as backgrounds for any Dark Matter search in clusters, they also open up the possibility to constrain the population of relativistic Cosmic Rays in the cluster. This in turn could have ramifications regarding the origin of the extra-galactic component in the observed Cosmic Ray spectrum at Earth, and is an interesting physics case on its own.

In preparation for MAGIC campaigns to observe clusters of galaxies, available candidates were drawn from a sample fo which the background due to Cosmic Ray interactions had been modeled using state of the art numerical approaches (GADGET-2 [179]) in [180].

While any AGN - induced background has to be considered on a case-by-case basis (AGN spectral energy distributions varying considerably), and in general the AGN emission is also time variable, the CR-induced component is expected to be steady and show

a spectrum that at TeV-energies can be described by a power-law of index ≈ 2.2 [181].

Predictions for nearby prominent clusters of galaxies are plotted in Fig. 40.
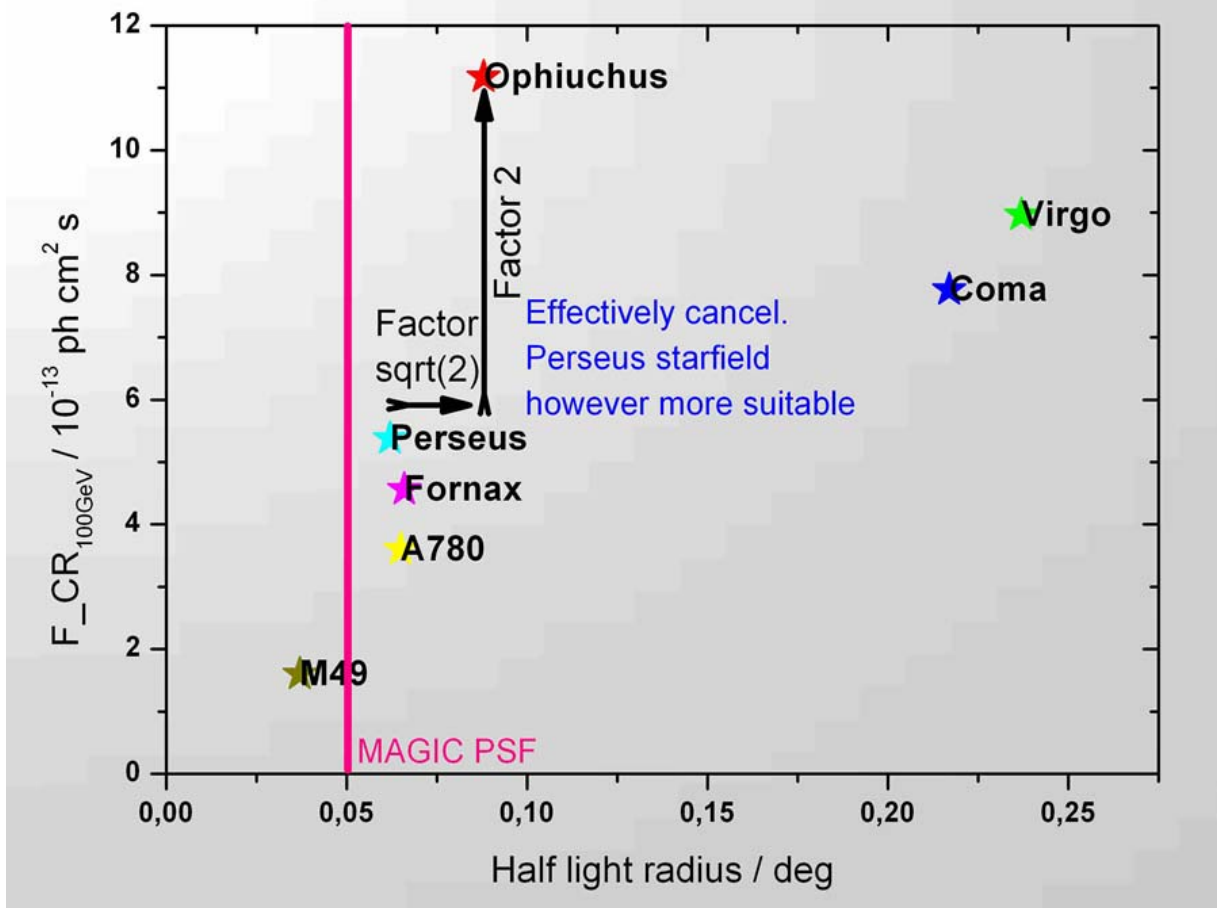
Figure 40: Expected flux of gamma-rays above 100GeV from Cosmic Ray interactions versus expected angular size of the region emitting half of the total intensity ("half light radius"). This is a relevant quantity since a point-like source is much easier to characterize using a Cerenkov telescope, and since in general the competing Dark Matter induced emission will be extended due to substructure in the cluster outskirts (see Section 5.3.2). MAGIC point spread function displayed by pink line for purposes of comparison. The higher expected flux from the Ophiuchus cluster is counterbalanced by larger size of emission region, and by a brighter star field (constellation Ophiuchus being in a rather bright part of the summer Milky Way), which is harmful to Cerenkov observations. Finally, Perseus Cluster and Virgo cluster were observed as cases representative of compact and extended expected emission. Plot created using input data from [180].

77

The conclusions for the campaign regarding indirect Dark Matter searches were clear: AGN as well as emission from CR-interaction are inevitable backgrounds. they have to be characterized, and in turn also represent interesting science cases, in case of the CR-interactions even a potential discovery of a process never observed before in the gamma-ray regime (which of course also means that the real flux level is not yet determined).

Observations of two very different clusters, Virgo (less compact, prominent AGN in the cluster center) and Perseus (compact cool core, high X-ray surface brightness [182]), were therefore carried out.

8.2 Virgo Cluster

The Virgo cluster of galaxies is the most nearby large cluster. At a distance of 16.5 ± 1 Megaparsecs, it has a total mass of $1.2 \times 10^{15} M_\odot$ [183].

In the center of the Virgo cluster, the prominent cD galaxy M 87 is located, which hosts an AGN. An optical image of the central 5 arcminutes of the Virgo cluster, including M87, can be seen in Fig. 41.

The center of the center of the Virgo cluster was observed by H.E.S.S., MAGIC and VERITAS in a prolonged multiwavelength campaign [184]. During this campaign, properties of the AGN could be constrained, including pinpointing the region of VHE emission to the immediate vicinity of the $6.4 \times 10^9 M_\odot$ black hole in M 87 [185].

Using data from these campaigns and excluding flaring states, it is also possible to extract constraints on a flux contribution from Dark Matter annihilation, despite the presence of the bright AGN.

The Dark Matter halo in the central region of the Virgo cluster / M 87 can be described with a NFW-type profile with the parameters $\rho_s = 3.2 \times 10^{-4} M_\odot\, pc^{-3}$ and $R_s = 560\, kpc$, drawn from observations of the X-ray surface brightness of the cluster [186].

The availability of multiwavelength data lends itself well to additionally considering a hard X-ray / soft gamma-ray component due to the inverse Compton up-scattering of photons by the charged annihilation products, which contributes (confer Section 3.4 and [55])

$$(\frac{d\Phi}{dE})_{ic} = \frac{1}{E}\frac{1}{4\pi r^2}\frac{<\sigma v>}{m_\chi^2}\int \rho_{NFW}^2(R)\, dV \times \int_{m_e}^{m_\chi}\frac{P(E, E')}{b(E')}\, dE' \int_{E'}^{m_\chi}\frac{dN_e}{d\widetilde{E}}\, d\widetilde{E}. \quad (77)$$

As target field, a blackbody radiation field with $T = 2.7 K$ and density $413\, cm^{-3}$ (the CMB) is considered, the simple most, and also inevitable, contribution.

Figure 42 summarizes the resulting fit to the observed multiwavelength spectrum, including prompt pion decay gammas and up-scattered CMB photons. To model the

Figure 41: Johnson B, V and R image of the central 5 arcminutes of the Virgo cluster, displaying M87, the system of globular clusters around this galaxy, and also the optical jet powered by the multi-billion solar mass black hole in the center of the galaxy. Image taken by D. Elsässer with the 1.2m MONET/North telescope.

underlying AGN, an implementation of the Synchrotron-Self-Compton (SSC) model was used [187]. Parameters for this fit were a Doppler factor of 3.9, a bulk Lorentz factor of 2.3, a source zone radius of 3.5×10^{13}cm, and a magnetic field strength of 3 Gauss. The injected electron distribution (exponentially cut-off power law) is obtained to a slope of 2.2, a maximum Lorentz factor of 10^8 and a normalization factor of $10^6 \, cm^{-3} \, s^{-1}$. The resulting injection luminosity is $L_{in} = 3 \times 10^{41} \, erg/s$, consistent with observations of large scale radio structures [188].

Although this is certainly a rather coarse and fiducial model, and the observational

data are not completely contemporaneous, it can be seen that the addition of a fiducial component due to annihilation of WIMPs with mass 4747 GeV and cross section $<\sigma v> = 3 \times 10^{-24}\,cm^3\,s^{-1}$, while allowing for an additional boost of the annihilation luminosity by a factor f=812, can slightly improve the already reasonable fit by the AGN model (reduced χ^2 of 1.6 vs. 2.5 for AGN only).

It should be noted that future, more sensitive observations, might allow for the simultaneous discrimination of prompt gamma-rays and IC up-scattered contributions, a tell-tale signature of WIMP annihilation.
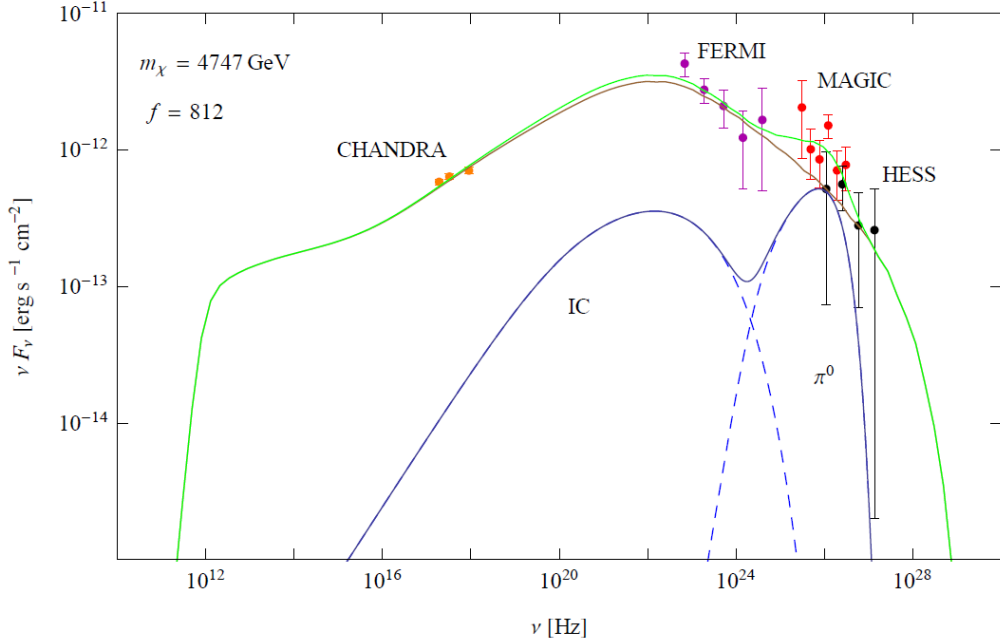
Figure 42: Spectral energy distribution of M87 in the center of the Virgo cluster. Data from Chandra [189], Fermi-LAT [190], MAGIC [191] and H.E.S.S. [192]. AGN-only model plotted as brown solid line, fiducial WIMP contributions as blue lines. Sum as green solid line. Note especially the improved fit to MAGIC data points for the sum contribution. Plot from our publication [55].

8.3 Perseus Cluster

The second cluster that was observed in the MAGIC campaign is the Perseus cluster of galaxies (Abell 426). Physical parameters for this system are summarized in Table 5.

Redshift z	Distance [Mpc]	$M_{200}\,[M_\odot]$	$T_X\,[keV]$	$L_X\,[erg/s]$	$R_{200}\,[Mpc]$
0.018	77.7	7.71×10^{14}	6.8	8.31×10^{44}	1.9

Table 5: Physical parameters for the Perseus cluster of galaxies [182, 193, 194].

The Perseus cluster was observed with the single-dish MAGIC I for 33.4 hours in November and December 2008 (zenith angles from 12 to 32 degrees) [195] in wobble mode, and for 99 hours from October 2009 to February 2011 with the stereoscopic system of both telescopes (zenith angles 12 to 36 degrees, again in wobble mode) [196]. From the single-dish campaign, 24.4 hours were retained after quality cuts, and 84.5 hours from the stereo campaign.
Analysis was done with the standard MAGIC analysis and reconstruction software.
The observations resulted in the first VHE detection of two AGN, NGC1275 in the cluster center, and IC310 located at a distance of 0.6 degrees off the center [197, 198].
Both objects show signs of variability. While NGC1275 exhibits a flux that rapidly decreases with energy (spectral index ≈ 4), and is not detected at energies above 600 GeV, IC310 by contrast shows a very hard spectrum (index -2.00 ± 0.14).
The hard emission from IC310 extends to TeV energies, making this object actually the hardest extragalactic TeV source yet detected.
Historically, IC 310 had been classified as a head-tail radio galaxy [199], i.e. a system characterized by interactions with the ICM.
The VHE and new radio observations, however, suggest a different picture [200, 201]: The "tail" at kiloparsec scales shares the direction and possibly the motion of the inner parsec-scale radio jet (the "head"), corresponding to a blazar-type system.
This would naturally explain the strongly suspected (hints at 3σ level [200]) short-term variability at TeV-energies, and actually make IC 310 the most nearby blazar, and therefore a fascinating object to study this yet-enigmatic class of cosmic accelerators. The hard spectrum extending to TeV energies might even hint at hadron acceleration [202].
Accordingly, a multiwavelength campaign including MAGIC, Fermi-LAT, SWIFT, optical monitoring, and VLBI with the EVN has been proposed and will be carried out within the next two years to study IC 310 in much greater detail.
While the detection and study of these two AGN certainly is an interesting and valuable outcome of this campaign, it also means that their contributions have to be considered when deriving limits onto the emission due to Dark Matter annihilation.
Figures 43 and 44 show the situation in terms of skymaps from the MAGIC stereo campaign.
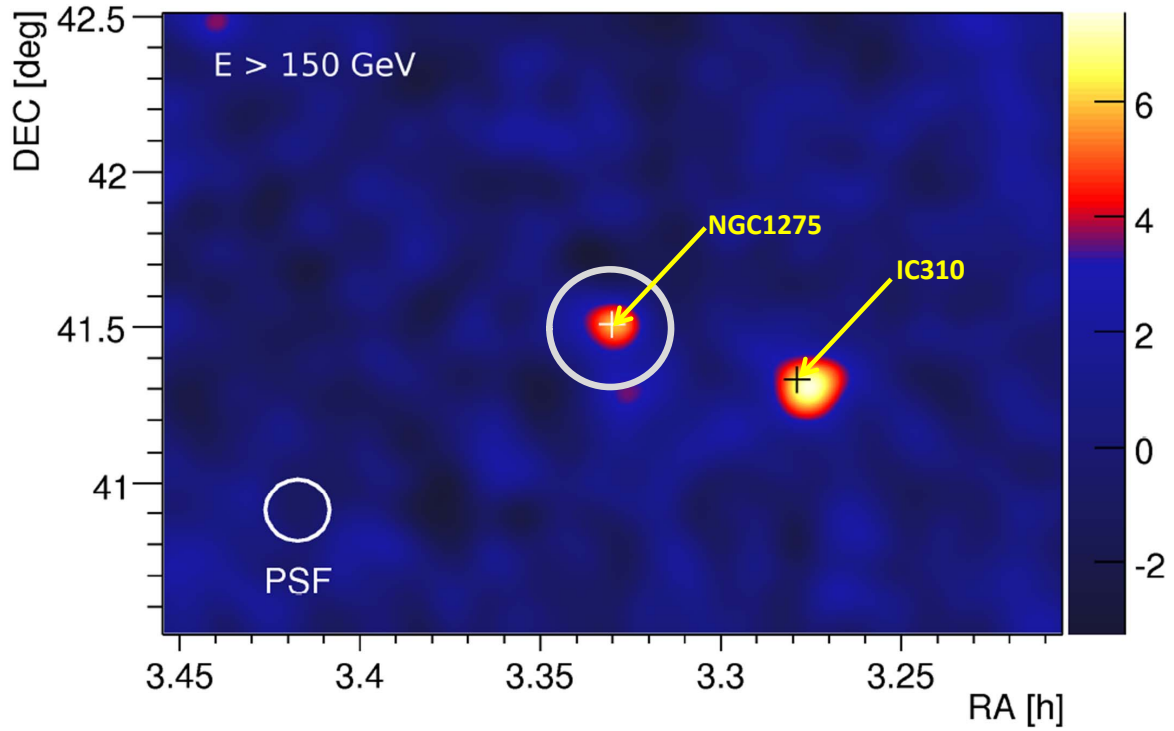
Figure 43: Skymap of the Perseus cluster field as seen in the MAGIC stereo campaign, for energies above 150GeV. Significance of detection color coded. Both NGC1275 and IC310 are detected as prominent sources. Light grey circle denotes the region of the cluster center around NGC1275 that is affected by the presence of NGC1275 for energies below $\approx 600\,GeV$. Basic plot from our publication [196], but modified for this work.
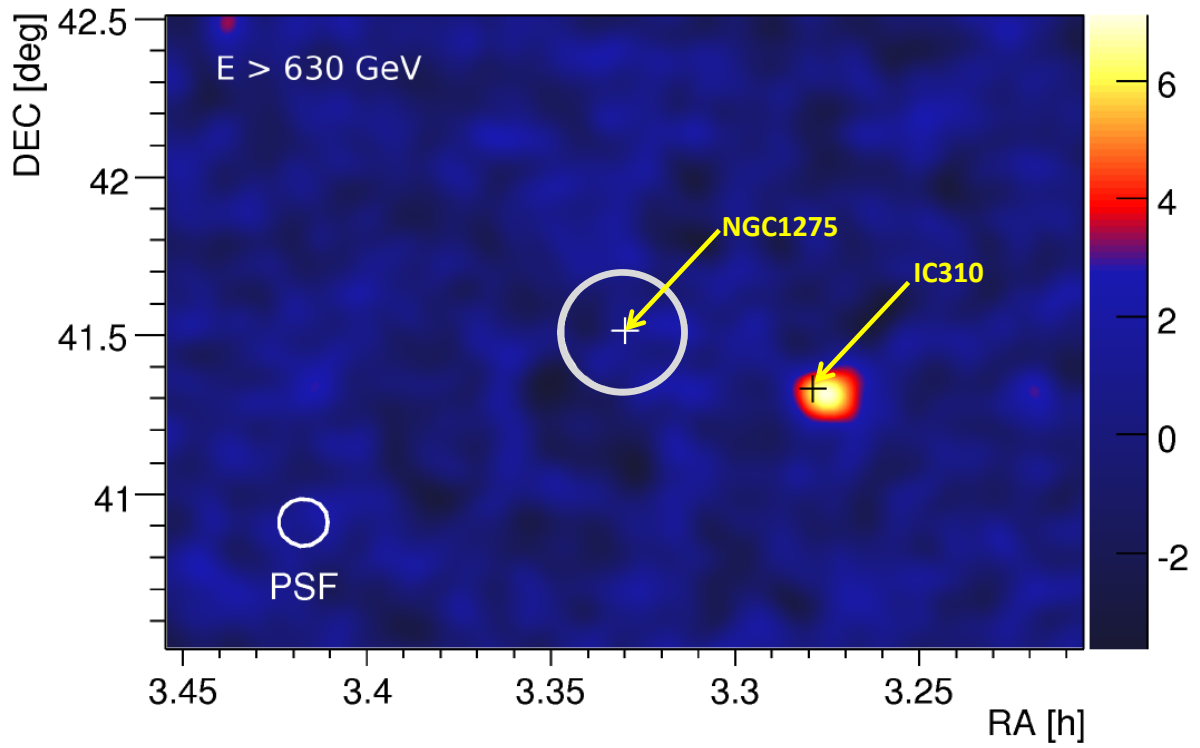
Figure 44: Skymap of the Perseus cluster field as seen in the MAGIC stereo campaign, for energies above 630GeV. Significance of detection color coded. Only IC310 remains as significant source. Basic plot from our publication [196], but modified for this work.

In terms of harvesting the resulting upper limit for constraining emission components other than the AGN, a two-fold approach is used:

Since IC 310 is considerably off the barycenter of the cluster, the sector where it is located can simply be discarded (since the adopted halo model is spherically symmetric, so will be the surface brightness of the DMA-induced emission component).

In the observing period November–December 2008, NGC1275 was in a very low state, also evident by checking the Fermi-LAT scans of the region from this period. It was not detected by MAGIC during this observations. For the central region as indicated in Figures 43 and 44, and below E=630 GeV, the upper limits deduced from this period are therefore the most constraining, and are subsequently used (Table 6).

For the regions outside the area affected by NGC 1275, and generally above energies of 630 GeV (where NGC1275 has never been detected by MAGIC, presumably due to the steep slope of the VHE spectrum), the limits from the stereo observations (October 2009 to February 2011) are used.

As is evident also by the detection of IC310 as an off-axis source, the stereo system for the first time allows for a competitive off-axis sensitivity. In order to harvest this sensitivity gain in terms of the potentially extended emission from Dark Matter annihilation, a relaxed θ^2 cut of $0.02 deg^2$ was used in the analysis [196].

The resulting upper limits are summarized in Table 6.

Energy threshold [GeV]	Flux U. L. [$10^{-13} cm^{-2} s^{-1}$]
100	65.5
630	3.22
1000	1.38
1600	1.18
2500	0.87

Table 6: Integral flux upper limits for the MAGIC Perseus cluster observations.

In terms of the emission due to CR interactions, this limits actually for the first time allowed to constrain the ratio of Cosmic Ray to thermal pressure X_{CR} for numerical simulations of Perseus-like clusters to $X_{CR} < 1.7\%$, or a factor of 1.25 below the self-consistent prediction from this simulation [196]. This is actually the first time that observational constraints from VHE observations limit the underlying physics of such a simulation. The result may suggest smaller than assumed acceleration efficiencies, or a non-negligible role of Cosmic Ray transport out of the cluster core region.

To place limits on Dark Matter annihilation, the halo profile for the Perseus cluster has to be determined. For a NFW-type profile (Eq. 56), the values for M_{200} and R_{200} from X-ray observations given in Table 5 can be used to constrain the profile parameters. In contrast to the sparse stellar dynamical tracers for the cases of dwarf galaxies, this actually results in a profile with a global uncertainty of less than a factor of two, and parameters $R_s = 0.384 Mpc$; $\rho_s = 1.06 \times 10^{15} M_\odot Mpc^{-3}$. Additionally, for cluster sized halos, surviving substructure must play a substantial role in enhancing the annihilation signal. While the total boost, as discussed in Section 5.3, cannot be evaluated with absolute precision, somewhat conservatively here a factor of 200 is assumed.

Resulting exclusion limits, calculated with the same recipe as described for the dwarf galaxies, are plotted in Fig. 45.
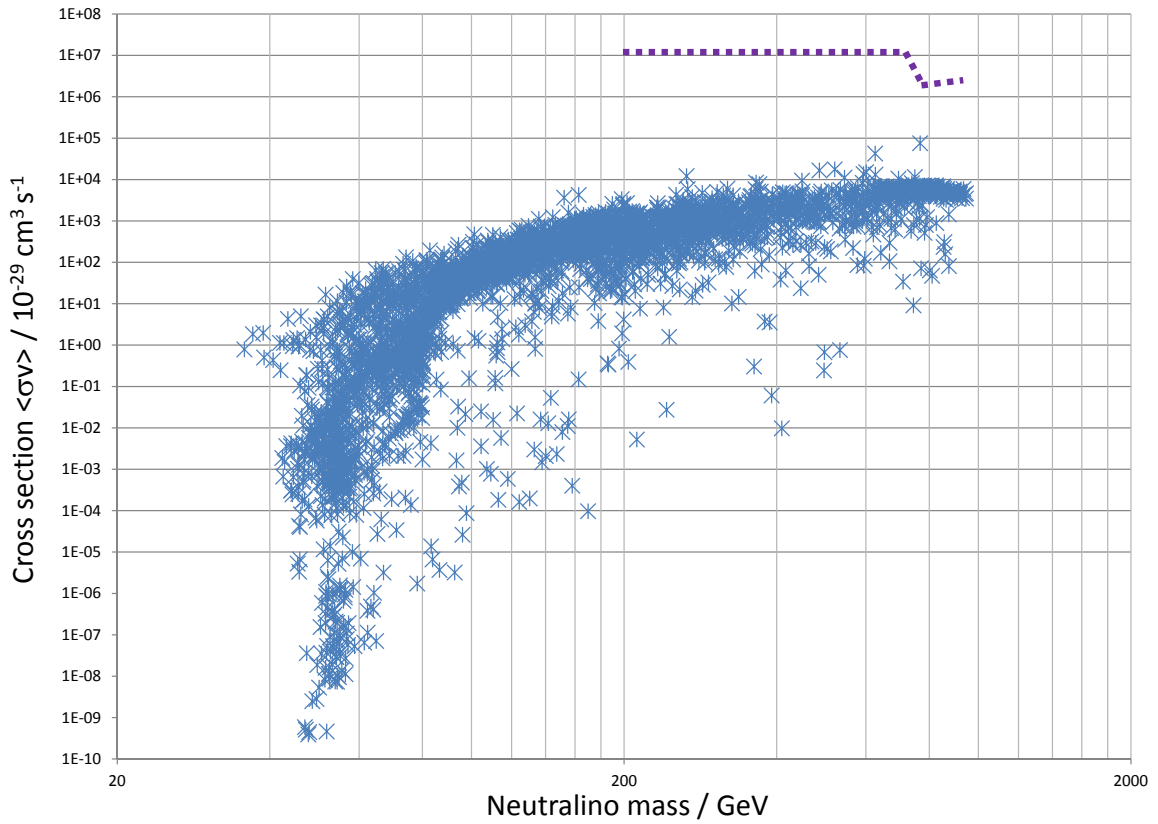
Figure 45: Indirect Dark Matter exclusion limits for the MAGIC observations of the Perseus cluster (violet short dashes). The discontinuity is due to the jump to much higher quality observational limits for the stereo dataset, as discussed in the text. Subhalo contribution factor of 200 is assumed.

9 Dark Matter powered Stars

The formation of the first stars in the Universe – the so called Population III stars – is an unsolved problem in modern Astrophysics [203].

In any case however, this takes place in a higher density environment compared to z=0, regarding both average baryonic- and Dark Matter density. Since collapse of the Dark Matter halos happens naturally before the surface of last scattering, low-mass Dark Matter halos will already be formed at this time, and may even act as "seeds", furthering the collapse of baryons by providing potential wells, thereby facilitating the first stages of protostellar collapse.

Though certainly speculative, it is conceivable that WIMPs may even play a more active role in the formation and evolution of the first stars: the number densities of these particles can be greatly enhanced by adiabatic contraction (the Dark Matter "following" the gravitational tug of the collapsing baryons in later phases of protostellar collapse) [204], or by Dark Matter capture into a (proto-)star for sufficiently large scattering cross sections [205].

Annihilation of the WIMPs in the center of this objects would then provide the forming "star" with an additional source of energy, which might even delay or altogether prevent further collapse and ignition of nuclear fusion – resulting in the formation of a Dark Matter powered object instead, a "Dark Star".

While presently, detection of either type of PopIII star has not been achieved, it is clear that a Dark Star would have different characteristics from a normal PopIII star: being less compact than a normal star, for a given luminosity the surface temperature will be smaller, in many cases resulting in temperatures too low to effectively ionize the surrounding hydrogen [204]. This means in principle, once a PopIII star. or, perhaps observationally more probable an entire star cluster of such objects, still enshrouded in the star forming cloud is detected, it would be possible to spectroscopically infer the temperature of the objects from the degree of ionization in the vicinity, and to subsequently decide whether the temperatures are more compatible with classical models of PopIII star formation, or those of Dark Star formation.

Here, a different approach to search for such objects is presented: with a forward-evolution model as presented in [206], it is possible to calculate the contribution of any species, including a putative Dark Star population, to the extragalactic background light (EBL). For typical Dark Star photospheric temperatures $T_{DS} \leq 10^4 \, K$ and formation redshifts of order ten, their contribution is most notable at micrometer wavelengths [207]. This contribution can then be compared to direct [208] or indirect (using the transparency of the Universe for TeV photons being limited by pair production n the EBL) measurements [209].

To this ends, realistic emission spectra of Dark Star photospheres have for the first time been calculated using PHOENIX version 16 [210].

Figure 46 demonstrates that, at least for rather extreme scenarios, EBL measurements can in fact be employed to constrain a population of Dark Stars in the early Universe. Should much more stringent measurements of the EBL become available in the future, constraints on the Dark Star population might become interesting also for less opti-

mistic models, and generally in terms of placing constraints on the WIMP properties, since the lifetimes of Dark Stars are dependent from the WIMP capture rate into the star (which is the rate with which the star can replenish the fuel it burns) [207], and thus from the elastic WIMP-proton scattering cross section. Thereby, another channel tapping into the elastic scattering parameter space would be opened up for indirect searches.
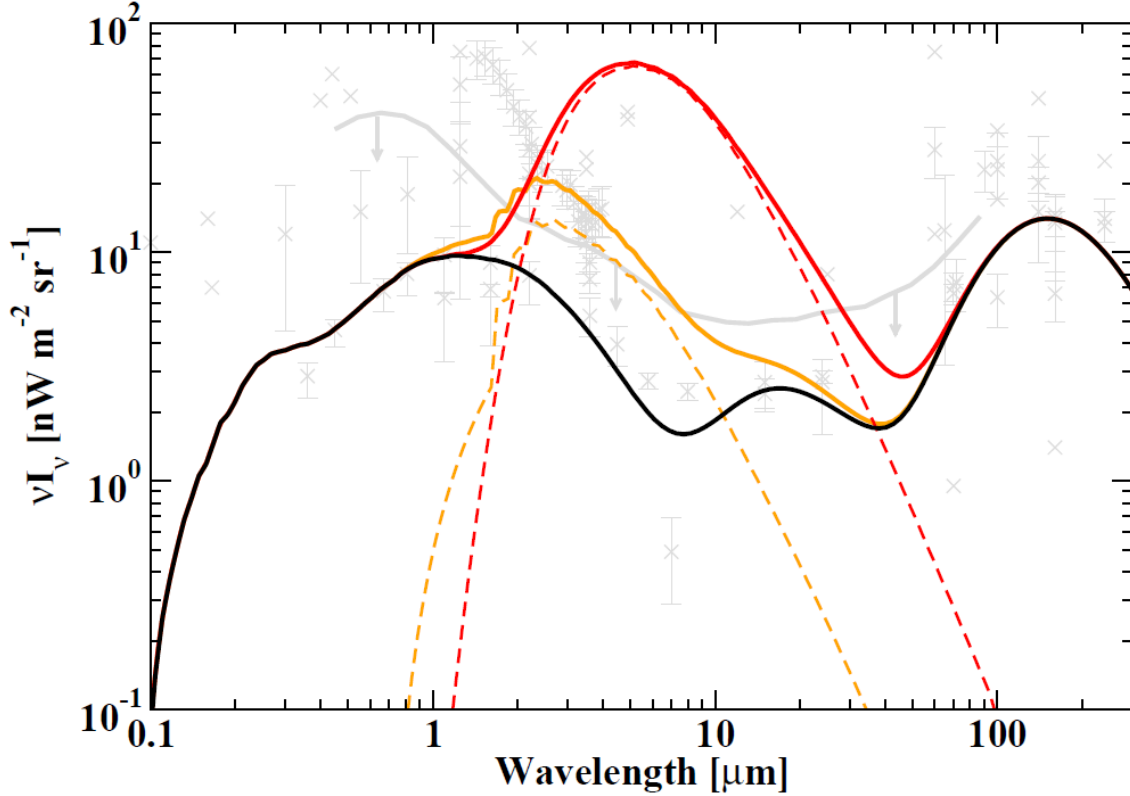
Figure 46: Contribution of fiducial Dark Star populations to the EBL, consisting of stars with mass $690 M_\odot$ and Temperature 7500K (orange) and $106 M_\odot/5000$K (red). EBL measurements and upper limit from TeV observations from [209]. Black line is EBL lower limit from [211]. Dark Star model parameters in both cases: formation rate equal to 10^{-3} of the standard PopIII formation rate [212], Dark Star lifetime $10^9 yrs$, and minimum redshift of formation $z_{min} = 5$. These are highly optimistic scenarios. Plot taken from our publication [207].

10 Combined Results and Prospects for the Type of Study Presented Here

Here, limits on the annihilation of weakly interacting massive particles from several channels were presented. Within the scientific program of the MAGIC telescope system, a portfolio of objects, ranging from dwarf galaxies to galaxy clusters, was observed, and here for the first time limits onto WIMP properties were deduced from these observations in a fully consistent way.

Also, the first direct limits onto the WIMP parameter space from the observations of the Perseus cluster were presented.

This consistent treatment now makes it feasible to combine this limits, and thereby substantially reduce the degree of uncertainty regarding the density profile and general parameters for each individual observed halo.

The limits for both Willman I and Segue I cover the same energy range (note that the observations do not constrain particles with masses exactly down to the energy threshold, due to the limited ($\approx 20\%$) energy resolution of Cerenkov telescope (meaning that fully employing the lowermost bin would use photons of higher energy than the WIMP mass for the constraints). Due to the higher value for the density integral, the Segue I data are rather more constraining, while the Willman I data still confirm the general method for a different halo. The Perseus cluster data extend to considerably higher energies, due to the superior performance of the stereo system, and much deeper exposure. What is probably even more important for our purposes, the Perseus data are much better constrained in terms of the used halo profile (one could however argue that his has to be traded against the assumption of substructure being present in the cluster – but then, we know for a fact (e.g. from the existence of the very same dwarf galaxies also observed in this project) that this must be the case at least to some extent). The combined limit therefore will be backed up by the Perseus data against a much weaker value that would otherwise have to be assumed in the region were the Segue I data are dominant, due to the uncertainties for the Segue I halo. In turn, the Segue I data are more constraining at lower energies, due to the absence of a bright AGN in the center of the field. This demonstrates the power of the approach to use observations of halos at different mass scales.

Figure 47 shows a compilation of both datasets.
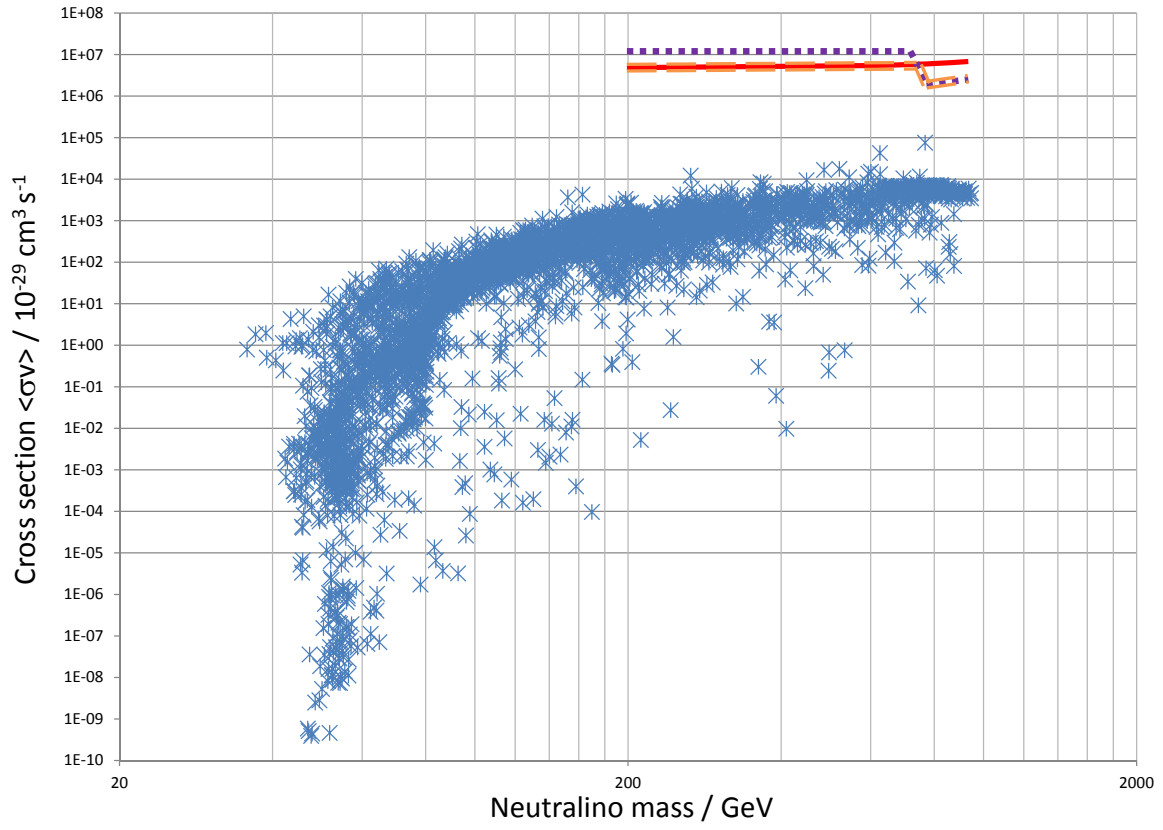
Figure 47: Exclusion limits from the Segue I observations (red) and the Perseus observations (violet). Combined exclusion limit indicated in orange.

This combined limit should now be compared to the state of the art in the field of indirect Dark Matter searches. Recently, the Fermi-LAT team released a very deep search for photons from Dark Matter annihilation from the position of a sample of Milky Way dwarf galaxies [170]. While the Fermi-LAT limit is more constraining at lower energies / WIMP masses, due to the inevitably much lower energies accessible to a space observatory, the situation changes for high-mass WIMPs: Even though more optimistic assumptions about some of the dwarf galaxy halos are made for the LAT-limit than employed here, and unless a very soft photon spectrum from the annihilations is assumed, both limits become equally constraining at TeV energies.
The limit presented here is therefore among the most constraining ones deduced to date from indirect Dark Matter searches.

Till now, constraints on very generic SUSY-WIMPs have been the focus of this work. However, the extracted limits can also be used to constrain less generic situations, which may result in drastically enhanced annihilation rates.

One example would be very high contributions of hard photons from internal Bremsstrahlung / final state radiation [213]. The limits presented here allow to constrain any such additional contributions to less than a factor of 10^3 for the mass range between 200 GeV and TeV. It should however be noted that more recent studies [214] concluded that such contributions anyhow would be sub dominant.

The other prolific case is Sommerfeld enhancement of the annihilation rates, a $1/v$ enhancement in the 1-loop amplitude for small velocities v, which could lead to resonant amplification of the s-wave cross section by orders of magnitude for small particle velocities as typically encountered for WIMPs in the late Universe [215].

This effect has been employed to invoke very high effective cross sections [216], generally needed to explain observed excesses in terms of Dark Matter annihilation.
Consider the case of Sommerfeld-enhanced annihilation of 800 GeV WIMPs with an effective (enhanced) cross section of a few times $10^{-23}\, cm^3\, s^{-1}$, as has been discussed as a combined explanation for the PAMELA and ATIC measured excesses [216]: as figure 48 shows, such a scenario is severely constrained by the Perseus data presented herein.
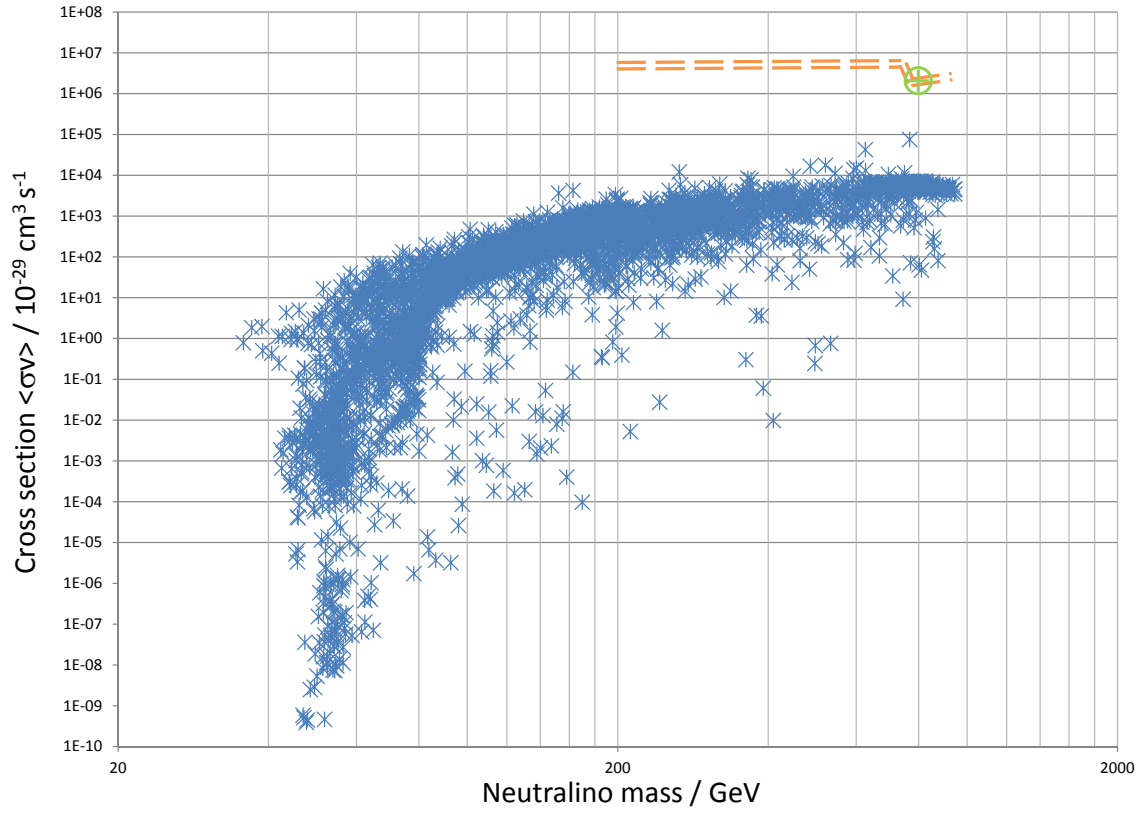
Figure 48: Sommerfeld-enhancement of high-mass WIMPs (model discussed in text depicted as green marker) being constrained by combined exclusion limit presented in this work.

Finally, the new indirect limits should be discussed in terms of up to date limits from elastic scattering experiments. This is done in Fig. 49. There, a limited set of the models from the Wuerzburg database is presented, all of which were required to have elastic scattering cross sections $\geq 10^{-11}\,pb$ and at the same time a WIMP mass $m \geq 400\,GeV$, in order to make comparison at all feasible in light of presently rather restricted coverage of the parameter space by both experimental approaches.

What can immediately be seen is that the approaches are far from closing the parameter space. However, an interesting feature is that there is no strict correlation between the strength of expected signals, so that both detection methods cut into very different parts of the parameter space, and are truly complemental. Note that it is not straight forward to also include limits from collider searches into such a consideration, since collider detection prospects (other than indirect searches for stable WIMPs) are strongly dependent from signals generated by short-lived but charged particles also present in the respective model, and e.g. for supersymmetric scenarios also for the constraints onto the detection of the lightest Higgs bosons.
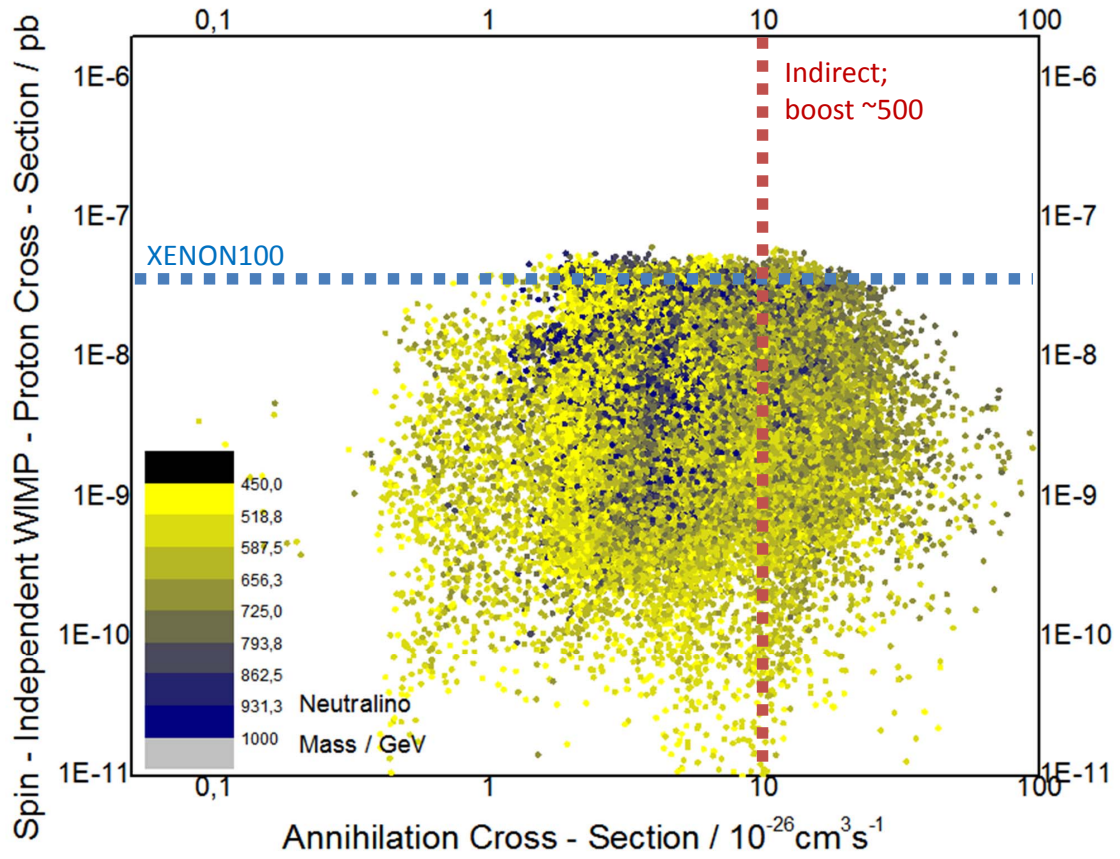
Figure 49: Comparison between direct [50] and indirect exclusion limits (this work, fiducial boost factor of 500 has additionally been assumed.)

11 Outlook

In this work, the first concrete limits onto the WIMP parameter space from observations of the Perseus cluster have been presented, as well as the first combined exclusion limits on WIMP annihilation from MAGIC observations. The results are among the presently strongest limits on indirect signatures of high-mass WIMPs. While the generic parameter space for WIMPs remains largely unexplored, the presently achieved limits are, together with signals from other wavelength regimes and messenger particles, sufficient to severely constrain scenarios with drastically enhanced effective annihilation rates, for example achieved via Sommerfeld enhancement.

The complementarity of collider, direct and indirect searches for Dark Matter strongly motivates a continuation of these efforts.

Regarding the strategy presented in this work, largest potential improvements that can be expected for the future are

- Construction of more sensitive facilities like the planned Cerenkov Telescope Array [217], or even dedicated Dark Matter telescopes [218] with also lower threshold energies would improve upon existing limits with deeper observations

- There are also dedicated and ongoing efforts by the H.E.S.S. and VERITAS collaborations to indirectly detect Dark Matter in the Universe [219, 220]. In principle, it ought to be feasible to include also the limits thus produced into a combined exclusion limit, then covering also higher energies and thereby WIMP masses than accessible to MAGIC.

Efforts to more precisely characterize astrophysical backgrounds due to AGN and CR-interactions should also be pursued with continuation of running programs.

Of course, confirmation of a concrete beyond-standard-model physics scenario, e.g. by the LHC experiments, would in turn allow for a much more focused probe into WIMP candidates from then-remaining parts of the parameter space.

List of Tables

List of Figures

References

[1] T. Standage. *The Neptune File: A Story of Astronomical Rivalry and the Pioneers of Planet Hunting.* Walker & Company, 2000.

[2] D. Cline (ed.). *Sources of Dark Matter in the Universe.* World Scientific, 1994.

[3] F. Zwicky. *Astrophysical Journal,* 86:217, 1937.

[4] P. J. McMillan. *Monthly Notices of the Royal Astronomical Society,* 414 (3):2446–2457, 2011.

[5] A. Mazure et al. (ed.). *Untangling Coma Berenices: a New Vision of an Old Cluster.* World Scientific, 1998.

[6] H. H. C. van de Hulst, E. Raimond and van Woerden. *Bulletin of the Astronomical Institutes of the Netherlands,* 14:1, 1957.

[7] V. Rubin et al. *ApJ Letters,* 255:107, 1978.

[8] M. Milgrom. *Astrophysical Journal,* 270:365–370, 1983.

[9] R. Wojtak et al. *Nature,* 477:567–569, 2011.

[10] J. P. Ostriker and P. J. E. Peebles. *Astrophysical Journal,* 186:467–480, 1973.

[11] P. Schneider. *Extragalactic Astronomy and Cosmology.* Springer, 2006.

[12] J. E. Gunn and J. R. Gott. *Astrophysical Journal,* 176:1, 1972.

[13] L. P. David et al. *Astrophysical Journal,* 380:39, 1991.

[14] C. L. Sarazin. *X-ray Emission from Clusters of Galaxies.* Cambridge University Press, 1988.

[15] A. Vikhlinin et al. *Astrophysical Journal,* 640 (2):691–709, 2006.

[16] A. N. Taylor et al. *Astrophysical Journal,* 501 (2):539, 1998.

[17] X. Wu et al. *Monthly Notices of the Royal Astronomical Society,* 301 (3):861–871, 1998.

[18] D. Clowe et al. *ApJ Letters,* 648 (2):109–113, 2006.

[19] J. Merten et al. *Monthly Notices of the Royal Astronomical Society,* 417:333–347, 2011.

[20] J. C. Mather et al. *Astronomical Journal,* 354:L37, 1990.

[21] E. Komatsu et al. *Astrophys.J.Suppl.,* 192:18, 2011.

[22] M. Arnaud et al. *Astronomy and Astrophysics*, 389:1–18, 2002.

[23] S. W. Allen et al. *Monthly Notices of the Royal Astronomical Society*, 353:457, 2004.

[24] G. Goldhaber and S. Perlmutter. *Physics Reports*, 307:325–331, 1998.

[25] A. V. Filippenko and A. G. Riess. *Physics Reports*, 307:31–44, 1998.

[26] M. Kowalski et al. *Astrophysical Journal*, 686:749–778, 2008.

[27] M. Viel et al. *Monthly Notices of the Royal Astronomical Society*, 399 (1):39–43, 2009.

[28] V. Mukhanov. *Physical foundations of cosmology*. Cambridge University Press, 2005.

[29] A. G. Riess et al. *Astrophysical Journal*, 699:539, 2009.

[30] W. J. Percival et al. *Monthly Notices of the Royal Astronomical Society*, 381 (3):1053–1066, 2007.

[31] S. Burles et al. *arxiv*, astro-ph/9903300:1, 1999.

[32] D. Tytler et al. *Physica Scripta*, 85:12, 2000.

[33] W. Hu and M. White. *Astrophysical Journal*, 471:30–51, 1996.

[34] P. J. E. Peebles. *The Large-Scale Structure of the Universe*. Princeton University Press, 1980.

[35] V. Springel et al. *Nature*, 435:629–636, 2005.

[36] W. H. Press and P. Schechter. *Astrophysical Journal*, 187:425–438, 1974.

[37] R. Cowsik and J. Mc Clelland. *Phys. Rev. Lett.*, 29:669, 1972.

[38] G. Jungman et al. *Phys.Rept.*, 267:195–373, 1996.

[39] B. W. Lee and S. Weinberg. *Phys. Rev. Lett.*, 39:165–168, 1977.

[40] B. Adeva et al. *Phys. Lett. B*, 252:518–524, 1990.

[41] A. Dubey for the D0 Collaboration. *Proceedings of the Hadron Collider Symposium 2009, Evian*, 1:74, 2009.

[42] J. Ellis. *Nature*, 448:297–301, 2007.

[43] CMS Collaboration. *Phys. Lett. B*, 698:196–218, 2011.

[44] M. Honma et al. *PASJ*, 59 (5), 2007.

[45] A. Green. *JCAP*, 1010:34, 2010.

[46] B. Censier. *Proc. of CYGNUS 2011, Aussois*, 2011.

[47] R. Bernabei et al. *EPJ C*, 67:39–49, 2010.

[48] C. E. Aalseth et al. *Phys. Rev. Lett.*, 106:131301, 2011.

[49] CDMS II Collaboration. *Science*, 327:1619–1621, 2010.

[50] G. Angloher et al. *arxiv*, 1109.0702:1, 2011.

[51] C. Savage et al. *Phys. Rev. D*, 70:123513, 2004.

[52] M. Pipe for the DRIFT Collaboration. *Journal of Physics: Conference Series*, 315:012017, 2011.

[53] N. Fornengo et al. *arxiv*, 1110.4337:1, 2011.

[54] I. V. Moskalenko. *arxiv*, 1105.4921:1, 2011.

[55] ... S. Saxena, ...D. Elsaesser. *EPJ C (accepted)*, arxiv:1111.3868:1, 2011.

[56] D. Hooper and J. Silk. *New J. Phys.*, 6:23, 2004.

[57] F. Halzen and D. Hooper. *New J. Phys.*, 11:105019, 2009.

[58] R. Hamerly and A. Kosovichev. *arxiv*, 1110.1169:1, 2011.

[59] C. Alcock et al. *Astrophysical Journal*, 542:281–307, 2000.

[60] J. Wess and B. Zumino. *Nuclear Physics B*, 70:39, 1974.

[61] S. Coleman and J. Mandula. *Physical Review*, 159:1251–1256, 1967.

[62] G. Ross. *Grand Unified Theories*. Westview Press, 1984.

[63] H. Georgi and S. Dimopoulos. *Nuclear Physics B*, 193:150, 1981.

[64] A. H. Chamseddine et al. *Phys. Rev. Lett.*, 49:970, 1982.

[65] S. P. Martin. *arxiv*, hep-ph/9709356:1, 1999.

[66] P. Gondolo et al. *JCAP*, 07:008, 2004.

[67] G. Belanger et al. *Comput.Phys.Commun.*, 182:842–856, 2011.

[68] P. Ullio. *Nuclear Physics B - Proceedings Supplements*, 110:82–84, 2002.

[69] T. Sjostrand et al. *Computer Phys. Commun.*, 178:852, 2008.

[70] T. Kaluza. *Sitzungsber. Preuss. Akad. Wiss. Berlin (Math. Phys.)*, K1:966, 1921.

[71] O. Klein. *Z. Phys.*, 37:895, 1926.

[72] T. Appelquist et al. *Phys. Rev. D*, 64:035002, 2001.

[73] H. C. Cheng et al. *Phys. Rev. Lett.*, 89:211301, 2002.

[74] T. Flacke. *AIP Conf. Proc.*, 1200:583–586, 2010.

[75] H. M. Niederhausen. *Astrophysikalische Suche nach Dunkler Materie in UED-Modellen.* Bachelorarbeit, Universität Würzburg, 2011.

[76] D. Elsässer H. M. Niederhausen and T. Flacke. *in preparation*, 2011.

[77] M. Kuster et al. *Axions - theory, cosmology, and experimental searches.* Springer, 2008.

[78] F. Wilczek. *Phys. Rev. Lett*, 40:223–226, 1978.

[79] S. Weinberg. *Phys. Rev. Lett.*, 40:279–282, 1978.

[80] G. Raffelt. *Proc. of the XVth Moriond Workshop: Dark Matter in Cosmology, Clocks and Tests of Fundamental Laws*, 1, 1995.

[81] K. Zioutas et al. *Nucl. Instrum. Methods Phys. Res.*, 425:480, 1999.

[82] K. Ehret et al. *arxiv*, hep-ex/0702023, 2007.

[83] S. Andriamonje et al. *J. Cos. Astropart. Phys.*, 4:10, 2007.

[84] K. Ehret et al. *Nucl.Instrum.Meth.A*, 612:83–96, 2009.

[85] A. De Angelis et al. *Phys Lett. B*, 659847:17, 2007.

[86] E. W. Kolb et al. *DARK98: Proceedings of the Second International Conference on Dark Matter in Astro and Particle Physics*, 1998.

[87] J.A. Formaggio et al. *Phys. Rev. D*, 57:7037–7040, 1998.

[88] M. Loewenstein and A. Kusenko. *Astrophysical Journal*, 714:652, 2010.

[89] The ROSAT All Sky Survey. *http://www.xray.mpe.mpg.de/cgi-bin/rosat/rosat-survey.*

[90] S. Cole and C. Lacey. *Monthly Notices of the Royal Astronomical Society*, 281:716, 1996.

[91] J. F. Navarro et al. *Astrophysical Journal*, 463:563, 1996.

[92] B. Moore. *Proc. of the 20th Texas Symposium*, 2001.

[93] A. Klypin et al. *Astrophysical Journal*, 573:597–613, 2002.

[94] G. R. Blumenthal et al. *Astrophysical Journal*, 301:27–34, 1986.

[95] B. Moore et al. *ApJ Letters*, 524:19–22, 1999.

[96] J. Einasto. *Trudy Inst. Astrofiz.*, 51:87, 1965.

[97] D. Merritt et al. *Astronomical Journal*, 132:2685, 2006.

[98] A. V. Kravtsov et al. *ApJ Supplements*, 111:73, 1997.

[99] V. Springel et al. *Nature*, 456:73–76, 2008.

[100] A. Green et al. *Monthly Notices of the Royal Astronomical Society*, 353:23–27, 2004.

[101] J. Lee. *Astrophysical Journal*, 604:73–76, 2004.

[102] K. V. Johnston et al. *Astrophysical Journal*, 451:598–606, 1995.

[103] L. Bergstrom et al. *Phys. Rev. Lett.*, 87:251301, 2001.

[104] T. C. Weeks. *AIP Conf. Proc.*, 198:3–11, 1990.

[105] E. Lorenz. *Nuclear Physics Proceedings Supplements*, 114:217–232, 2003.

[106] T. C. Weeks et al. *Astrophysical Journal*, 342:379, 1989.

[107] W. Hofmann et al. *Proceedings of ICRC 2001*, pages 2785–2788, 1989.

[108] T. C. Weeks et al. *Astroparticle Physics*, 17:221–243, 2002.

[109] C. Baixeras et al. *Nuclear Instruments and Methods in Physics Research A*, 518:188–192, 2004.

[110] H. Anderhub et al. *HEAD 2010*, arXiv:1010.2397, 2011.

[111] A. N. Otte for the MAGIC collaboration. *Proc. of the 30TH INTERNATIONAL COSMIC RAY CONFERENCE*, 2:827–830, 2008.

[112] MAGIC collaboration. *Science*, 322:1221–1224, 2008.

[113] $http://heasarc.gsfc.nasa.gov/docs/cgro/egret/egret_tech.html$.

[114] R. C. Hartman et al. *ApJ Supplements*, 123:79–202, 1999.

[115] S. D. Hunter et al. *Astrophysical Journal*, 481:205, 1997.

[116] P. Sreekumar et al. *ApJ Supplements*, 494:523, 1998.

[117] A. W. Strong et al. *Astrophysical Journal*, 613:956–961, 2004.

[118] S. Mereghetti et al. *AIP Conf. Proc.*, 515:467–473, 2000.

[119] J. Carson for the Fermi-LAT coll. *Journal of Physics: Conference Series*, 60:115–118, 2007.

[120] Fermi-LAT collaboration. *arxiv*, 1108.1435, 2011.

[121] G. Johannesson for the Fermi-LAT collaboration. *Proc. of the XLIV Rencontres de Moriond*, 2009.

[122] Fermi-LAT collaboration. *Phys. Rev. Lett.*, 104:101101, 2010.

[123] C. Boehm et al. *Phys. Rev. Lett.*, 92:101301, 2003.

[124] The COMPTEL collaboration. *Astronomy and Astrophysics Supplement*, 143:145–179, 2000.

[125] R. Diehl et al. *Astronomy and Astrophysics Supplement*, 97:181–184, 1993.

[126] Sonja Boyer. *Diplomarbeit, Universität Würzburg*, Korrelation der Gammastrahlen-Emission aus dem Zerfall von radioaktiven Al-26 in der Milchstrassee mit Supernova-Überresten, 2011.

[127] J. Greiner et al. (incl. D. Elsässer). *Experimental Astronomy*, (arXiv:1105.1265), 2011.

[128] D. Elsässer A. Summa and K. Mannheim. *Astronomy and Astrophysics*, 533:A13, 2011.

[129] R. Ramaty et al. *ApJ Supplements*, 40:487, 1979.

[130] G. Bertone et al. *Phys. Rept.*, 405:279–390, 2005.

[131] O. Adriani et al. *Nature*, 458:607–609, 2009.

[132] J. Chang et al. *Nature*, 456:362–365, 2008.

[133] P. J. Fox and E. Poppitz. *Phys. Rev. D*, 79:083528, 2009.

[134] S. Profumo. *Central European Journal of Physics*, 10:1–31, 2011.

[135] K. Mannheim and D. Elsässer. *Physik Journal*, 02/2009:19, 2009.

[136] D. Hooper et al. *Phys. Rev. D*, 76:083012, 2007.

[137] M. Ackermann et al. *arxiv*, 1109.0521, 2011.

[138] M. Aguilar et al. *Physics Reports*, 366:331–405, 2002.

[139] D. Elsässer and K. Mannheim. *Astroparticle Physics*, 22:65–72, 2004.

[140] D. Elsässer and K. Mannheim. *Phys. Rev. Lett.*, 94:171302, 2005.

[141] F. Acero et al. *Science*, 326:1080–1082, 2009.

[142] V. A. Acciari et al. *Nature*, 462:770–772, 2009.

[143] A. A. Abdo et al. *ApJ Letters*, 709:152, 2010.

[144] D. Elsässer K. Mannheim and O. Tibolla. *arxiv*, 709:1010.2185, 2010.

[145] N. F. Bell and T. D. Jacques. *Phys. Rev. D*, 79:043507, 2009.

[146] F. Aharonian et al. *Phys. Rev. Lett.*, 97:221102, 2006.

[147] K. Tsuchiya et al. *ApJ Letters*, 606:115–118, 2004.

[148] K. Kosack et al. *ApJ Letters*, 608:97–100, 2004.

[149] J. Albert et al. (MAGIC coll.). *ApJ Letters*, 638:101, 2006.

[150] S. Markoff et al. *ApJ Letters*, 489:47–50, 1997.

[151] V. Schönfelder et al. *Astron. Astrophys. Suppl. Ser.*, 143:145–179, 2000.

[152] M. P. Ulmer et al. *Proceedings of the 2nd INTEGRAL Workshop*, page 253, 1996.

[153] A. Atoyan and C. D. Dermer. *Astrophysical Journal*, 617:123–126, 2004.

[154] Revnivtsev M.G. et al. *Pis'ma Astron. Zh.*, 430:253, 2004.

[155] M. A. Sanchez-Conde et al. *Proceedings of the 8th UCLA Symposium*, 1166:191–196, 2009.

[156] MAGIC collaboration. *Astrophysical Journal*, 679:428–431, 2008.

[157] V. Belokurov et al. *Astrophysical Journal*, 654:897–906, 2007.

[158] M. Geha et al. *Astrophysical Journal*, 692:1464–1475, 2009.

[159] J. D. Simon et al. *Astrophysical Journal (submitted)*, arXiv:1007.4198, 2010.

[160] G. D. Martinez et al. *JCAP*, 0906:014, 2009.

[161] E. Domingo-Santamaria et al. (MAGIC coll.). *Proceedings of the International Cosmic Ray Conference 2005*, astro-ph/0508274, 2005.

[162] J. Aleksic et al. (incl. D. Elsässer). *JCAP*, 06:035, 2011.

[163] R. Essig et al. *Phys. Rev. D*, 82:123503, 2010.

[164] B. Willman et al. *Astronomical Journal*, 129:2692–2700, 2005.

[165] J. Sitarek and R. Mirzoyan. *MAGIC TDAS Note*, 08-03.

[166] E. Aliu et al. (incl. D. Elsässer). *Astrophysical Journal*, 697:1299–1304, 2009.

[167] L. E. Strigari et al. *Astrophysical Journal*, 678:614, 2008.

[168] L. Pieri et al. *Phys. Rev. Lett.*, 95:211301, 2005.

[169] H. Zechlin et al. (incl. D. Elsässer). *Astronomy and Astrophysics*, accepted, 2011.

[170] Fermi-LAT coll. *Phys. Rev. Lett.*, in press:arxiv:1108.3546, 2011.

[171] A. Geringer-Sameth and S. Koushiappas. *Phys. Rev. Lett.*, in press:arxiv:1108.2914, 2011.

[172] D. Nieto for the MAGIC coll. *Proc. of the ICRC2011*, arXiv:1111.0879, 2011.

[173] N. Gehrels et al. *Astrophysical Journal*, 611:1005, 2004.

[174] L. Feretti et al. *New Astronomy Reviews*, 48:1137, 2004.

[175] R. Schlickeiser. *Cosmic ray astrophysics*. Springer, 2002.

[176] P. Blasi and S. Colafrancesco. *Astroparticle Physics*, 12:169, 1999.

[177] A. C. Fabian. *Annual Review of Astronomy and Astrophysics*, 32:277–318, 1999.

[178] A. Pinzke et al. *arxiv*, 1105.3240:277–318, 2011.

[179] V. Springel. *Monthly Notices of the Royal Astronomical Society*, 364:1105, 2005.

[180] C. Pfrommer. *Monthly Notices of the Royal Astronomical Society*, 385:1242, 2008.

[181] A. Pinzke and C. Pfrommer. *Monthly Notices of the Royal Astronomical Society*, 409:449, 2010.

[182] T. H. Reiprich and H. Boehringer. *Astrophysical Journal*, 567:716, 2002.

[183] P. Fouque et al. *Astronomy and Astrophysics*, 375:770, 2001.

[184] A. Abramowski et al. (incl. D. Elsässer). *Astrophysical Journal*, accepted, 2011.

[185] V. A. Acciari et al. (incl. D. Elsässer). *Science*, 325:444, 2009.

[186] D. E. McLaughlin. *Astrophysical Journal*, 512:9, 1999.

[187] M. Rueger et al. *Monthly Notices of the Royal Astronomical Society*, 401:973, 2010.

[188] P. E. Hardee. *Astrophysical Journal*, 261:457, 1982.

[189] D. E. Harris et al. *Astrophysical Journal*, 699:305, 2009.

[190] A. A. Abdo et al. *Astrophysical Journal*, 707:55, 2009.

[191] K. Berger for the MAGIC coll. *arxiv*, 1109.5879, 2011.

[192] F. Aharonian et al. *Science*, 314:1424, 2006.

[193] A. Pedlar et al. *Monthly notices of the Royal Astronomical Society*, 246:477, 1990.

[194] E. Churazov et al. *Astrophysical Journal*, 590:225, 2003.

[195] J. Aleksic et al. (incl. D. Elsässer). *Astrophysical Journal*, 710:634–647, 2010.

[196] J. Aleksic et al. (incl. D. Elsässer). *arXiv:1111.5544*, submitted to Astronomy and Astrophysics, 2011.

[197] MAGIC coll. *ATEL*, 2916, 2010.

[198] J. Aleksic et al. (incl. D. Elsässer). *ApJ Letters*, 723:207–212, 2010.

[199] J. M. Riley. *Monthly Notices of the Royal Astronomical Society*, 161:167, 1973.

[200] D. Eisenacher. *Diplomarbeit, Universität Würzburg*, Die Radio-Galaxie IC 310: Ein hadronischer Beschleuniger?, 2011.

[201] M. Kadler et al. sumitted to Astronomy and Astrophysics, 2011.

[202] K. Mannheim. *Astronomy and Astrophysics*, 269:67–76, 1993.

[203] V. Bromm and R. B. Larson. *Ann. Rev. Astron. Astrophys.*, 42:79–118, 2004.

[204] D. Spolyar et al. *Phys. Rev. Lett.*, 100:051101, 2008.

[205] F. Iocco et al. *Monthly Notices of the Royal Astronomical Society*, 390:1655–1669, 2008.

[206] T. M. Kneiske et al. *Astronomy and Astrophysics*, 386:1–11, 2002.

[207] A. Maurer et al. (incl. D. Elsässer). *Proceedings of the 25th Texas Symposium on Relativistic Astrophysics*, online: *http : //pos.sissa.it/cgi − bin/reader/conf.cgi?confid* = 123, 2010.

[208] G. G. Fazio et al. *ApJ Supplements*, 154:39–43, 2004.

[209] D. Mazin and M. Raue. *Astronomy and Astrophysics*, 471:439–452, 2007.

[210] P. H. Hauschildt and E. Baron. *Astronomy and Astrophysics*, 509:36, 2010.

[211] T. M. Kneiske and H. Dole. *Astronomy and Astrophysics*, 515:19, 2010.

[212] M. Trenti and M. Stiavelli. *Astrophysical Journal*, 694:879–892, 2009.

[213] T. Bringmann et al. *JHEP*, 1:049, 2008.

[214] M. Cannoni et al. *Phys. Rev. D*, 81:107303, 2010.

[215] J. L. Feng et al. *Phys. Rev. D*, 82:083525, 2010.

[216] N. Arkani-Hamed et al. *Phys. Rev. D*, 79:015014, 2009.

[217] P. Brun for the CTA coll. *Proceedings of the Annual meeting of the French Society of Astronomy and Astrophysics*, 2011.

[218] L. Bergstrom et al. *Phys. Rev. D*, 83:045024, 2011.

[219] A. Abramowski et al. *Astroparticle Physics*, 34:608–616, 2011.

[220] V. A. Acciari et al. *Astrophysical Journal*, 720:1174–1180, 2010.

Lebenslauf

Name: Dominik Martin Elsässer

Geburtsdatum: 15.07.1980

Geburtsort: Alzenau

Staatsangehörigkeit: deutsch

Eltern: Klaus und Rebecca Elsässer

Wohnort: Hauptstrasse 80, 97218 Gerbrunn

Grundschule: 09/1987-07/1991: Grundschule Kleinkahl

Gymnasium: 09/1991-06/2000 Spessart-Gymnasium Alzenau

Zivildienst: 07/2000-04/2001 Krankenhaus Gelnhausen

Universitätsstudium (Physik): 04/2001-04/2005 Fakultät für Physik und Astronomie, Universität Würzburg

Abschluss: Dipl. Phys. (04.04.2005)

Seit 01/2006: Wissenschaftliche Arbeiten zur Promotion in Physik (Lehrstuhl für Astronomie, Universität Würzburg)

Fremdsprachen: Englisch, Latein

Beruf: Wissenschaftlicher Angestellter, Universität Würzburg

Danksagungen

Mein aufrichtigster Dank gebührt Prof. Dr. Karl Mannheim, der diese Arbeit betreut hat. Sein fachlicher und persönlicher Rat war und ist stets von unschätzbarem Wert, und seine herausragende Forscherpersönlichkeit ein grosses Vorbild.

Ebenfalls danke ich allen Mitgliedern des Lehrstuhls für Astronomie, sowie des Graduiertenkollegs 1147 an der Uni Würzburg, für anregende Diskussionen und wissenschaftliche Zusammenarbeit.

Ebenso geht mein aufrichtiger Dank an alle Mitglieder der Gamma-Arbeitsgruppe am Lehrstuhl Astronomie, mit denen es stets eine Freude ist, zu diskutieren und zu arbeiten.

Weiterhin danke ich der MAGIC Kollaboration für den Betrieb dieser einzigartigen Instrumente, sowie für ausserordentlich produktive wissenschaftliche Diskussionen und Zusammenarbeit.

Für finanzielle und ideelle Unterstützung danke ich dem BMBF (MAGIC), der DFG (Graduiertenkolleg 1147), der Helmholtz-Gesellschaft (VIHKOS, NAVI und HAP) und dem Elitenetzwerk Bayern.

Carolin Liefke, liebste Seilgefährtin beim Erklimmen auch der höchsten (realen und ideellen) Berge auf allen leichten und schwierigen Wegen.

Meinen Eltern, denen ich alles verdanke, und die mich immer unterstützt haben, auch wenn meine Ziele sicher nicht immer leicht erkennbar waren.

Eidesstattliche Versicherungen und Erklärung zur Einhaltung der Regeln über gute wissenschaftliche Praxis

Hiermit versichere ich an Eides statt, dass ich die vorliegende Dissertation eigenständig, d.h. insbesondere selbstständig und ohne Hilfe einer kommerziellen Promotionsberatung, angefertigt habe, und dass ich keine anderen als die angegebenen Quellen und Hilfsmittel benutzt habe.

Ebenfalls versichere ich an Eides statt, dass ich die Gelegenheit zum Promotionsvorhaben nicht kommerziell vermittelt bekommen habe, und insbesondere keine Person oder Organisation eingeschaltet habe, die gegen Entgelt Betreuer bzw. Betreuerinnen für die Anfertigung von Dissertationen sucht.

Ich erkläre hiermit ausserdem, dass ich die Regeln der Universität Würzburg über gute wissenschaftliche Praxis eingehalten habe.

Ort, Datum

Dominik Elsässer